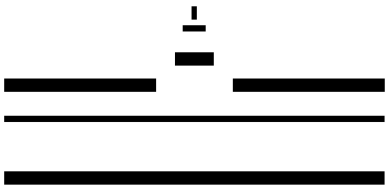

Westfälische
Wilhelms-Universität
Münster

Master of Science

Efficiency determination of a radon detection system for practical exercises in nuclear physics

Effizienzbestimmung eines Radondetektionssystems im kernphysikalischen Praktikum

Institut für Kernphysik
Mathematisch-Naturwissenschaftliche Fakultät
Westfälische Wilhelms-Universität Münster

Erstgutachter : Prof. Dr. Alfons Khoukaz

Westfälische Wilhelms-Universität Münster

Zweitgutachter : Prof. Dr.Marcos Aurelio González Álvarez

Universidad de Sevilla

Manuel Pérez Mayo

A la memoria de mi padre.
Zur Erinnerung an meinen Vater.
To memory of my father.

Contents

Introduction 1

1. Motivation 5
   1.1. The importance of Radon . . . 6
   1.2. Start point, work and improvements . . . 7

2. Theoretical principles of alpha spectrometry 9
   2.1. The radioactive decay law . . . 10
      2.1.1. Radioactive decay chains . . . 11
   2.2. Dosimetry . . . 12
   2.3. Alpha decay . . . 16
      2.3.1. The barrier penetration . . . 18
   2.4. Multi alpha peaks analysis . . . 20
   2.5. Semiconductor systems . . . 24
      2.5.1. Semiconductor properties . . . 24
      2.5.2. Silicon Surface Barrier detectors . . . 28
      2.5.3. Solid angle correction . . . 30
      2.5.4. Dead-time . . . 32
   2.6. Global efficiency of a system . . . 32

3. Experimental setup 35
   3.1. Cryogenic system . . . 37
      3.1.1. Water trap . . . 38
      3.1.2. Radon trap . . . 42
      3.1.3. Cold head . . . 47
   3.2. Electronic system . . . 50
      3.2.1. Detection system . . . 50

3.2.2. Temperature measurement system 58

4. Calibration and radon air sample 65
4.1. Calibration 66
4.1.1. Calibration source 67
4.1.2. Calibration test 68
4.2. The radioactive source 68
4.2.1. Working with the radioactive source 69

5. Modifications of the setup and results 71
5.1. Radon in detection system V 2.0 72
5.2. Radon in detection system V3.1 74
5.3. Radon in detection system V 3.2 81
5.3.1. New tube system with new valve and vacuum sensor 82
5.3.2. Temperature card modification 85
5.3.3. Temperature control with Temp V2.5 85
5.3.4. Exchange of a vacuum pump in the gas system 88

6. Radon measurements 95
6.1. Calculation of radon concentration in air 96
6.2. Measurements of basement samples 97
6.3. Measurements of floor samples 101
6.4. Measurements of background samples 104

7. Conclusions 107

A. Plots 109
A.1. Calibrations 110
A.2. Measurements with setup V3.1 111
A.3. Measurements with setup V3.2 117
A.4. Measurements of basement samples 119
A.5. Measurements of floor samples 120
A.6. Measurements of background samples 121

B. Relative and absolute corrections 123
B.1. Absolute correction 123
B.2. Relative correction 125

C. Measurement protocol V3.2 127
C.1. Calibration protocol 127
C.2. Radon air measurement protocol 133

D. CAD-drawings 147

E. Electronic diagrams 151

F. Radon properties and extra information 157

G. Tables 161
G.1. Measurements with setup V2.0 161
G.2. Measurements with setup V3.1 163
G.3. Measurements with setup V3.2 170
G.4. Measurements of basement samples 173
G.5. Measurements of floor samples 176
G.6. Measurements of background samples 179

Bibliography 183

Introduction

Every act of creation is first of all an act of destruction
Pablo Picasso.

Radioactivity and radiation are well known words today. Radioactivity is defined as the emission of ionizing radiation or particles caused by the spontaneous disintegration of atomic nuclei. Radiation is the emission of charged particles with high energy or electromagnetic energy. Radiation can be classified in α, β^+, β^-, γ, or neutrons. In the first case α-radiation is composed by helium nuclei and is the most ionizing radiation, but easily to stop. The second and the third case are positrons and electrons. The β-radiation is a penetrating radiation due to the light mass of these particles. The γ-radiation is electromagnetic radiation or photons this radiation is one of the most penetrating radiation. The last one is the neutron radiation. This radiation consists of free neutrons result of nuclear fission or nuclear fusion, these free neutrons react with nuclei of other atoms forming new isotopes.
The central theme of this master thesis will be α-radiation, in particular the α-decay of Radon-222. The importance of radon detection is based on studies showing that the exposition of a high radon concentration is directly related with the probability of lung cancer. Radon is an alpha emitter. When a radon particle goes into the lung the particle is catched by the lung tissue, radon decays into polonium-218 and polonium-214 via α-emission.
The α-particles have a strong ionizing power in short distances, that means in a lung tissue, a radon particle is a principal factor causing cancer.
With these argument radon detection plays a important role for lung cancer prevention. Nevertheless the detection of radon is not easy. There are standard devices to detect the radon concentration using chemical processes but the detection of a low radon concentration in air probes is still a task under development.
For this reason the objective of this work is oriented to improve an experimental setup which was built up to detect radon in air probes. The first version of this

setup was developed by Martin Nettebrock in his Phd thesis to measure radioactive isotopes in natural probes. After that Andrea Nustede has modified the setup in the framework of her Diploma thesis to measure solid and gaseous radioactive probes. This device should allow for radon concentration measurements and is used in the practical exercises of the institute. The global efficiency determination of the setup and some tests of radon probes were done. The conclusion was a low efficiency but the possibility to do radon measurements. For these reasons the necessity to improve the experimental setup for radon air probes still remains.
The task of this master thesis will be the efficiency determination of the setup and improvements in the cryogenic system, temperature control, gas system and the optimal electronic configuration will be done. To finish this master thesis, radon measurements will be measured and shown in the last chapter.
The structure of this thesis will follow the next outline:

Chapter 1 presents the motivation of this work. Some typical radon concentration will be presented. In this brief chapter the history of radon and arguments to measure it will be discussed.

Chapter 2 will give a brief overview of the α-spectrometry. Information about typically used units, the radioactive decay law and in more detail the alpha decay are presented. The fit function to analyze the alpha spectra used in this master thesis will be explained. In addition theory of the semiconductor detectors, dead time and formulation to calculate the detection efficiency can be found.

Chapter 3 will deal with the experimental setup. This chapter shows the experimental components and parts of the system. A description of the characteristic modules used and optimal configuration of the them are given.

Chapter 5 describes the realized modifications in the system. The chapter is divided into three parts. Every part explains the development of the system during this master thesis. The first part will deal with the original setup. The second one shows the first modifications. In the last part of this chapter the final setup and their improvements are presented.

Chapter 6 exposes the radon concentration measurements of this master thesis. For this purpose several air samples from different locations in the institute have been collected and analyzed. In total six samples from the basement, seven samples from the floor and two samples from the background of the laboratory were studied.

Chapter 7 is the conclusion of this thesis including an outlook of possible improvements.

1. Motivation

1.1. The importance of Radon

Radon is a radioactive, colorless, odorless and tasteless gas. This chemical element can be obtained as decay element of uranium and thorium. In normal conditions radon is a gas, for this reason, radon has been considered to be a health hazard. The principal problems of this radiative substances are the daughter nuclei. These elements are solid and can remain on surfaces in particular tissues. When contaminated air is inhaled these particles remain in the airways and alpha radiation is emmited, the consequence can be the development of lung cancer.
Radon is responsible for the majority of the radiation exposure background. This element is accumulated in buildings especially in basements and attics. The EPA (United States Environmental Protection Agency) [epa] established that Radon is the second cause of lung cancer after cigarette smoking. It is also known that high exposure of approximately $1\,\mathrm{MBq/m^3}$ can be found in radon mines. In 1879 Herting and Hesse identified the high radon concentration with lung cancer in their investigations of miners from Schneeberg in Germany.
The Radon concentration varies widely from place to place. A typical domestic exposure is $100\,\mathrm{Bq/m^3}$ indoors, but radon may accumulate in basements and seep into an indoor through construction junctions or for the water supply. On Table 1.1 values of a estimated concentration in different places can be seen.

$\mathrm{Bq/m^3}$	Places
1	Large oceans
10	Continental concentration in open air
100	Typical indoor domestic concentration
1000	High concentration, houses built on soils with a high uranium concentration or high permeability of the ground
10000	Concentration in a uranium mines

Table 1.1.: Guide value of typical radon concentration in different places. Source: [con]

Radon emanation varies with the soil type and of course with the content of uranium. Radon concentration can be an indicator that there are local inputs of ground water. For this reason the radon concentration can be detected for earthquake predictions. The idea is, if there is an increase of radon concentration,

it is due to the generation of new cracks below ground.

Radon levels are different during the day, for example the maximal concentration is during the coolest part of the day when the pressure differential is the greatest.[1] In 2009 a maximal recommended value of 100 Bq/m^3 by the national reference level was established. In USA the EPA [epa] recommends to take actions if the radon concentration is higher than 74 Bq/m^3, but the European Union recommends action to be taken at 400 Bq/m^3 in old houses and 200 Bq/m^3 for new ones.

1.2. Start point, work and improvements

The initial point of this master thesis was to do the improvements developed by A. Nustede in her Diploma thesis. The implementation of a new configuration to perform a background measurement parallel to the radon cooling measurement was the first task. The next and important objective was the efficiency determination, for that a high number of radon measurements was required. With the obtained results and the observed instabilities, three improvements were developed .
A new computer program to control the temperature of all parts of the system was developed in the framework of this master thesis. An improper control of the temperature was the first suggestion as reason for a too low measured radon concentration. The radon air detection system is composed of two cryogenic devices and, in every device the temperature must be restricted in a specific range. If the temperature is not sternly controlled the radon concentration can be lost.
The second modification was in order to avoid the loss of radon before of the measurement. In the original system the radon concentration was expanded over a long gas tube system. In the new setup a new tube configuration to concentrate radon only in a short part of the gas system was developed.
The third modification was the exchange of a vacuum pump of the gas system, due to some observed instabilities in the measurements and the vacuum pressure.
With the done improvements, measurements with radon probes of the basement and floor samples of the institute of nuclear physics were done. The air sample collection were done in places where a high radon concentration was expected. To compare with low radon concentration, radon air measurements in the corridor of every floor were measured.

[1] For more information see [God]

2. Theoretical principles of alpha spectrometry

2.1. The radioactive decay law

During the investigation of properties of radiation emitted by radioactive elements, Rutherford and Soddy found that:
"In all cases where one of the radioactive products has been separated, and its activity examined independently of the active substance which gives rise to it, or which it in turn produces, it has been found that the activity under all condition investigated fall off in a geometrical progression with time".[Hod97]
Actually this citation is known as the law of radioactive decay. The "activity" of a radiative substance is only the number of decays per time. The "decay rate" is called λ and this value is characteristic of a radiative substance. When a nucleus has more than one mode of decay, then λ is the sum of the separate constants for each mode.

$$\lambda = \lambda_1 + \lambda_2 + \lambda_3... \tag{2.1}$$

In a sample of N nuclei, the number of nuclei decaying in a time dt would be:

$$\frac{dN(t)}{dt} = -\lambda N(t). \tag{2.2}$$

Integrating formula 2.2 it gives:

$$N(t) = N_0 e^{-\lambda(t-t_0)} \tag{2.3}$$

where N_0 is the number of nuclei at t_0. Every radiative substance has a specially λ, in praxis it is more habitual to use the term "life-time" τ_m.

$$\tau_m = \frac{1}{\lambda} \tag{2.4}$$

Normally in a calculation the parameter "half-life" $T_{1/2}$ will be used. It is defined as the time a sample takes to decay to one-half of the original activity. Thus,

$$\frac{1}{2} = e^{-\lambda T_{1/2}} \tag{2.5}$$

leads to

$$T_{1/2} = \frac{1}{\lambda}\ln(2) = \tau_m \ln(2). \tag{2.6}$$

The activity $A(t)$ of a radioactive nuclei is defined as:

$$A(t) \equiv \lambda N = N_0 \lambda e^{-\lambda(t-t_0)} = A_0 e^{-\lambda(t-t_0)} \tag{2.7}$$

with A_0 is the initial activity.
The activity depends on the amount of source material. Some units for the activity were introduced, the outdated unit was "Curie" (Ci). It was defined as the activity of a 1 g of pure radium-226.

$$1\,\text{Curie(Ci)} = 3.7 \times 10^{10}\,\text{Decay/s} \tag{2.8}$$

Curie was a large unit and normally in the laboratory μ-Curies or less can be found. Actually the SI-derived unit fot the activity is "Becquerel" and it is defined as

$$1\,\text{Becquerel(Bq)} = 1\,\text{Decay/s}. \tag{2.9}$$

2.1.1. Radioactive decay chains

Normally a situation in which a nucleus decays in a daughter nucleus can be found. The daughter nucleus disintegrates into another unstable nucleus and so on. For this example one can consider the first two alpha decays of the radium scheme: [Leo94]

$$^{226}Ra \rightarrow^{222} Rn \rightarrow^{218} Po \tag{2.10}$$

To explain this theoretical example three arbitrary nuclei A, B, C will be used:

$$\text{A} \rightarrow \text{B} \rightarrow \text{C} \tag{2.11}$$

Applying the formula 2.2, in this case:

$$\left(\begin{array}{l} \frac{dN_a}{dt} = -\lambda_a N_a \\ \frac{dN_b}{dt} = \lambda_a N_a - \lambda_b N_b \\ \frac{dN_c}{dt} = \lambda_b N_b \end{array} \right) \tag{2.12}$$

If one consider initially $N_b(0) = 0$ and $N_c(0) = 0$, the solution of these equations can be written:

$$\left(\begin{array}{l} N_a(t) = N_a(0) e^{-\lambda_a t} \\ N_b(t) = N_a(0) \frac{\lambda_a}{\lambda_b - \lambda_a} \{e^{-\lambda_a t} - e^{-\lambda_b t}\} \\ N_c(t) = N_a(0) \{1 + \frac{1}{\lambda_b - \lambda_a} [\lambda_a e^{-\lambda_b t} - \lambda_b e^{-\lambda_a t}]\} \end{array} \right) \tag{2.13}$$

One can remember the activity definition 2.7 that delivers:

$$\left.\begin{array}{l} A_a(t) \equiv \lambda_a N_a = A_a(0)e^{-\lambda_a t} \\ A_b(t) \equiv \lambda_b N_b = A_a(0)\frac{\lambda_b}{\lambda_b-\lambda_a}\{e^{-\lambda_a t} - e^{-\lambda_b t}\} \\ A_c(t) \equiv \lambda_c N_a = \lambda_c N_a(0)\{1 + \frac{1}{\lambda_b-\lambda_a}[\lambda_a e^{-\lambda_b t} - \lambda_b e^{-\lambda_a t}]\} \end{array}\right) \tag{2.14}$$

In general the chain is described as a series.

$$N_1 \xrightarrow{\lambda_1} N_2 \xrightarrow{\lambda_2} N_3 \xrightarrow{\lambda_3} N_4 \xrightarrow{\lambda_4} ...N_n \tag{2.15}$$

It is possible to write the activity of the family member n starting at N_0. In this case the Bateman[1] equations can be used.

$$A_n(t) = N_0 \sum_{i=1}^{n} C_{n,i} e^{-\lambda_i t} \tag{2.16}$$

where:

$$C_{n,i} = \frac{\lambda_1\lambda_2\lambda_3\lambda_4...\lambda_n}{(\lambda_1-\lambda_i)...(\lambda_{i-1}-\lambda_i)(\lambda_{i+1}-\lambda_i)...(\lambda_n-\lambda_i)} = \frac{\prod_{k=1}^{n}\lambda_k}{\prod_{k=1;(k\neq i)}^{n}(\lambda_k-\lambda_i)} \tag{2.17}$$

In nature three natural radioactive family scheme can be found. Due to the experimental setup and a radium source used in this master thesis only the decay series of ^{238}U will be shown. Figure 2.1 shows the decay scheme of ^{238}U series, this scheme shows the α-decays that will be studied in this master thesis.

2.2. Dosimetry

Dosimetry is the measurement of the absorbed dose in matter and tissue resulting from the exposure to ionizing radiation.
The absorbed dose is defined [Pro]:

$$D = \frac{dE_{\text{abs}}}{dm} = \frac{1}{\rho}\frac{dE_{\text{abs}}}{dV}. \tag{2.18}$$

Where dE_{abs} is the absorbed energy per mass or volume, ρ is the density matter. The absorbed dose is reported in Gray (Gy):

$$1\,\text{Gy} = 1\,\text{J/kg} \tag{2.19}$$

[1]More information in [Ama]

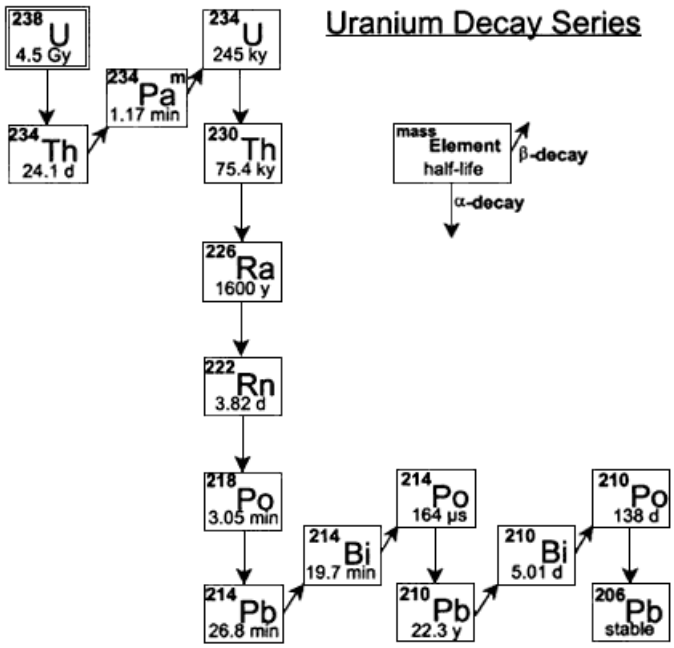

Figure 2.1.: Decay scheme ^{238}U chain. In the practical exercise, the alpha decays starting with ^{226}Ra and finishing in ^{214}Pb will be studied. [ap]

In older books other unit can be found, today is not used because the Gray is more extended. It is called 1 rad. [Pro]

$$1\,\text{rad} = 100\frac{erg}{g} = 100\frac{(\frac{g \cdot cm^2}{s^2})}{g} = 0.01\,\text{Gy} \tag{2.20}$$

Here the type of radiation is not considered. In the case of tissues biological effects of radiation are correlated with the energy absorbed by ionization in unit mass. [Leo94]
The absorbed dose does not give indications of the harm, for this reason the "equivalent dose" is defined:

$$H_T = w_R \cdot D_R \tag{2.21}$$

The "equivalent dose" H_T is the absorbed dose multiplied by the radiation weighting factor w_R. When there are more than one radiation, the sum must be used:

$$H_T = \sum_R w_R \cdot D_{T,R} \tag{2.22}$$

The new index R is because there is an absorbed dose by the organ T and with radiation type R. [Leo94]

The Sievert Sv is the unit used today to measure the "equivalent doses" or "absorbed dose in a tissue or organ". Sievert has the same units that Gray (J/kg).

$$1\,\mathrm{Sv} = \mathrm{J/kg} \tag{2.23}$$

This unit is normalized to measure the biological effects due to irradiation. The normalizer factor w_R is different to every radiation type. Different values of this factor can be found on Table 2.1

Radiation type and energy	**Radiation weighting factor** w_R
Photons, all energies	1
Electrons, myons, all energies	1
Neutrons	
$< 10\,\mathrm{keV}$	5
$10\,\mathrm{keV}$ to $100\,\mathrm{keV}$	10
$> 100\,\mathrm{keV}$ to $2\,\mathrm{MeV}$	20
$> 2\,\mathrm{MeV}$ to $20\,\mathrm{MeV}$	10
$> 20\,\mathrm{MeV}$	5
Protons $> 2\,\mathrm{MeV}$	5
Alpha particles, fission fragments, heavy nuclei	20

Table 2.1.: Radiation weighting factor or "w_R". Excluding Auger electrons emitted from nuclei bound to DNA. [Leo94]

Effective Dose

To measure the probability of developed biological effects such as cancer or genetic anomalies due to the radiation on the specific organ or tissue other term have to be defined. It has to be weighted with a new "tissue weight factor" or w_T. It is a non-dimensional factor equivalent to the last one, but with other meaning. [Leo94]
Some differences are clear:
*Is defined only for organs of the body

*The w_T is independent of the radiation and energy.
*Is normalized to 1.

The "Effective Dose" is defined as:

$$E = \sum_T w_T H_T \tag{2.24}$$

Where T is the sum factor for all parts of the body. In the table 2.2 all values to the w_T factor can be found.

Organ	**Tissue weighting factor** w_T
Gonads	0.20
Colon	0.12
Bone marrow (red)	0.12
Lung	0.12
Stomach	0.12
Bladder	0.05
Chest	0.05
Liver	0.05
Thyroid gland	0.05
Oesophagus	0.05
Skin	0.01
Bone surface	0.01
Remainder	0.05

Table 2.2.: Tissue weighting factor or "w_T". Remainder includes: Adrenals, brain, small intestine, kidney, muscle, pancreas, spleen, thymus and uterus. [Leo94]

2.3. Alpha decay

Alpha decay is the emission of a charged particle α of a nucleus X. One can make a description of this phenomenon with the next equation. [Leo94]

$$ {}^{A}_{Z}X \longrightarrow {}^{A-4}_{Z-2}X + {}^{4}_{2}He^{2+} \tag{2.25} $$

Normally a daughter nucleus in the ground state can be found. An α-decay has a defined alpha energy but that is not always the case. For example in the alpha decay of ^{226}Ra this problem can be shown.^{226}Ra decays into ^{222}Rn with a probability 94.6 % in the ground state, but the remaining probability shows that there are other decays in excited state of radon (see Figure 2.2).

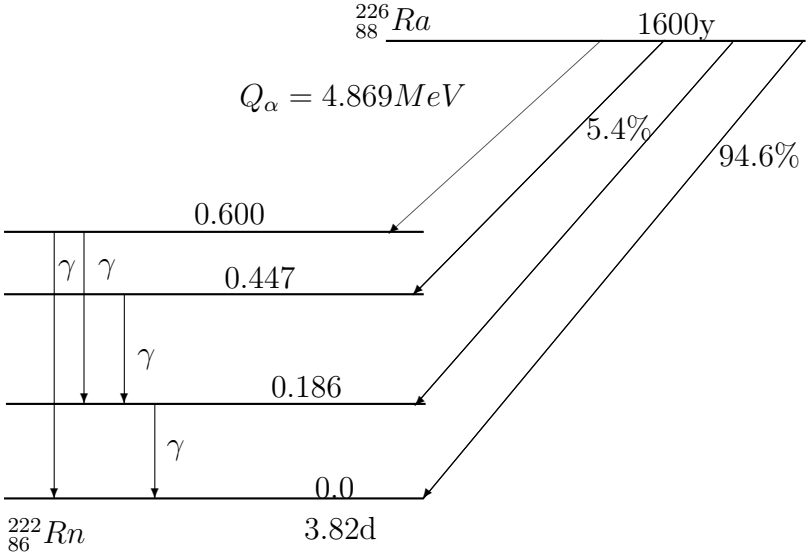

Figure 2.2.: Alpha decay of the source ^{226}Ra. The oblique arrows represent α emissions with the branching ratios indicated, leading to excited states of ^{222}Rn. The vertical arrows represent successive γ-decays. [Hod97]

Alpha decay is only possible if the mass of the parents atoms are greater than the sum of the daughter atoms masses and the ^{4}He . That means α-decay is possible if the kinetic energy Q_α is greater than:

$$ Q_\alpha = (M(Z,A) - M(Z-2,A-4) - M(^{4}He))c^2 \tag{2.26} $$

It is only possible if there is a nuclei with $A \geq 140$ [Hod97]. The origin of this condition is due to a potential barrier that the α-particle must go through. It can be done if there is a non-negligible probability different to zero. In general if $Q_\alpha > 0$

the energy can be divided into two parts. One part can be the energy of the excited daughter nucleus E_{exc} and the other one the kinetic energy E.

$$Q_\alpha = E_{exc} + E \tag{2.27}$$

Considering energy and momentum conservation, a part of E is provided to the α-particle, considering the α-emitter at rest [Hod97]:

$$M_\alpha \nu_\alpha = M_R \nu_R \tag{2.28}$$

$$E_\alpha = E\frac{M_R}{M_\alpha + M_R} \approx (1 - \frac{4}{A}) \tag{2.29}$$

In this case the kinetic energy of an α-particle is not sufficient for a α-emission. Of course this phenomenon is possible because the α-particle must surmount the Coulomb barrier by tunnel effect. The α-particles have normally a well defined range in air $\Re$. For α-particle with energy between 3 and 8 MeV, the range in air (in cm) is[2]:

$$\Re \approx 0.325 E_\alpha^{3/2} \tag{2.30}$$

Where E_α is in MeV for the α-particle, Geiger and Nuttall found out that the range is connected with the decay constant λ, and the decay constant is related with the energy of the alpha particle [Hod97]:

$$\log(\Re) = A + B\log(\lambda) \tag{2.31}$$

$$\log(\lambda) = C\log(E_\alpha) - D \tag{2.32}$$

A, B, C, D are constants. Equations 2.31 and 2.32 are experimental formulas. To explain these laws, Gamow, Condon and Gurney developed a theory of the quantum mechanical tunnelling of the α-particle through the Coulomb barrier. The next section will explain this process.

[2]Experimental equation obtained by [Hod97]

2.3.1. The barrier penetration

This section wants to show the transmission of a plane wave through a one-dimensional barrier. It is a fast method to explain the alpha emission.

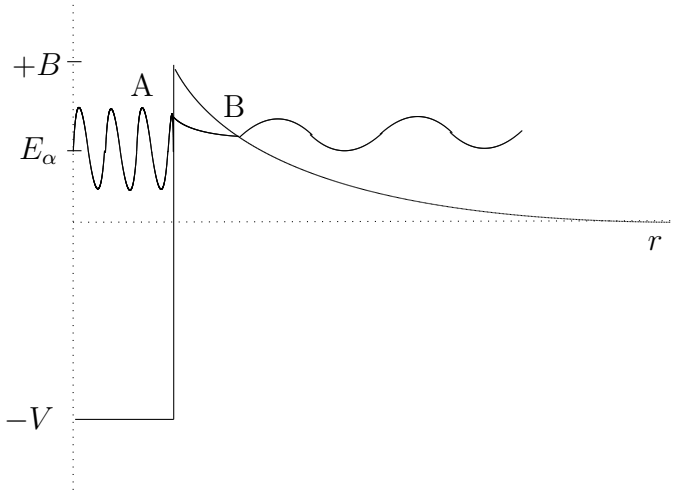

Figure 2.3.: Nuclear potential and the α-wave function in α-decay. E_α is the energy of the α-particles, A and B are the input and output of the α-wavefunction, $-V$ is the nuclear potential, $+B$ is the connection point between well-potential and the Coulomb potential. r is the spherical axis, due to the spherical symmetry. [Hod97]

Considering a one-dimensional barrier and a spherical symmetry, it is possible to use the WKB approximation. The barrier penetration factor T will be given by the ratio between the incident and the transmitted flux: [Hod97]

$$T \approx \ e^{-G} = \exp(-2\frac{\sqrt{2M_\alpha}}{\hbar}\int_R^b (V(r) - E_\alpha)^{1/2} dr), \tag{2.33}$$

with the Coulomb potential:

$$V(r) = \frac{1}{4\pi\varepsilon_0}\frac{2Ze^2}{r}. \tag{2.34}$$

Introducing the Coulomb potential in the equation 2.33 and integrating it leads to

$$T \approx \ e^{-G} = \exp(-2\sqrt{\frac{M_\alpha Ze^2 b}{\pi\varepsilon_0\hbar^2}}[\cos^{-1}(\sqrt{\frac{R}{b}}) - \sqrt{\frac{R}{b} - (\frac{R}{b})^2}] \tag{2.35}$$

In this equation, G is the Gamow factor, Z is the charge of the daughter nucleus, $b = \frac{Ze^2}{2\pi\varepsilon_0 E_\alpha}$ and for all natural α-emitters is $r = b \ggg r = A$. For that one can say that the square bracket is approximately $(\frac{\pi}{2} - 2\sqrt{\frac{R}{b}})$, it is:

$$T \approx \exp(-\frac{e^2 Z}{\varepsilon_0 \hbar v_\alpha} + 8\sqrt{\frac{M_\alpha R Z e^2}{4\pi\varepsilon_0 \hbar^2}}), \tag{2.36}$$

where $v_\alpha = \sqrt{2E_\alpha/m_\alpha} \propto \sqrt{E_\alpha}$ and for natural radioactive substances $82 \leq Z \leq 92$ its mean: $9.06 < \sqrt{Z} < 9.59$. In this case, it is possible to consider that the second term only varies 6% for the natural α-emitters. We obtain:

$$T \approx \exp(-\frac{C_2 Z}{\sqrt{E_\alpha}} + C_1), \tag{2.37}$$

where C_1 and C_2 are constants. Thus

$$\log(T) = C_1 - C_2 \frac{Z}{\sqrt{E_\alpha}}. \tag{2.38}$$

It is necessary to remember that T is the lead term in the expression of the decay rate, therefore:

$$\log(\lambda) = C_1 - C_2 \frac{Z}{\sqrt{E_\alpha}} \tag{2.39}$$

For the most radiative substances one can make a good approximation:

$$-\log(E_\alpha) \propto \frac{Z}{\sqrt{E_\alpha}} \tag{2.40}$$

One can see that 2.32 and 2.40 are equivalent. Geiger and Nuttal found this relation through a purely empirical fitting to the experimental data. The validity of the equation 2.40 for the same α-emitters is shown on the Figure 2.4 .

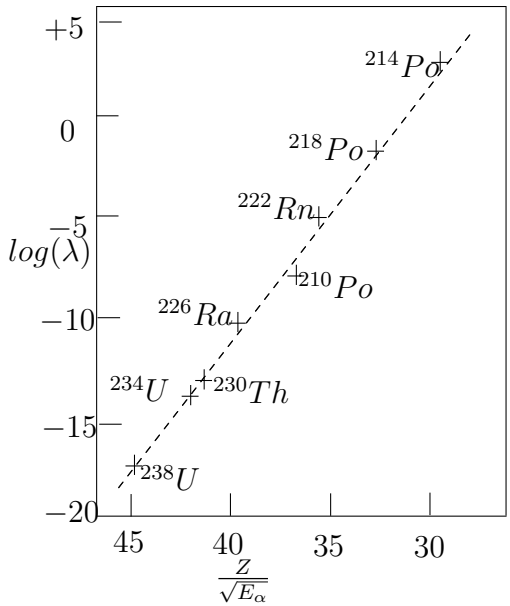

Figure 2.4.: Validity of the Gamow-Condon-Gurney relation (2.15) in the case of even-even α-emitters of the uranium series. [Hod97]

2.4. Multi alpha peaks analysis

To analyze the alpha spectra the analytical function cited in [Bor] will be used. This function can be used for multi-alpha-peaks. In this case spectra with three decays of ^{222}Ra will be analyzed. In the abstract, the fit function is called as convolution of a Gaussian and weighted by sum of two exponentials. In the following lines, the analysis for only one peak will be explained and will extrapolate then for more than one. Normally the function for alpha peaks is written as a convolution product

$$f(u) = G(u) * E(u)H(-u), \tag{2.41}$$

where:
$f(u)$ is the joint-probability-density function,
u is the energy variable,
$G(u)$ is a normalized Gaussian function,
$E(u)H(-u)$ is a left-sided exponential.

Alpha emission is a random process, characterized with a symmetry probability-density function $p_x(x)$ and with a purely asymmetric probability-density function. Considering now x and y as independent random variables, $p_x(x)$ is defined as.

$$p_x(x) = \frac{1}{\sqrt{2\pi\sigma^2}} e^{-\frac{x^2}{2\sigma^2}}. \tag{2.42}$$

The function 2.42 is used in $-\infty < x < +\infty$ and is the Normalized Gaussian function. The next function function $p_y(y)$ is:

$$p_y(y) = \frac{1}{\tau} e^{\frac{y}{\tau}} H(-y). \tag{2.43}$$

The function 2.43 is used in $-\infty < x < +\infty$ and is a left-sided exponential. The joint-probability-density function to characterize the random variable $u = x + y$ is:

$$p_u(u) = \int_{-\infty}^{0} p_y(y) p_x(u - y) dy. \tag{2.44}$$

With equation 2.43 in 2.44 and integrating it leads to

$$p_u(u) = \frac{1}{2\tau} e^{\frac{u}{\tau} + \frac{\sigma^2}{2\tau^2}} \mathrm{erfc}[\frac{1}{\sqrt{2}}(\frac{u}{\sigma} + \frac{\sigma}{\tau})]. \tag{2.45}$$

Some modifications will be done, the first one: the area is A instead of 1. The centroid position can be determined by μ. Finally the function for a single peak can be written by

$$f(u)_1 = A p_u(u) = \frac{A}{2\tau} e^{\frac{u-\mu}{\tau} + \frac{\sigma^2}{2\tau^2}} \mathrm{erfc}[\frac{1}{\sqrt{2}}(\frac{u-\mu}{\sigma} + \frac{\sigma}{\tau})]. \tag{2.46}$$

The authors have described:
Alpha peak symmetry is relatively well described by such a model. However, according to our experience, tailing in spectra from essentially massless sources measured with ionimplanted detectors is not adequately dealt with by an expression which contains a single exponential asymmetry function. We therefore adopt a sum of exponentials and a constant. [Bor]
In praxis there is not only one peak, other terms must be introduced to weight the function. The general function described by G. Bortels and P. Collaers in [Bor], for m peaks is

$$\begin{aligned} f(u) = &\textstyle\sum_{i=1}^{m} \frac{A_i}{2} \{(\frac{1-\eta}{\tau_1}) \exp(\frac{u-\mu_i}{\tau_1} + \frac{\sigma^2}{2\tau_1^2}) \mathrm{erfc}[\frac{1}{\sqrt{2}}(\frac{u-\mu_i}{\sigma} + \frac{\sigma}{\tau_1})] \\ &+ \frac{\eta}{\tau_2} \exp(\frac{u-\mu_i}{\tau_2} + \frac{\sigma^2}{2\tau_2^2}) \mathrm{erfc}[\frac{1}{\sqrt{2}}(\frac{u-\mu_i}{\sigma} + \frac{\sigma}{\tau_2})]\}. \end{aligned} \tag{2.47}$$

In the experimental calculation, there are three peaks. To obtain the area of ^{222}Rn, ^{218}Po and ^{214}Po all spectra will be analyzed with the function 2.48.

$$
\begin{aligned}
&f(A_{222};A_{218};A_{214};x;\eta;\mu_1;\mu_2;\mu_3;\tau_1;\tau_2;\sigma) = \\
&+\tfrac{A_{222}}{2}\{(\tfrac{1-\eta}{\tau_1})\exp(\tfrac{u-\mu_1}{\tau_1}+\tfrac{\sigma^2}{2\tau_1^2})\mathrm{erfc}[\tfrac{1}{\sqrt{2}}(\tfrac{u-\mu_1}{\sigma}+\tfrac{\sigma}{\tau_1})] \\
&+\tfrac{\eta}{\tau_2}\exp(\tfrac{u-\mu_1}{\tau_2}+\tfrac{\sigma^2}{2\tau_2^2})\mathrm{erfc}[\tfrac{1}{\sqrt{2}}(\tfrac{u-\mu_1}{\sigma}+\tfrac{\sigma}{\tau_2})]\} \\
&+\tfrac{A_{218}}{2}\{(\tfrac{1-\eta}{\tau_1})\exp(\tfrac{u-\mu_2}{\tau_1}+\tfrac{\sigma^2}{2\tau_1^2})\mathrm{erfc}[\tfrac{1}{\sqrt{2}}(\tfrac{u-\mu_2}{\sigma}+\tfrac{\sigma}{\tau_1})] \\
&+\tfrac{\eta}{\tau_2}\exp(\tfrac{u-\mu_2}{\tau_2}+\tfrac{\sigma^2}{2\tau_2^2})\mathrm{erfc}[\tfrac{1}{\sqrt{2}}(\tfrac{u-\mu_2}{\sigma}+\tfrac{\sigma}{\tau_2})]\} \\
&+\tfrac{A_{214}}{2}\{(\tfrac{1-\eta}{\tau_1})\exp(\tfrac{u-\mu_3}{\tau_1}+\tfrac{\sigma^2}{2\tau_1^2})\mathrm{erfc}[\tfrac{1}{\sqrt{2}}(\tfrac{u-\mu_3}{\sigma}+\tfrac{\sigma}{\tau_1})] \\
&+\tfrac{\eta}{\tau_2}\exp(\tfrac{u-\mu_3}{\tau_2}+\tfrac{\sigma^2}{2\tau_2^2})\mathrm{erfc}[\tfrac{1}{\sqrt{2}}(\tfrac{u-\mu_3}{\sigma}+\tfrac{\sigma}{\tau_2})]\}.
\end{aligned}
\tag{2.48}
$$

In all measurements the equation 2.48 was the model equation used to determine the area of the^{222}Rn peak. The parameters A_{222}, A_{218}, A_{214} are the area of every peaks. The parameter x is the number of channel. Parameters μ_i are referred to the centroid of every peak, parameters τ_i are the adjust parameter between the two gauss function of every peaks (the fit function and the normal distribution), finally the parameter σ is a global parameter of the full function.

In Figure 2.5 a example of a fit has been shown. In this case, one can see the fit using the fit function 2.48. A initial value of the parameters μ_i must be introduced in the program to find the convergence. In a theoretical and perfect setup the values of μ_i using the calibrated source will be the same. During the measurements of the efficiency determination only in a short number of measurements the initial values μ_i have been modified, due to some instabilities in the measurement.
In the majority of the fits realized the fit has been done without difficult. For every peaks two gauss functions have been used in the fit function, it can see in the formula 2.48, the idea come from the authors and the argument is a best fitting according to the experience. [Bor]
This function was used in the last work realized on this setup. In the Diploma thesis of [Nus11], this function was tested and confirmed as the best option for the SSB detector here used. For this reason the use of this function are based in the last Diploma thesis realized on this experimental setup. [Nus11]

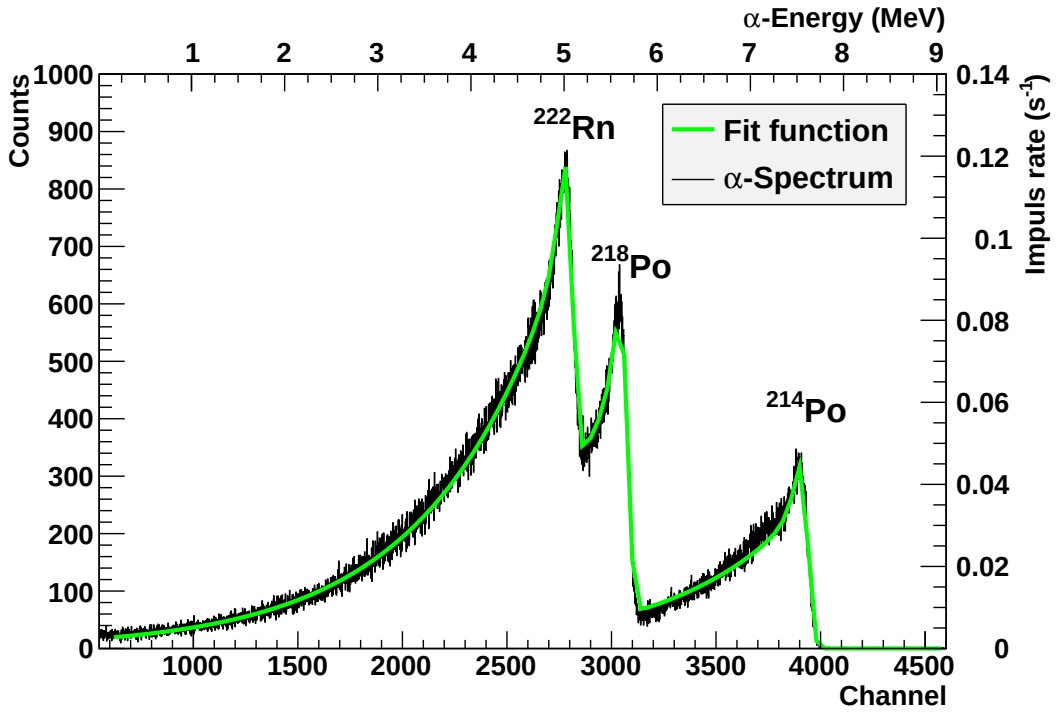

Figure 2.5.: Measurement for the efficiency determination, date: 30.09.2011. In this picture a fit of a measurement has been shown. In the horizontal axis the channel and a calibration of the energy has been plotted. In the vertical axis the number of counts and a calibration of the impulse rate have been included. With black color the experimental data, in green the fit function used in the calculation.

2.5. Semiconductor systems

To measure charged particles semiconductor devices are normally used. Crystalline semiconductor material is a medium where the ionizing radiation can pass as well as electron-hole pairs can be created. To collect the particles an electrical field is used. Using electronic devices it is possible to register the final pulse. The principal advantages of semiconductor are a great density to stop the particles, the compact size and the fast response time have been considered.

2.5.1. Semiconductor properties

In this section the basic properties of semiconductor materials will be shown. A scheme of the semiconductor material can be found on Figure 2.6.

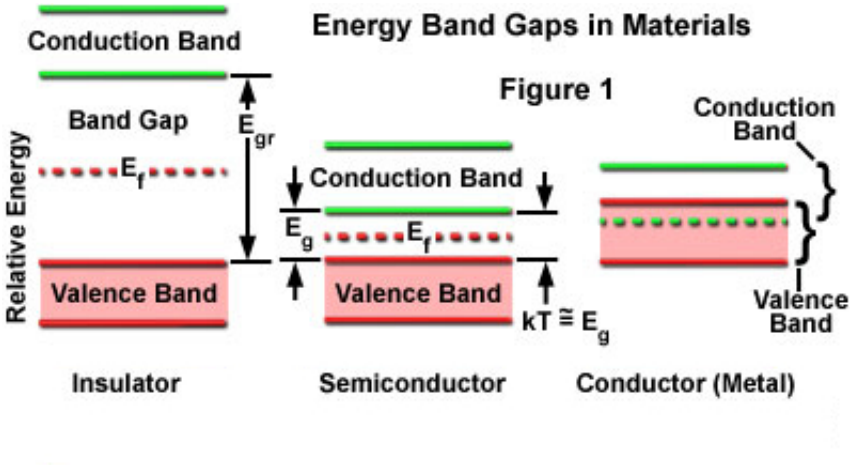

Figure 2.6.: Energy band structure of Insulator, semiconductor and conductor by [War]. In the vertical axis the energy is represented. E_f indicates the Fermi energy and E_g the energy gap.

The principal difference between an insulator, semiconductor or conductor is the "energy gap". In conductors the energy gap doesn't exist and at insulators it is huge. Normally the electrons are in the valence band. If an electric field is applied: in the case of an insulator electrons don't have sufficient energy to cross the gap. In the case of a conductor there isn't gap and thermally excited electrons jump into the conduction band. For semiconductors the energy gap will be approximately of $E_g \approx 1\,\text{eV}$ and a current is only possible if an electrical field is applied. Of course the energy gap depend on the temperature and the pressure.

The depletion depth

The depletion depth is created when two doped materials, p-type and n-type, are together. Two different concentrations of holes and electrons make an initial diffusion (see Figure 2.7). An electric field gradient across the junction will be created. Due to the electrical field there is a potential across the junction it is called the contact potential V_0, generally this potential is the order of $V_0 \approx 1V$.

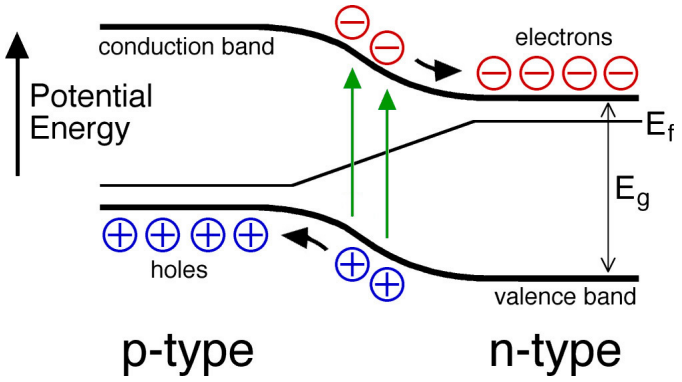

Figure 2.7.: Schematic diagram of a n-p junction, E_f is the Fermi energy, E_g is the energy gap. In the vertical axis the potential energy has been shown. The vertical arrows show the electrical field created by the contact potential. Figure extracted from [dep]

A calculation of the depletion zone is interesting because in the experimental particle detection a plane capacitor will be used. To calculate the depth and the charge density distribution $\rho(x)$ the Poisson equation can be used. [Leo94]

$$\frac{d^2V}{dx^2} = -\frac{\rho(x)}{\varepsilon} \tag{2.49}$$

A uniform charge distribution is necessary to consider. Denoted with x_n the depletion zone in the n-side and x_p the depletion zone on the p-side.

$$\rho(x) = \begin{cases} eN_D \leftrightarrow 0 < x < x_n \\ -eN_A \leftrightarrow -x_p < x < 0 \end{cases} \tag{2.50}$$

N_D and N_A are the "donor" and "acceptor" impurity concentrations. The total charge is conserved

$$N_A x_p = N_D x_n \tag{2.51}$$

Integrating and applying the boundary conditions the electric field $\overrightarrow{E}$ will be calculated as

$$\overrightarrow{E} = -\frac{dV(x)}{dx} = \begin{cases} -\frac{eN_D}{\varepsilon}(x - x_n) \Longleftrightarrow 0 < x < x_n \\ -\frac{eN_A}{\varepsilon}(x + x_p) \Longleftrightarrow -x_p < x < 0 \end{cases} \tag{2.52}$$

The solutions must join at $x = x_n \mapsto V(x_n) = V_0$ and $x = -x_p \mapsto V(-x_p) = 0$ and integrating leads to:

$$V_0 = \frac{e}{2\varepsilon}(N_D x_n^2 + N_A x_p^2) \tag{2.53}$$

Using 2.51 and 2.53,

$$x_n = \sqrt{\frac{2\varepsilon V_0}{eN_D(1 + N_D/N_A)}} \qquad x_p = \sqrt{\frac{2\varepsilon V_0}{eN_A(1 + N_A/N_D)}} \tag{2.54}$$

The depletion zone can be written as

$$d = x_n + x_p = \sqrt{\frac{2\varepsilon V_0}{e}\frac{(N_A + N_D)}{N_A N_D}}. \tag{2.55}$$

In praxis $N_A \gg N_D$ it is $x_n \gg x_p$ is assumed as

$$d \simeq x_n \simeq \sqrt{\frac{2\varepsilon V_0}{eN_D}}. \tag{2.56}$$

The conductivity of a n-type semiconductor is $\frac{1}{\rho_n} \simeq eN_D\mu_e$ using the conductivity in the expression 2.56:

$$d \simeq \sqrt{2\varepsilon\rho_n\mu_e V_0}. \tag{2.57}$$

In a detector setup an electric potential is applied into the detector, it means the depletion zone will be increased. The expression 2.57 will be replaced by

$$d \simeq \sqrt{2\varepsilon\rho_n\mu_e(V_0 + U_{apply})}. \tag{2.58}$$

Finally to obtain detector capacity the equation of a plane capacitor[3] $C = \varepsilon\frac{A}{d}$ will be used:

$$C = \varepsilon\frac{A}{\sqrt{2\varepsilon\rho_n\mu_e(V_0 + U_{apply})}}. \tag{2.59}$$

Dates of Silicon and germanium can be found on Table: 2.3. A typical value of V_0 for a high-resistivity n-type silicon at room temperature is $V_0 = 0.6\,\mathrm{V}$. Source: [Nus11]

[3] $\varepsilon = \varepsilon_0\varepsilon_r$

Properties	**Si**	**Ge**
Atomic number Z	14	32
Atomic Weight A	28.09	72.6
Atoms ($1/cm^3$)	5.0×10^{22}	4.42×10^{22}
Breakdown Field (V)	approx. 3×10^5	approx. 1×10^5
Crystal Structure	Diamond	Diamond
$N_A(1/cm^3)$	2.8×10^{19}	1.04×10^{19}
$N_D(1/cm^3)$	1.04×10^{19}	6.0×10^{18}
ρ (g/cm^3)	2.328	5.3267
ϵ_r	11.9	16.0
Electron Affinity (V)	4.05	4
E_g at 300K (eV)	1.12	0.66
$n_i(1/cm^3)$	1.45×10^{10}	2.4×10^{13}
Intrinsic Resistivity ($\Omega \cdot cm$)	2.3×10^5	47
Lattice Constant ($\AA$)	5.43095	5.64613
Melting Point (°C)	1415	937
μ_e ($cm^2 \cdot V^{-1} \cdot s^{-1}$), electrons	1500	3900
μ_p ($cm^2 \cdot V^{-1} \cdot s^{-1}$), holes	475	1900
Optical Phonon Energy (eV)	0.063	0.037
Specific Heat (J/g)	0.7	0.31
Thermal Conductivity at 300 K (W/cm)	1.5	0.6

Table 2.3.: Physical properties of silicon and germanium at 300 K. Information extracted from: [sil]

2.5.2. Silicon Surface Barrier detectors

The most typical detectors used to measure charged particles are the detectors SSB (Silicon Surface Barrier). These detectors consist of a semiconductor material n-type or p-type and a metal. The n-type are build with gold and the p-type with aluminium.
If a semiconductor and metal are together, the Fermi level will be changed and a depletion zone will be created. It is the same case of a pn junction, but now the junction is called *Schottky Barriers* (see Figure: 2.8). The same characteristic of a pn junction can be found, for this reason the depletion depth can be calculated using formula 2.58. The SSB detectors present many advantages, the first one is

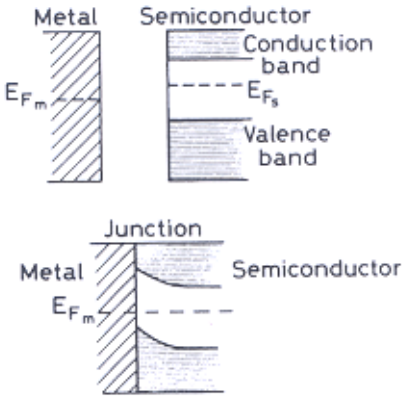

Figure 2.8.: Schematic diagram of a Schottky Barriers junction [Leo94]. In the first picture materials before the junction have been represented, E_{F_m} indicates the Fermi energy of the metal material and E_{F_s} the Fermi energy of the semiconductor, in this case they are different. In the second picture the junction has been realized and the consequently the conduction band and the valence band have been curved. In this case there is only one E_{F_m}.

this devices can be build by deposing a thin layer of gold with evaporation at room temperature. It is necessary to allow the surface to oxidize before deposition. The SSBs can be made with different thickness and regions. It is a perfect device to measure energy deposition of passing charged particles.
Disadvantages of the SSB are its high sensitivity to light. The thin gold covering is insufficient to stop the ambient light.

There are many possible configuration to build a SSB. In Figure 2.9 a SSB made for the company (EG & G ORTEC, Oak Ridge, TN) is shown.

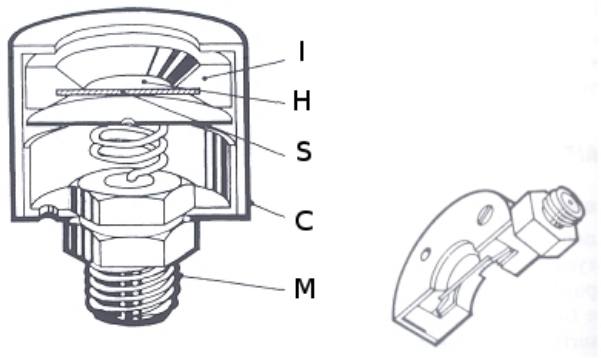

Figure 2.9.: Schematic diagram of a Schottky Barriers junction [Leo94].
(I) Insulating ring
(H) Metalized surface
(S) Silicon Wafer
(C) Metal case
(M) Connector

"Construction and mounting of silicon junction detector:
Surface barrier mount with a coaxial connector (M) at rear. The silicon wafer (S) is mounted in a ceramic ring (I) with electrical contact made between either side of the junction and opposite metalized surface of the ring. The front of surface is connected to the outer case (C) and grounded, whereas the back surface is connected to the center conductor of the coaxial connector".[4]

[4]Mounting description of a SSB by EG & G ORTEC, Oak Ridge, TM. [Kno89]

2.5.3. Solid angle correction

Solid angle correction is an experimental correction which has to be taken in this experimental setup due to the number of particles who the detector can detected is restricted by the geometrical configuration. Values of the solid angle Ω goes from 0 to 4π. For this reason the number of particle detected by the detector must to be corrected by 2.60:

$$\Omega_{\text{system}} = (\frac{4\pi}{\Omega}) \tag{2.60}$$

The equation 2.60 gives the value 1 or 100% when the detector can measure all particles emitted by the source. Besides, it gives the percent of particles that can arrived with a fixed geometrical configuration. The equations 2.60 is restricted for small values of the solid angle Ω and no angular distribution of radiation.

In the experimental exercise the program *Average Solid angle calculation* described in [R.W02] was used (see Figure 2.10). This program uses the Monte-Carlo-Simulation to obtain a value of the solid angle with a fixed geometrical configuration. For all air radon measurements of this master thesis the same experimental conditions were used. The optimal parameters of the measurement have been taken from [Nus11] and [Net94]. To calculate the value of the solid angle Ω_{system} first, it is necessary obtain the value of thickness and the diameter of the sample film. During the injection of the radon on the cold head a circular film is created. The thickness and the diameter of the sample film will be given by the optimal parameters of the injection. All parameters were studied, tested and assumed as optimal parameter in the works of [Nus11] and [Net94] and in the present master thesis these values were assumed.
Otherwise other measurements can be measured with other values. If other values of flow or injection distance between the injector and the cold head are used the value of the new source radius will change. In the present master thesis, the values presented by [Nus11] used to calculate the efficiency of the experimental setup have been used.

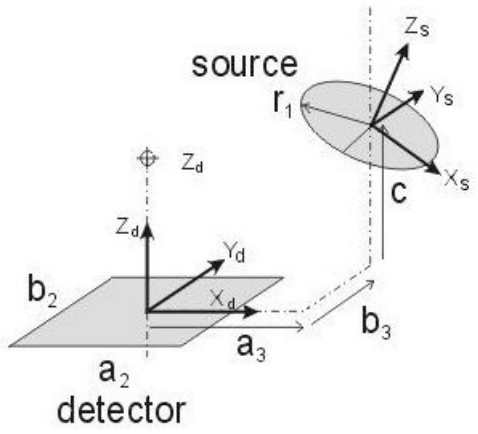

Figure 2.10.: Geometry parameters of the program *Average Solid angle calculation.* [R.W02] In the experimental setup the detector is quadratic and the source is a circular film. To make easier the geometrical calculation of the solid angle, the detector and the source have been built in the coaxial axis. It means that parameters a_3 and b_3 are zero

To obtain the experimental value used, the program *Average Solid angle calculation* will be running with the next parameters:

☑Circular source
☑Rectangular detector face
☑Source and detector coaxial
☐Source rotated or tilted
- Source Radius[5]=8 mm
- Detector length; $a2 = 24\,\text{mm}$
- Detector length; $b2 = 24\,\text{mm}$
- Elevation; $c = 4\,\text{mm}$

Finally the value obtained of the solid angle with the optimal parameters is:[6]

$$\Omega = (4.23 \pm 0.24)\,\text{Sr} \tag{2.61}$$

[5]This value is obtained by M. Nettebrock. [Net94]
[6]The work conditions are the same during the efficiency, basement, floor and background sample measurements.

2.5.4. Dead-time

In every detection setup a finite time between two independent events (particle detected) needs to be controlled. This time is denominated "dead time" and it is characteristic to the system. This time is normally too short and would be optimal if this time is zero. The dead time depends on the setup, it is: the electronic modules, cables, detector, etc. For this reason this time must be controlled to detect a problem during the measurement. In the experimental setup the dead time is showed by the program *Maestro* [Orta]. See Figure: 2.11

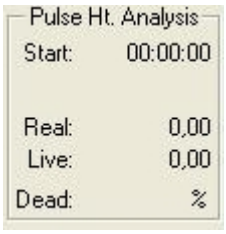

Figure 2.11.: Catch of the program *Maestro* with the times: t_{real}, t_{life}, $t_{dead}(\%)$. For more information see: [Orta]

The program shows values of the electronic dead time in percent and does automatically the calculation of the real and life times. The real time is the time between the measurement is started and finished. The time during events can be operated is considered as live time.

2.6. Global efficiency of a system

The efficiency of the radon air detection system is defined as the activity measured divided by the calculated activity:

$$\varepsilon_{\text{system}} = \frac{A_{\text{measurement}}}{A_{\text{calculated}}}. \tag{2.62}$$

The measured activity for ^{222}Rn is the area under the fit peaks divided by the measurement time "life-time" and corrected by the solid angle (see Section 2.60) and by the probability of the decay into the ground level of ^{222}Rn.

$$A_{\text{measurement}} = (\frac{\text{Area}_{^{222}Rn}}{t_{\text{life}}}) \cdot (\frac{4\pi}{\Omega}) \cdot (\frac{1}{P_\alpha}) \tag{2.63}$$

The calculated activity is obtained by the initial activity of the ^{222}Rn contained in the cylinder and corrected by the differential time.

$$A_{\text{calculated}} = A_{\text{air-sample}} e^{-\lambda_{Rn} t_{\text{diff}}} \tag{2.64}$$

The activity of the ^{222}Rn obtained by the calibrated source ^{226}Ra can be calculated by formula 2.14 with the initial activity of the radium source (see value 4.2), and corrected by the *emanation factor* (see value 4.3):

$$A_{\text{air-sample}} = A_{Ra,0}\left(\frac{\lambda_{Rn}}{\lambda_{Rn} - \lambda_{Ra}}\right)\left(e^{-\lambda_{Ra} t_{\text{enr}}} - e^{-\lambda_{Rn} t_{\text{enr}}}\right)\left(1 - \frac{A_{Rn}}{A_{Ra}}\right). \tag{2.65}$$

Where:
*$Area_{^{222}Rn}$ is the peak integral of the ^{222}Rn fitted with the program ROOT.
*t_{life} is the measurement time.
*$\Omega = (4.23 \pm 0.24)\,\text{sr}$ is the solid angle to every measurement, in our case it is the same for all efficiency measurements (see Value 2.61).
*$P_\alpha = 0.99992$ [7]
*$A_{Ra,0} = (2604 \pm 6\,\text{Bq})$ is the activity of the Radium source (see value 4.2).
*$\lambda_{Ra} = 1600\,\text{y}$
*$\lambda_{Rn} = 3.823\,\text{d}$
*t_{diff} is the time between the creation of a radon air sample and starting of measurement.
*t_{enr} is the enrichment time between two radon samples created by the calibrated source ^{226}Ra.
*$(1 - \frac{A_{Rn}}{A_{Ra}}) = (0.382 \pm 0.016)$ is the emanation factor (see value 4.3).

[7] ($^{222}_{86}Rn$ has two decays into $^{218}_{84}Po$): The first one in $^{218}_{84}Po(2+)$ (second excited state of the atom) with energy 4.986 MeV and probability 0.0785%, the second one in $^{218}_{84}Po(0+)$ (ground excited state of the atom) with energy 5.4897 MeV and probability 99.992%.

3. Experimental setup

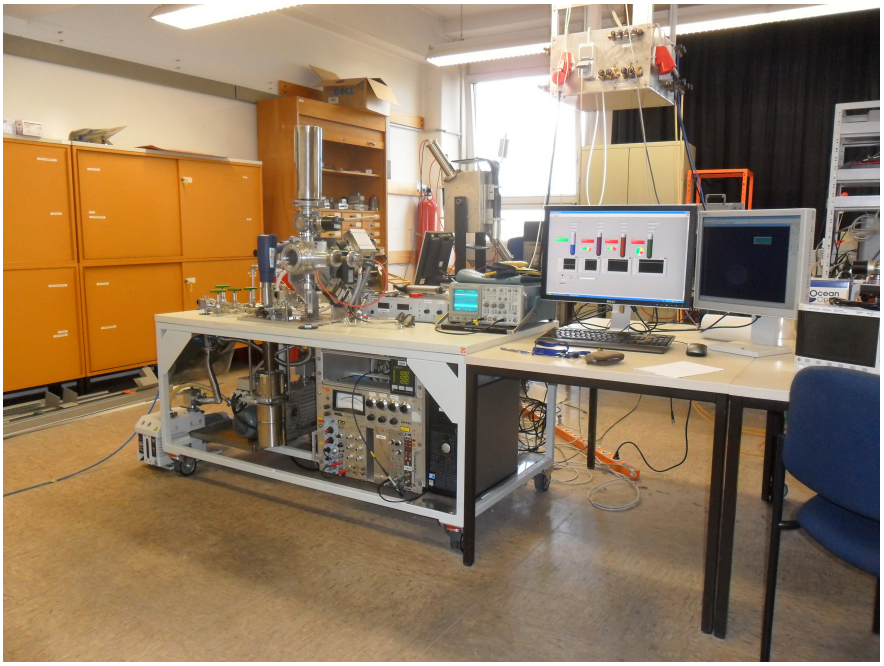

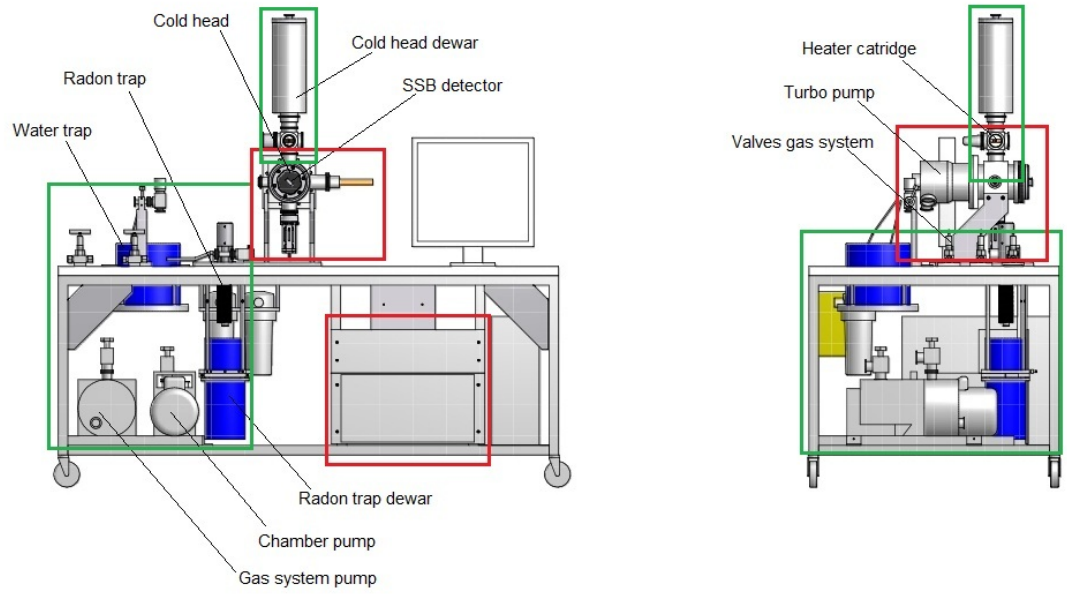

Figure 3.1.: CAD figure of the experimental setup drawn by D. Bonaventura. In the left figure a description of all parts of the setup can be observed. The cryogenic system composed by the water trap, the radon trap and the cold head is presented in a green box. The electronic system composed by the detection system and the temperature measurement system can be found in a red box.

During the next section the radon detection system will be presented. To explain the system, the setup will be divided in two parts: *The cryogenic system* and the *Electronic system*.

The first module is the *The cryogenic system*. This module has the finality to filter the radon element of the air sample concentration, freeze out the radon concentration and inject it on a cold surface creating a thin solid of radon film. The next module is the *Electronic system*, this module is composed by the detection system used to detect, amplify convert and register the alpha particles. The temperature measurement system is used to measure and controller the temperature in the cryogenic modules.

In operating order first, the water concentration is filtered of the air sample, this task will be realized by the water trap. The next step is to freeze the sample, it will be realized by the radon trap. This process will be done to finish with all gas kept in the sample bag. In this process radon element is deposited on the spiral freezing the radon. After, vacuum will be done to eliminate the rest of air. The frozen radon will

be sublimated and injected on a cold surface "cold head" using as carrier gas N_2. Created the radon solid sample with the injection parameters described in [Net94], the detector will be put under the sample and the measurement can be started.
To not change the geometrical parameter of the solid angle, the optimal parameter developed in [Net94] of: Flow during the injection, creation of the sample and preparation of the radon will be used.
Original electronic parameters have been used of [Nus11] but due to some modifications during this thesis the new optimal parameters will be described.

3.1. Cryogenic system

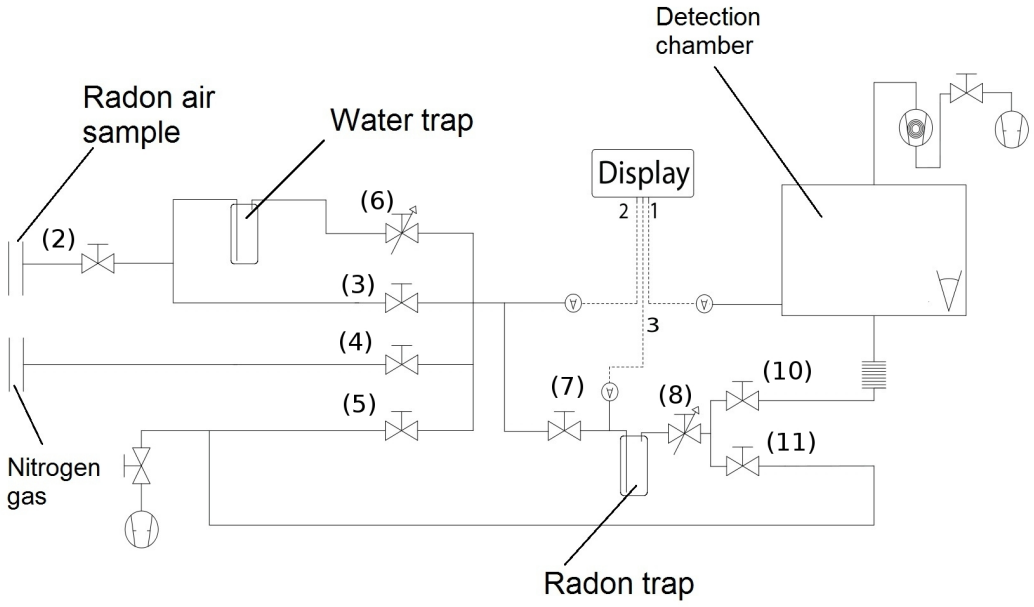

Figure 3.2.: Scheme of the last configuration of the radon detection system: In this picture, one can see the modules of the cryogenic system. In order are: water trap, radon trap and finally finishing in the detection chamber the cold head. The mix air bag is put in the input of the *Radon air sample* and the carrier gas N_2 is injected by the inputs of the *nitrogen gas*. The valves are indicated with (*Number*) and the vacuum detectors with *number*

In this section a description of the cryogenic modules as well as temperature evolution in every phase will be given. To extract the radon, the cryogenic system disposes two sub-phases. The first one is called "the water trap" whose function is eliminate the water component. The second one is the "radon trap". This device will contain all radon concentration freezing the sample and after sublimating the radon concentration. The last device is the "cold head", this devices is used to maintain the film sample during the measurement, this device doesn't work on the radon, only is used to maintain the sample solid during the measurement.
The actual scheme of the radon detection system is shown in the Figure 3.2. During the freezing of the radon, the optimal flow will be fixed in $< 2.5\,\mathrm{ml/s}$ [Net94], with this flow the sample bag with a capacity of 10 l will be empty in 2 h. The optimal flow will be reached opening the valve (6) in seven lines and the valve (8) in two lines. The flow during the injection will be 0.25 ml/s, it corresponds to 0.70 lines of the valve (8) and a pressure of the N_2 flask of 0.60 bar. With the optimal flow the sample created on the cold head will have a radius of $(8 \pm 2\,\mathrm{mm})$ [Nus11]. Considering the values of elevation and source radius the solid angle will be the value expressed in the formula 2.61.
Due to the flow was a point treated in the last work about this setup, during the next lines one will treat the evolution of the temperature in the cryogenic devices. For this reason devices will be explained from the temperature point of view. Evolution of the parts of the setup will be explained in the next sections as modification of the setup to solve instabilities.

3.1.1. Water trap

The water trap consists of a spiral tube where the gas mixture enters trough an external input surrounding an spiral and loses the water gas concentration. The input of the water trap starts in the external part of the spiral and goes to the central point. The design has been developed to filter the water component progressively in order to guarantee that in the center the temperature will be more stable.
To filter the water components of the gas mixture, the temperature control plays an important role. In this device the temperature must keep it between $-60\,^{\circ}\mathrm{C}$ and $-40\,^{\circ}\mathrm{C}$ [Nus11]. In any case a temperature below $-60\,^{\circ}\mathrm{C}$ must be achieved, because the boiling point of radon[1] is $-62\,^{\circ}\mathrm{C}$ at room pressure. A photo of the water trap is shown in Figure 3.3.

[1]Radon boiling point at room pressure, see appendix F

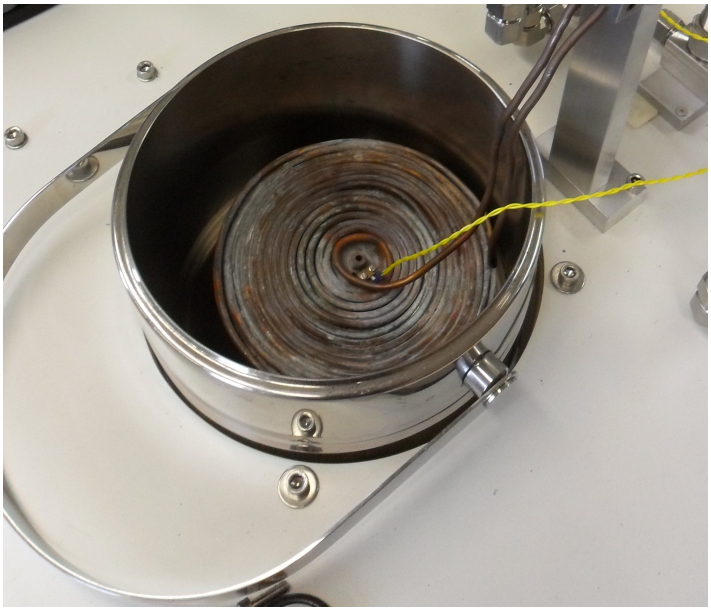

Figure 3.3.: Water trap spiral: The spiral is supported by a plate without contact with the liquid N_2, below the spiral the vessel is filled with liquid N_2. The cooling down of the spiral will be done by vapor of liquid N_2. The spiral dispose a thermometer PT100 placed in the central point to measure the temperature. The gas input is though the external part and in the central point of the spiral the gas output can be found.

To measure the temperature in this device a resistance thermometer *PT100* was used. The resistance was fixed at the support in the central point of the spiral. A current of 1 mA proportionated by a preamplification card of the temperature measure system will feed the resistor. The voltage between the resistor terminals is amplified by a factor 83.5, and afterwards a card *NI USB-6008/6009* will convert this value into a digital data .
To control the temperature in this device a new program *temp 2.5* has been developed (see Figure 3.6). A visual alarm has been implemented when the temperature is crossing the limit of $-60\,°C$ as well as a temperature monitor shows the temperature evolution in one minute. The program displays the temperature, voltage and resistance values of the *PT100* and includes the possibility to save all data. In Figure 3.4 temperature evolution of a measurement is shown. In this figure, one can see the instability when the cooling-down is starting. This process happens always and approximately two hours are required to reach a stable temperature. To maintain

the optimal temperature in order to avoid loss of radon concentration in the water trap, recharges of liquid N_2 are necessary every 6 minutes.

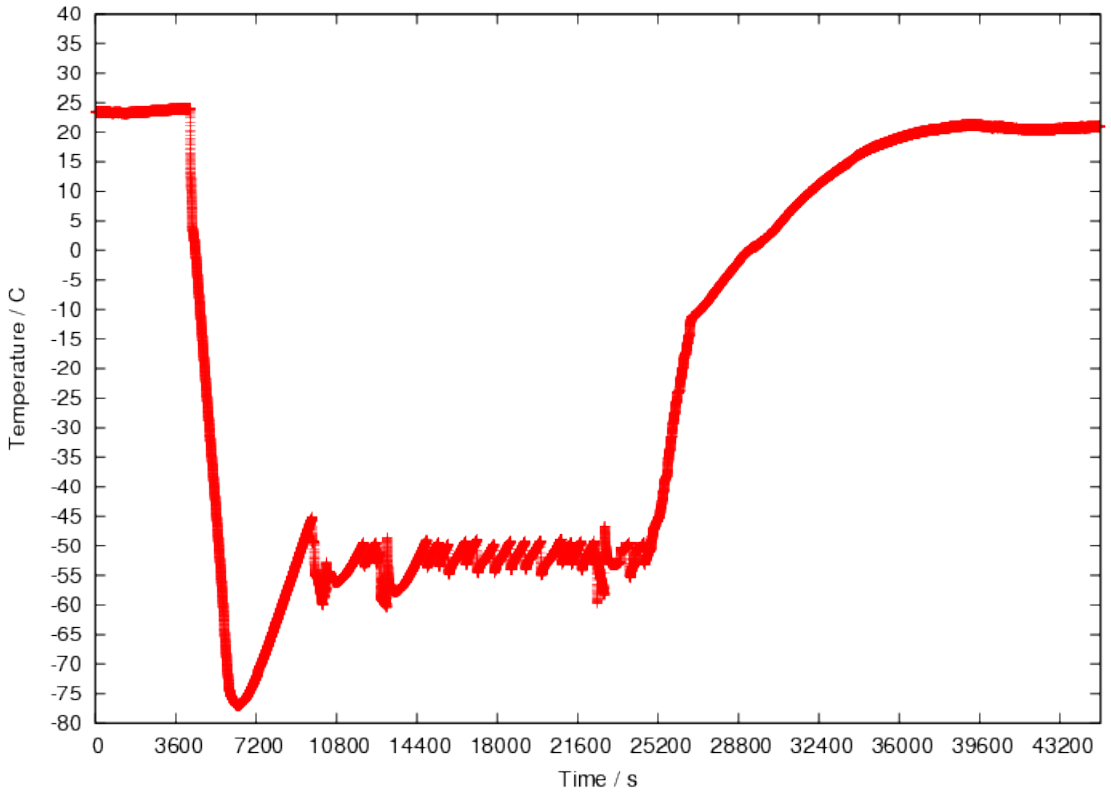

Figure 3.4.: Water trap temperature in an ordinary measurement. The time between the second 7000 s and the second 14000 s is for stabilization of the temperature in the spiral. The radon cooling down starts in the second 14400 s and finishes in the second 21600 s. The radon cooling down last two hours: (7200 s).

In Figure 3.5 a example of radon cooling-down is shown. In this case short recharges have been realized in order to avoid lost of radon.
The flow of the gas will be given by the precision valve after the spiral output *Valve (6)*. The optimal flow of the water trap was adjusted by [Net94] with 8.75 ml/s ("seven lines") in the water trap. Nonetheless the final flow of the whole system will be given by the valve after the radon trap *Valve (8)* these valve will be commented in the next section (see Figure 3.2).

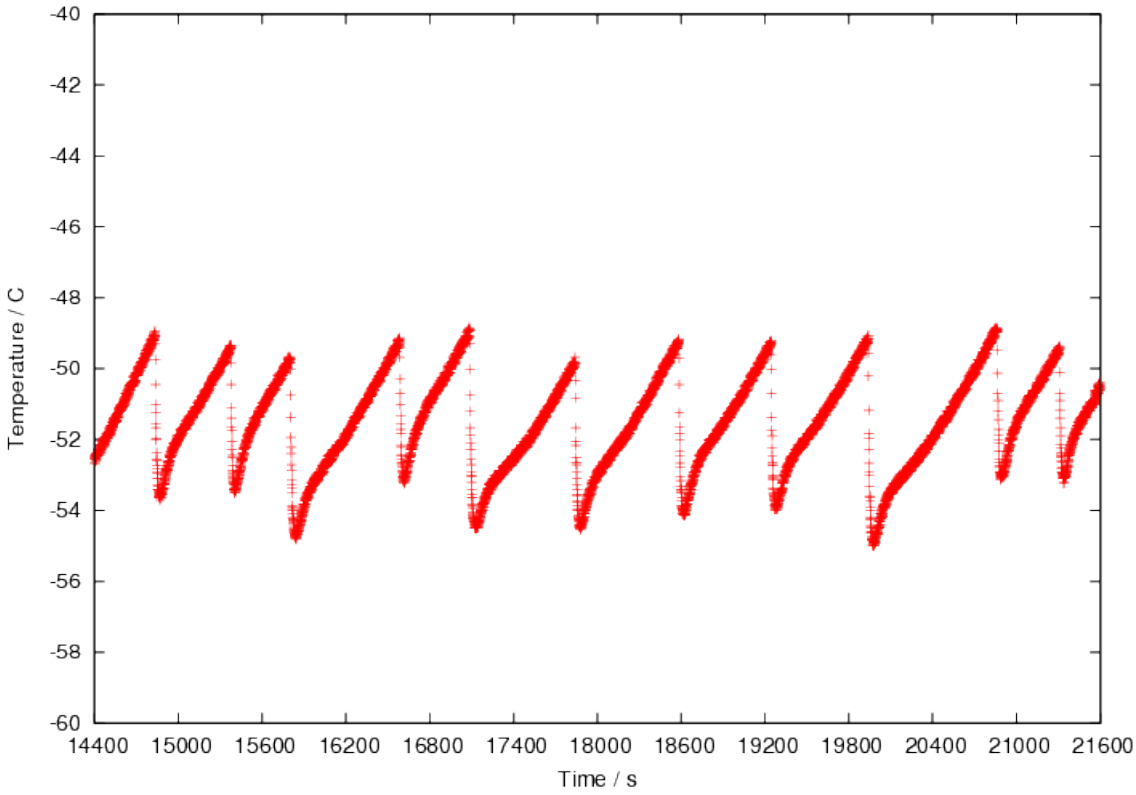

Figure 3.5.: Zoom of a liquid N_2 recharge. During the process of the cooling down, temperature in the water trap oscillates between the maximal and the minimal values permitted. A high number of short recahrges of liquid N_2 is advisable to maintain a stable temperature.

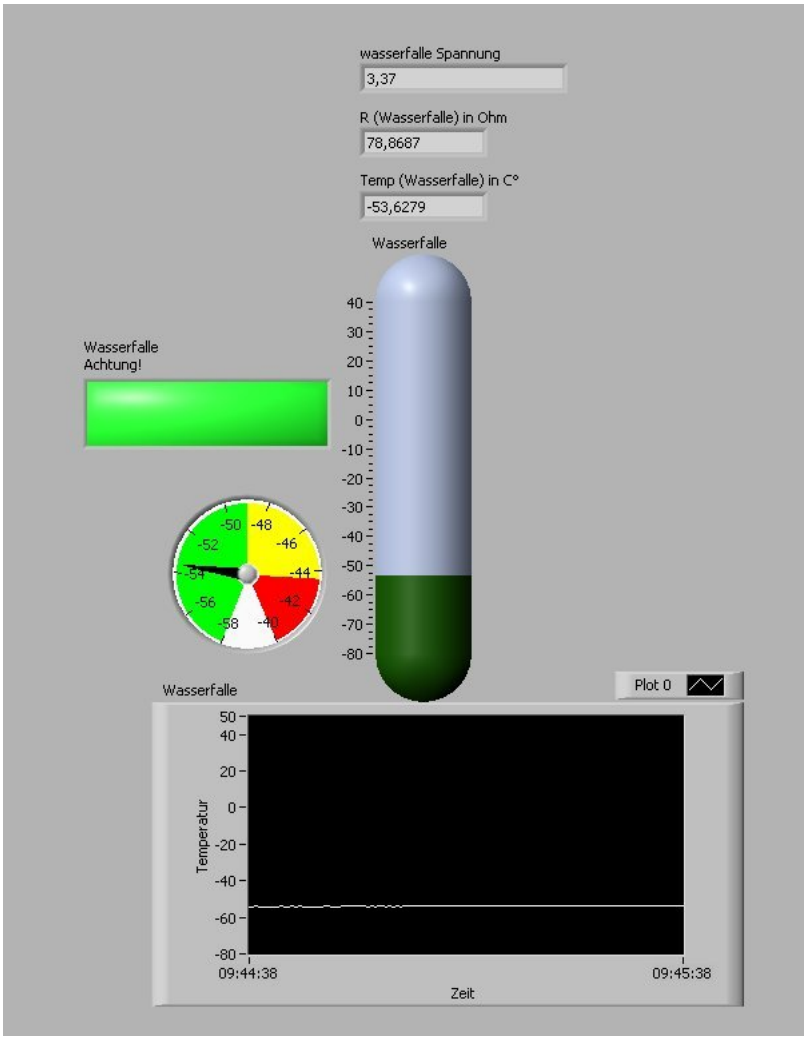

Figure 3.6.: Water trap temperature control. For the water trap, in the new program *temp 2.5* two graphic monitors have been implemented. The program dispose a red alarm when the temperature is not in the optimal range. The monitor shows the dynamic temperature in the range of one minute, the program shows the voltage, resistance and temperature values of the *PT100*.

3.1.2. Radon trap

The radon trap is the second active module of the cryogenic system. It consists of a long spiral tube submerged in liquid N_2 where the radon and other gas components will be liquefied (see Figure 3.7). To submerge the tube spiral a dewar vessel of the company *Thermos KGW Isotherm* mounted in a guide tube was used. The tube is coiled in a hollow cylinder connected with a heating system (see Figure 3.8). Using

a hot air gun in the input of the hollow cylinder the liquefied components in the radon trap will be evaporated before the injection.

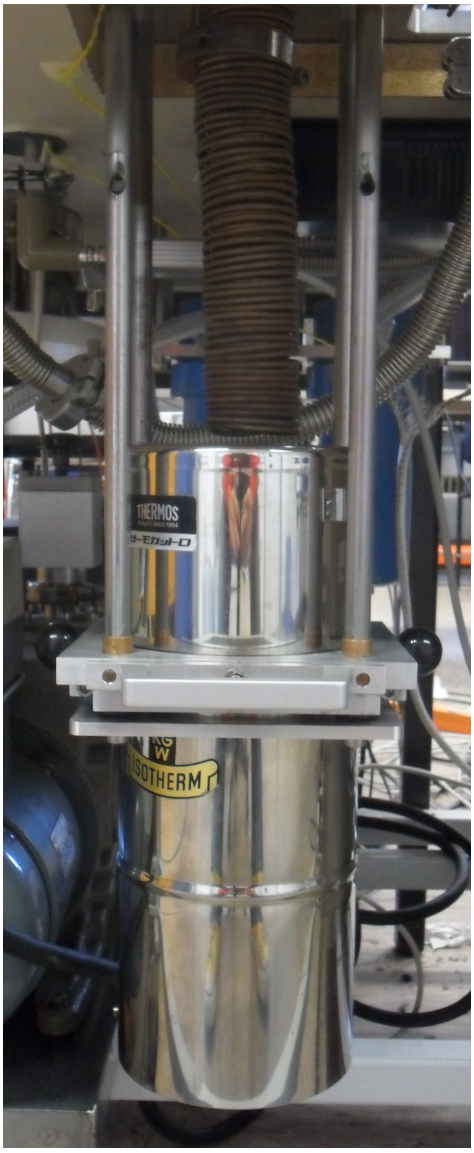

Figure 3.7.: Radon trap spiral: In the superior part of this photo the spiral can be observed. Connected with four guides the dewar vessel to contain the liquid N_2 can be found. To recharge the vessel first, it is necessary stop the flow, to go down the dewar vessel, to fill the container and to lift up the dewar vessel through the guide. During the filling, the spiral stays without cooling fluid, which means that temperature of the spiral will reach higher temperatures.

Figure 3.8.: Heat input for the spiral: Spiral of the radon trap is surrounding by a hollow cylinder, on the top of the cylinder a device to support a hot air gum has been developed. The hot air is injected on the central axis of the cylinder heating and reaching in around 10 min room temperature. Before the injection the gas will be sublimated using this configuration.

Due to the radon trap will be always submerged on the dewar vessel, all gas component with a boiling point below −160 °C will be liquefied. The working temperature of the radon trap will be the boiling point of the liquid N_2: −195.9 °C at room pressure [liq]. The reason why all gas components with boiling point below −160 °C will be liquefied is because during filling of liquid N_2 a temperature of −160 °C will be reached and gas elements with boiling point above −160 °C will be lost (see Figure 3.10), in any case the radon component remains in the radon trap because the local pressure will be 1000 mbar and in this case the boiling point of the radon will be −62 °C (see Appendix F).
In order to avoid radon losses, the optimal flow of 2.5 ml/s was fixed by [Net94]. The optimal flow fixes the pressure in the gas system close to 1000 mbar during the radon cooling down. In this case the boiling point of radon will be around −62 °C, it assures that radon will remain in the radon trap even if a liquid N_2 filling will be

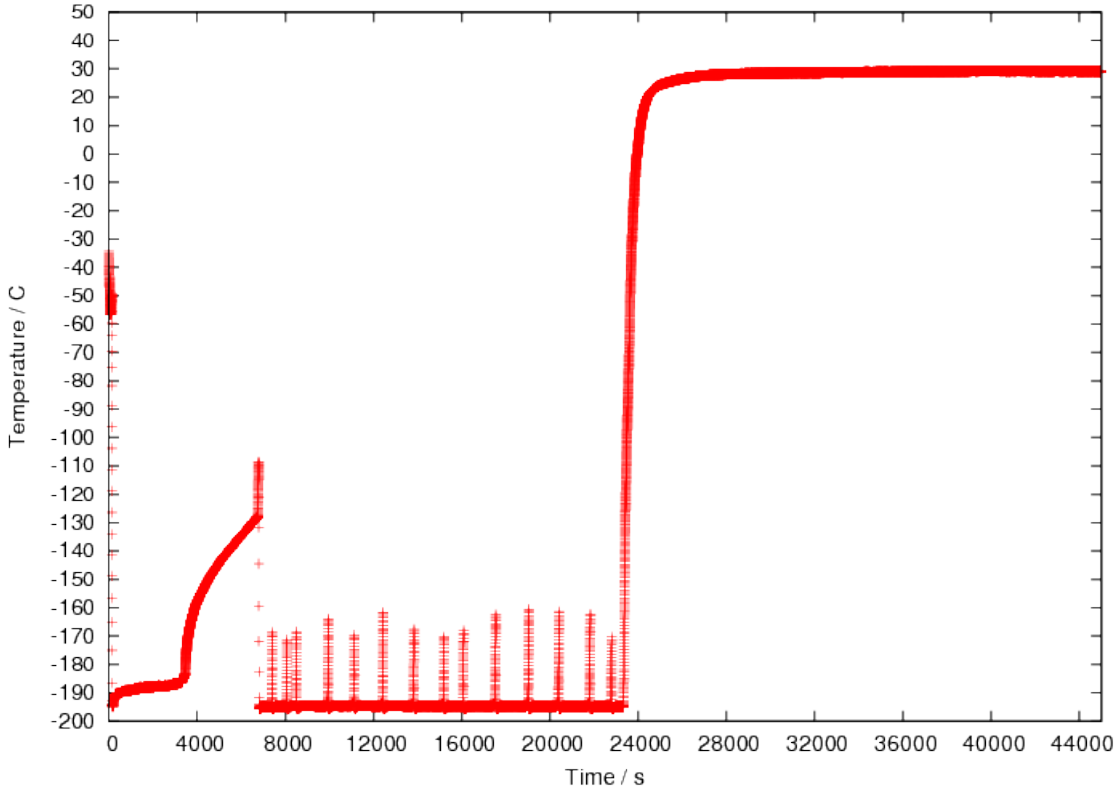

Figure 3.9.: Radon trap temperature in an ordinary measurement. The first 8000 s are to stabilize the temperature in the radon trap. The cooling down process start in the second 14400 s and last to the second 21600 s. The injection of the radon in the cold head is realized after the second 24300 s when the room temperature has been reached.

done.

With the optimal flow, the cooling time is approximately two hours, considering that the sample bag is full filled with the radon gas test. The temperature evolution of the radon trap in a measurement has been shown in Figure 3.9. The cooling down process of the radon sample after 14400 s has been started. Every peak shows the filling of liquid N_2, the working time in a filling must be in the minimal time as possible in order to avoid radon losses (also see Figure 3.10).

The temperature evolution of heating up the radon trap has been shown in Figure 3.11. In this process the radon trap is heated to the room temperature using the hot air gun.

To measure the temperature in the radon trap a resistance thermometer *PT100* has

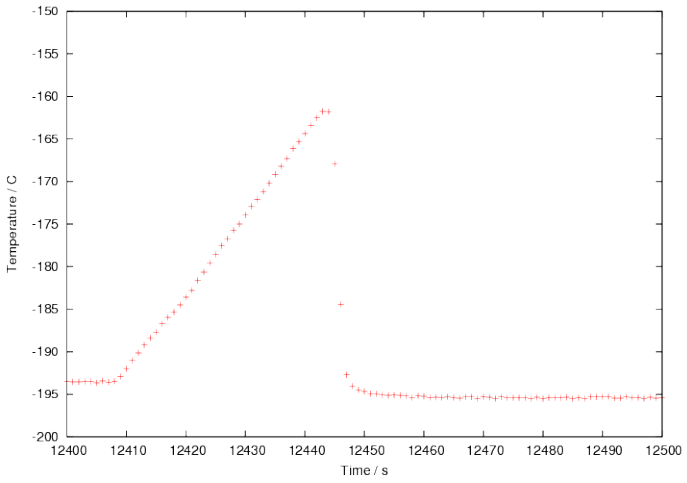

Figure 3.10.: Zoom of a liquid N_2 recharge in the radon trap. In this example a liquid N_2 recharge has been done in 40 s. During the filling, the radon trap stays without liquid N_2 and temperature is increased. A filling in the minimal time as possible is recommended.

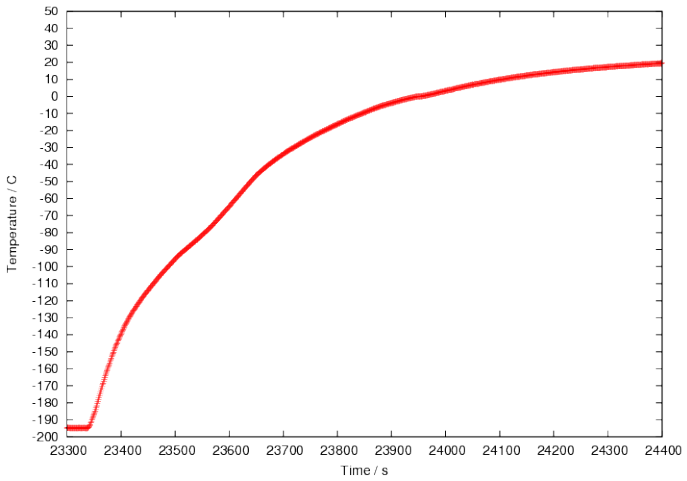

Figure 3.11.: Zoom of the heating up. Before the injection, radon in the radon trap must be heated to reach room temperature. To heat up the radon, the hot air gun will be used. This device introduces hot air in the central axis of the container cylinder of the radon trap.

been used. As well as in the last module, electronic to control this devices was the same as in the water trap used.

3.1.3. Cold head

The cold head is the third and passive cryogenic system. It consists of a metal surface connected with a cryogenic system. The cryogenic system is a vessel full filled with liquid N_2 and sealed. To decrease the pressure of the liquid nitrogen, vacuum on top of the vessel can be done. In this case the low pressure of the liquid N_2 maintain the temperature of the cold head under $-200\,^{\circ}\mathrm{C}$ (see Figure F.2).

Figure 3.12.: Cold head: The cold head is a metal surface where a solid film of radon will be created. To cooling down this surface a cryogenic dewar flask is connected through a stem. The dewar flask is sealed and on top of the flask there is a gas output to decrease the pressure in the vessel. This setup is used to decreases the pressure in the dewar flask and to maintain a constant temperature in the cold head. The cold head is placed in the detection chamber and is used to create the solid sample injecting on the cold surface and to maintain the sample. Between the cold surface and the dewar flask a heater cartridge has been placed. This heater device disposes a PT100 thermometer included to monitor the temperature during the heating up. On the other side, the cold head disposes a PT100 to monitor the temperature on the metal surface.

Figure 3.13.: Measurement configuration: In this photo the measure position can be observed. Created the radon sample on the cold head temperature must be maintained during the measurement at −204 °C. Finished the injection, the injector must be displaced to the position 0 mm. The injection process remains around 6 min, after the injection detector can be placed under the cold head to start the measurement.

In Figure 3.12 a photo of the cold head can be observed as well as in Figure 3.13 the measure configuration using the detector in the chamber can be also found.
The cold head temperature will be measured by a resistance thermometer *PT100* fixed on the surface. In the connector cylinder between the cold head and the cryogenic vessel there is a cartridge heater and a *PT100* integrated. The heater cartridge has a double task, the first one is to monitoring the temperature between the cold

head and the cold head dewar, and the second one will be heat up the cool head when the measurement will finish. The maximal power of the cartridge heater is 150 W but due to overheating working with a maximal power of 120 W has been determined. A new modification respect to the last setup was the amplification factor used in the heater cartridge. In this case the factor was changed from 83.5 to 46.2 because during the heating up of the cold head 50 °C was the maximal monitored temperature.
The temperature of the cool head did not show any instabilities. A required temperature must be −204 °C before the radon injection. An example of the temperature of the cold head during a radon measurement can be found in Figure 3.14.

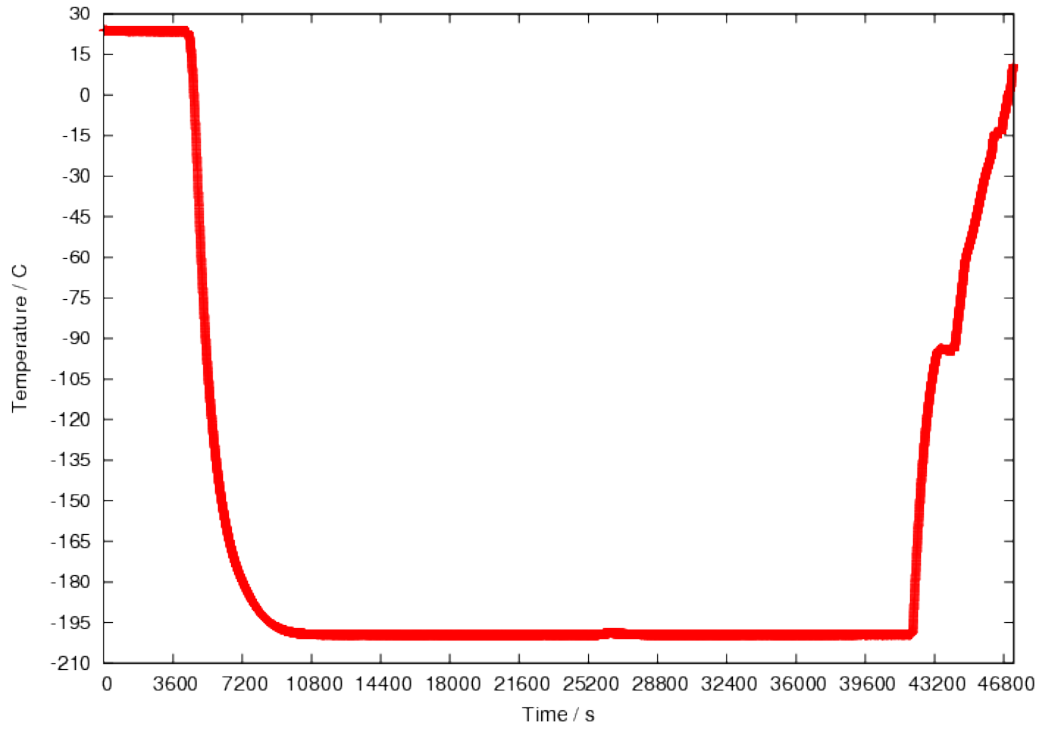

Figure 3.14.: Working temperature curve of the cold head. In this plot the temperature during a radon measurement has been shown. The temperature on the cold head does not present problems of instabilities because the flask is filled with liquid N_2 and sealed. To reach the injection temperature it must be waited for approximately 2 h (second 10800). The heater cartridge will be used to reach the room temperature when the measurement will be finished. It would be advisable not to work with the maximal power of the heater cartridge 150 W (values in the power source below 3 A and 50 V). Reaching a temperature of −90 °C in the cold head, it will be necessary decrease the power in the heater cartridge due to overheating, it can be observed in the second 43200.

3.2. Electronic system

3.2.1. Detection system

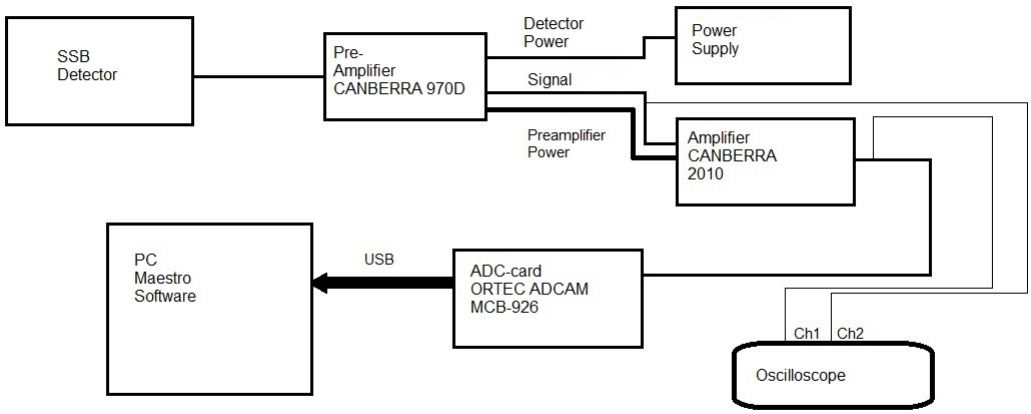

Figure 3.15.: Detection scheme used in the experimental setup. The configuration for α-detection was obtained in [Nus11]. The system is composed by a SSB detector, a preamplifier, amplifier and gauss pulse converter, a ADC card and finally the impulse is registered by a computer using the program *Maestro*®. In this case an analogical oscilloscope has been introduced to monitoring the pulse and control the electric noise. Two inputs of the oscilloscope has been connected parallel to the amplifier before and after the pulse amplification.

The detection system has the finality to register the α-particle. Figure 3.15 shows the scheme of the particle detection module in the radon detection system. At this setup a SSB detector followed by a preamplifier and an amplifier system of the company *Canberra* were used. The silicon detector is feed by a power supply with high current sensibility. The connection cable between the detector and the preamplifier has an impedance of $(75 \pm 3)\,\Omega$. The connection cable between preamplifier and amplifier is a standard cable with impedance $50\,\Omega$. To convert the analogical signal to a digital pulse a *ADC card of the company ORTEC model 926* with output USB connected at the output of the amplifier was employed.
To count the pulses and save all dates the program *Maestro*® in a computer running under windows operation system has been used. To study the analogical signal a analogical oscilloscope was used.

The detector

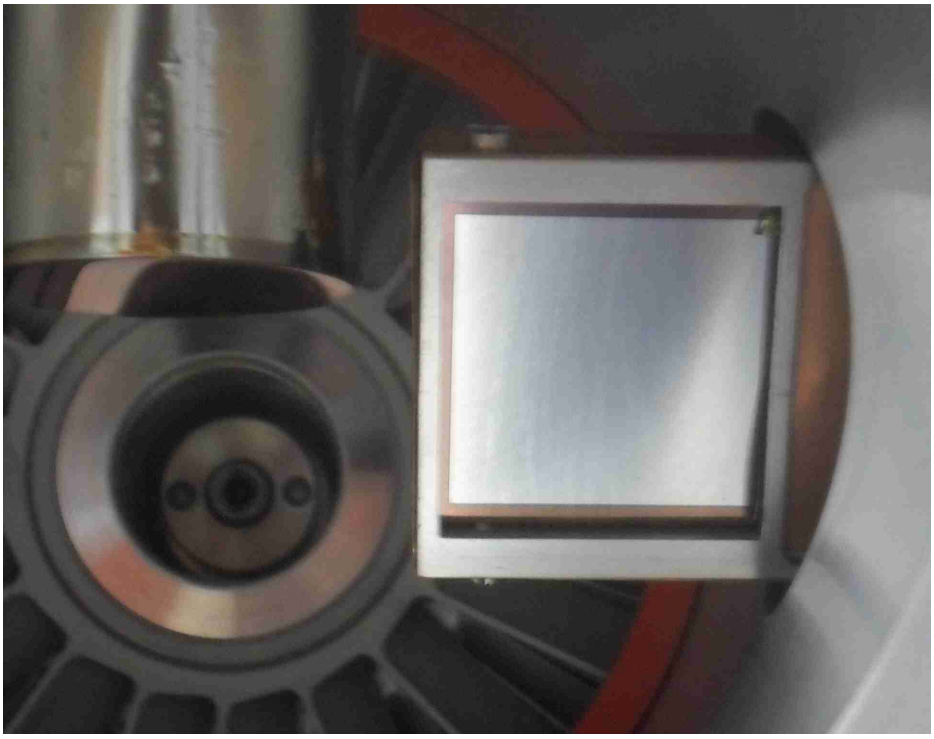

Figure 3.16.: SSB (Silicon Surface barrier) detector of the company *Schlumberger*. The detector is settled under the cold head to do a measurement. Detector is mounted in a driver guide able to turn by 180 ° and displace horizontally. In this picture one can see the detector during the changing of place, the detector has a surface of 576 mm^2 (24 mm × 24 mm).

The detector used in the setup is a silicon detector type SSB (Silicon Surface Barrier) of the company *Schlumberger* (see Figure 3.16), built through ion implantation [Nus11] and [Net94]. All technical dates of this detector can be found in Table 3.1.

The detector was mounted in a mobile support, able to turn by 180 °. There are two different possible positions, to measure the sample on the cold head and to measure using the measure table. The working voltage of the detector is 65 V and the current observed is 250 nA. The capacitance of the detector using formula 2.59 can be calculated, in this case considering a silicon detector SSB and properties of the silicon (see table 2.3), the detector has: $\varepsilon_r = 11.9$, $d = 250\,\mu$m, $A = 250\,\text{mm}^2$ the theoretical capacitance has been calculated and resulted $C = 245\,\text{pF}$.

Properties	**Detector**
Company	Schlumberger
Type	IPE $24 \times 24 - 100 - 35$
Surface	$576\,\mathrm{mm}^2$ ($24\,\mathrm{mm} \times 24\,\mathrm{mm}$)
Active deep (μm)	$200 - 300$
Working voltage (V)	$60 - 70$
Working current (nA)	$100 - 200$
FWHM	30 keV maximal to 5 MeV paticles

Table 3.1.: Technical dates of the SSB detector. Source: [Nus11]

Preamplifier

The preamplifier phase was developed with the preamplifier *Canberra* model 970*D* (see Figure 3.17).

Canberra 970*D* is a preamplifier designed to Silicon Surface Barrier Detectors at room temperature. The resolution depends on the detector capacity (see Table 3.2). The degradation resolution due to additional capacitance is less than 12 (eV/pF). A scheme of the *Canberra* 970*D* can be found in Section E.1 as well as properties[2] about this preamplifier can be found in Table 3.3.

Detector capacitance (pF)	Noise FWHM (keV) Silicon	Rise time (ns)	Typical slopes (eV/pF)
0	2.5	8	12
100	3.7	10	12
200	5.5	13	18
300	7.5	16	20
400	9.5	18	20
500	11.0	20	20

Table 3.2.: Noise due to additional capacitance for detector connection [Ind].

[2] All information obtained by [Ind]

Figure 3.17.: Picture of the preamplifier Canberra 970D: Photo obtained of the instruction manual [Ind]. The preamplifier disposes two inputs *HV* (high Voltage) and *Test* (to introduce a simulated signal). The output are *Timing* and *Energy*. The detector is fed by the power supply through the preamplifier.

Properties	**Preamplifier**
Company	Canberra
Type	$970D$
Detection Input	Pulse from detector
Test input	$100\,\mathrm{mV/MeV}$ input impedance $93\,\Omega$
Power supply	$+12\,\mathrm{V}$ at $40\,\mathrm{mA}$, $-12\,\mathrm{V}$ at $15\,\mathrm{mA}$
HV input in DC (V)	$0-3000$
nonlinearity	0.05% for $0-5\,\mathrm{V}$
Charge sensitivity (mV/MeV)	20

Table 3.3.: Technical description of the preamplifier Canberra 970D. Information obtained from the instruction manual: [Ind]

Amplifier

To register a count the first step is a preamplification. The second step will be the conversion of this pulse into a Gaussian pulse. For this task the module *Canberra 2010 Spectroscopy Amplifier* was needed (see Figure 3.18).

Figure 3.18.: Amplifier Canberra 2010: The amplifier is used to amplify and convert into a Gaussian pulse the original signal. The amplifier disposes an amplification from $\times 10$ to $\times 3000$. The Pole zero can be adjust, as well as the Gaussian shaped using time constants of 0.25, 1, 2, 4, 8 or 12 μs. The input accepts positive or negative linear pulses with amplitude 0 V to ± 12 V. Disposes an unipolar output with delayed 2 μs and ± 10 V full scale linear output, and a bipolar output with a double differentiated linear output and $+10$ V full scale linear output.

The optimal configuration for α-spectroscopy measurements using the module *Canberra 2010 Spectroscopy Amplifier* can be found in Table 3.4.

Properties	**Value**
Coarse gain	$X100$
Fine gain	$X5.00$
Pole zero	configured
Shaping	$X1$
Unipolar restorer mode	off
Unipolar output restorer rate	Low
Restorer threshold	$100MV$
Input polarity	Negative
Unipolar output DC level	Negative
Unipolar output polarity	Positive
Signal input	Preamplifier cable
Unipolar output	ADC card cable
Bipolar output	non-use
93Ω unipolar output (back)	non-use
93Ω bipolar output (back)	non-use
Signal input (back)	non-use
Restore busy (back)	non-use
Preamplifier power	Preamplifier cable

Table 3.4.: Optimal value configuration. Module *Canberra 2010 Spectroscopy Amplifier*

More details about the *Canberra 2010 Spectroscopy Amplifier* controls can be found in appendix E.2 and E.3.

ADC-card with adaptor DPM-USB

The last step of the pulse converting is carried out with the module *ORTEC model 926 ADCAM multichannel Buffer*.

Figure 3.19.: Module *ORTEC model 926 ADCAM multichannel Buffer*: In this picture the front panel and the rear panel of the module Ortec 926 has been shown. In the front panel the manual controls of Zero and LLD can be observed, also the ground voltage is possible to adjust. In the rear panel the inputs *Gate*, *PUR*, and *Busy* can be found. The data outputs are the *Parallel port*, it is a standard IBM PC printer port and the *Dual-port memory*, it is an optional 37-pin connector provides the PC with a communication link and direct access to the Model 926's internal data memory. [Ortb]

The module *ORTEC model 926 ADCAM multichannel Buffer* is a multichannel buffer with an integrated microprocessor designed to data acquisition in nuclear spectroscopy. The module has a resolution of 8192 channels, a data memory of $2^{31} - 1$ counts per channel and a dead time per event of $8\,\mu$s. The module disposes a microprocessor *Intel 80C188* Dual-Port RAM with battery backup.
The screwdriver Zero and LLD can be also configured, in this case for α-spectroscopy both of them were configured with optimal values to eliminate the background at low channels.
Detailed information about the input/output of this card will be shown on Table 3.5

Properties/indicator	**Value/information**
CPU busy	indicate the activity of the microprocessor
ADC busy	every flash is a pulse digitalized
Screwdriver Zero	range $\pm 250\,$mV (configured for maestro)
Screwdriver LLD	range $0 - 10\,\%$ (configured for maestro)
ADC input	Positive unipolar signal, range $0 - 10\,$V in dynamic range semi-Gaussian-shaped two connectors on front and rear panels.
Gate input (front)	non-use
Gate input (back)	non-use
PUR (back)	non-use
BUSY (back)	non-use
Dual-Port Memory (back)	using adaptor DPM-USB
Printer (back)	non-use
Parallel port (back)	non-use

Table 3.5.: Technical information of module *ORTEC model 926 ADCAM multichannel Buffer*. The optimal values of the *screwdriver Zero* and *screwdriver LLD* have been configured for the program *Maestro* . Source:[Ortb]

Power supply

The power supply used to feed the detector is a *ORTEC model 210*.

Figure 3.20.: Power supply ORTEC 210: The front panel dispose all control of the power supply. The Voltage range go from $0-1000\,\mathrm{V}$ disposed in four channels, the amplification factor is manual controlled with the *Meter*. The ammeter can be used in only in one channel, scaled in μA, also the power supply dispose the possibility to invert the current *Polarity* in positive or negative.

The power supply disposes 4 voltage outputs from $0\,\mathrm{V}$ to $1000\,\mathrm{V}$ (configure the *Meter* in $\times 1$ or $\times 10$), a high sensibility ammeter with a scale from $0-3\,\mu\mathrm{A}$ and the possibility to invert the current. Due to the high sensibility of the detector the output number 3 was used.

3.2.2. Temperature measurement system

Temperature measure system is the second module of the electronic system. This part of the system will be used to detect, amplify, convert and register the temperature signal in every cryogenic device (see Figure 3.21). The temperature measurement system dispose four resistance thermometers PT100, one in every cryo-module. Temperature will be measure using these devices because they are linear in a high operation range. The amplifier card impose a constant current in every unit, the voltage will be the output data consequence of variation of the resistance due to changes in the temperature. The measured voltage will be amplified by an amplifier card developed in the workshop of the electronic nuclear physics. After the amplified voltage will be converted into a digital signal with the ADC card *National Instrument USB-6009*, finally data is processed with a new program developed in this master thesis *Temp V2.5*.

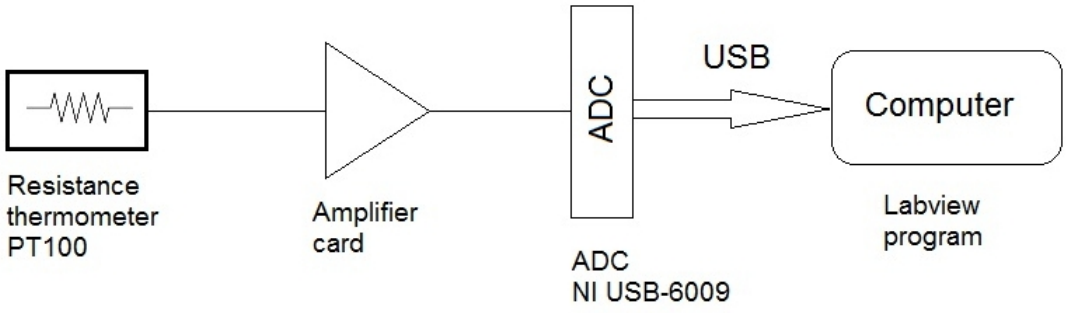

Figure 3.21.: Scheme of the temperature measure system: A constant current of 1 mA is imposed in every resistor PT100, the measure variable will be the voltage supported by variations of the voltage due to changes in the resistance. The voltage will be amplified in a factor depending on the resistor. The voltage will be converted with a ADC *National Instrument* USB-6009 module. The final data will be analyzed with the software *Temp V2.5* and registered as temperature data.

Resistance thermometer PT100

The resistance thermometer PT100 are the most standard devices used to measure temperature. These devices obey the European Norm EN 60751 (IEC 751 in Germany). The norm EN 60751 establishes that in every temperature range the resistance will be given by:
→ Temperature range between −200 °C and 0 °C:

$$R(T) = R_0(1 + AT + BT^2 + C(T - 100°C)T^3). \tag{3.1}$$

→ Temperature range between 0 °C and 850 °C:

$$R(T) = R_0(1 + AT + BT^2). \tag{3.2}$$

Where T is in °C, R in Ω, and the coefficients will be given by:
$A = 3.9083 \times 10^{-3°}C^{-1}$
$B = -5.775 \times 10^{-7°}C^{-2}$
$C = -4.183 \times 10^{-12°}C^{-3}$

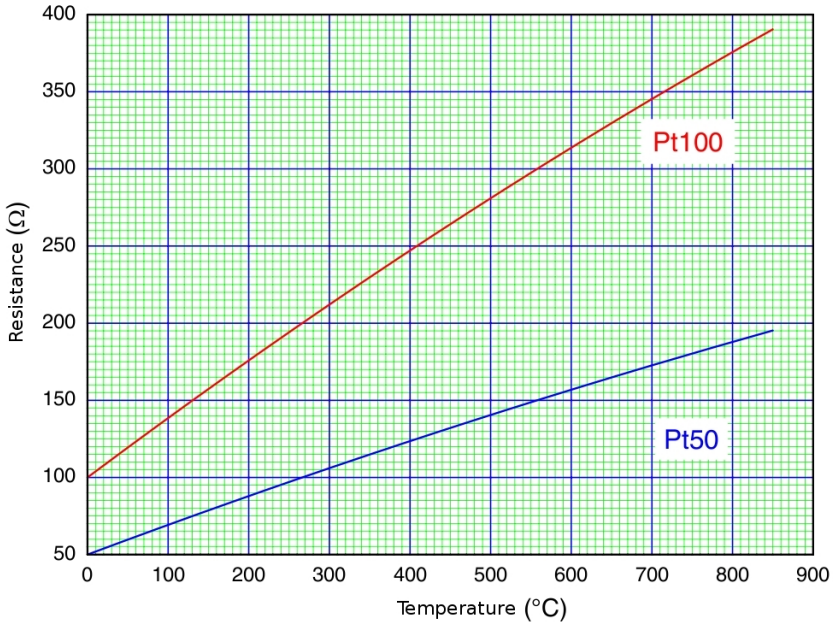

Figure 3.22.: PT100 and PT50 temperature diagrams:
The red line correspond to a PT100 resistor and the blue line to a PT50 resistor. Source [nIDE]

The evolution of the resistance with the temperature can be observed in Figure 3.22. In the practical exercise the equations used to calculate the temperature are the inverse functions of the equation 3.1 and 3.2, they are:

$$T(R) = \frac{-0.39083 + \sqrt{(0.152748089) + 0.000231(100 - R)}}{-0.0001155} \Longleftrightarrow T > 0° \quad (3.3)$$

$$T(R) = -5.67 \cdot 10^{-6} R^3 + 0.0024984 R^2 + 2.22764 R - 242.078 \Longleftrightarrow T < 0° \quad (3.4)$$

Amplifier and ADC NI cards

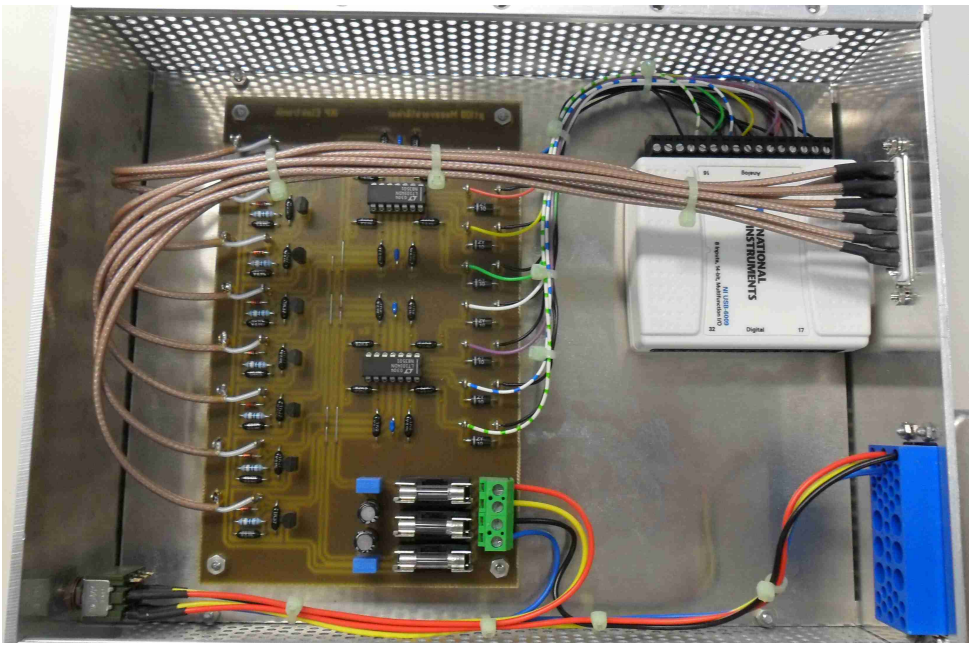

Figure 3.23.: Temperature module: To the left part, the amplifier card developed in the electronic workshop can be observed. Every pair of cables are from a thermometer, there are 8 inputs (black and white cables). To the right part of the card there are the amplifier voltage outputs (color cables). The amplifier voltage is converted with the module *National Instrument USB-6009* (white box).

The temperature module can be observed in the Figure 3.23. This module was developed in the workshop of the electronic physics. The preamplifier card dispose 8 voltage inputs, every input impose a DC current of 1 mA to feed the thermometer resistors. The outputs of the preamplifier card and the inputs in the *National Instrument USB-6009* card are showed in Table 3.6. In the actual setup only 4 thermometers are doing used, in every case the preamplifier card dispose a different value of amplification, it can be observed in Table 3.7. In the original setup all resistor had the same amplifier factor, but during this master thesis due to improvements in the temperature system new values have been modified (see Section 5.3.2).
The amplifier voltage is converted into a digital signal with the ADC card *National Instrument USB-6009*. This card dispose a maximal input signal of +10 V connected in mode RSE and using *floating signal source* (see Figure 3.24).

After the modification a new calibration of all resistor was necessary. To realize it, a variable resistor was placed in the place of every PT100. First the variable resistor was configured with a know resistance, afterwards the data with the acquisition program was measured, finally the new calibration have been obtained in:

Heater cartridge:
$R(V) = 207.023 - 21.0963V$
Cold head:
$R(V) = 120.319 - 12.1117V$
Radon trap:
$R(V) = 116.064 - 11.9896V$
Water trap:
$R(V) = 119.279 - 11.985V$
The last equations have been implemented in the program *Temp V 2.5*, where resistance is calculated in Ω and the voltage is introduced in V

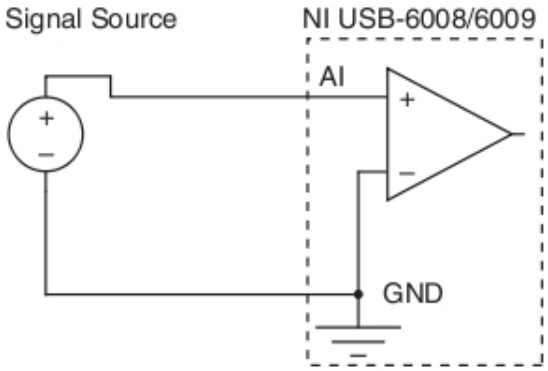

Figure 3.24.: Configuration mode used in the experimental setup: The photo was obtained by [ni]. This connection correspond the mode RSE with floating signal source. It means the resistors and the ground of the card is connected into the same ground of the amplifier card and with the NIM crate.

channel	Sub-D 25pol	Thermometer	NI card
1	1	Ground	GND
1	2	Heater cartridge	AI 0
	3	non-use	AI 4
2	4	Ground	GND
2	5	Cold head	AI 1
	6	non-use	AI 5
3	7	Ground	GND
3	8	Radon trap	AI 2
	9	non-use	AI 6
4	10	Ground	GND
4	11	Water trap	AI 3
	12	non-use	AI 7
	13	Ground	GND
	14	non-use	AO 0
	15	non-use	AO 1
	16	non-use	GND

Table 3.6.: Configuration table of the thermometer resistors: Every channel gives the pair of cable correspond to one thermometer, the sub-D 25pol indicates the input for the ADC card *National Instrument USB-6009*, every thermometer has been placed in a AI (Analogic input).

Cryo-device	**Value**
Water trap	×83.5
Radon trap	×83.5
Cold head	×83.5
heater cartridge	×46.2

Table 3.7.: Amplification factor used in the amplifier temperature card: In the original setup all resistor had the same amplification factor. Now the amplification factor in the heater cartridge has been changed to monitoring the temperature in a high range.

Temperature version 2.5

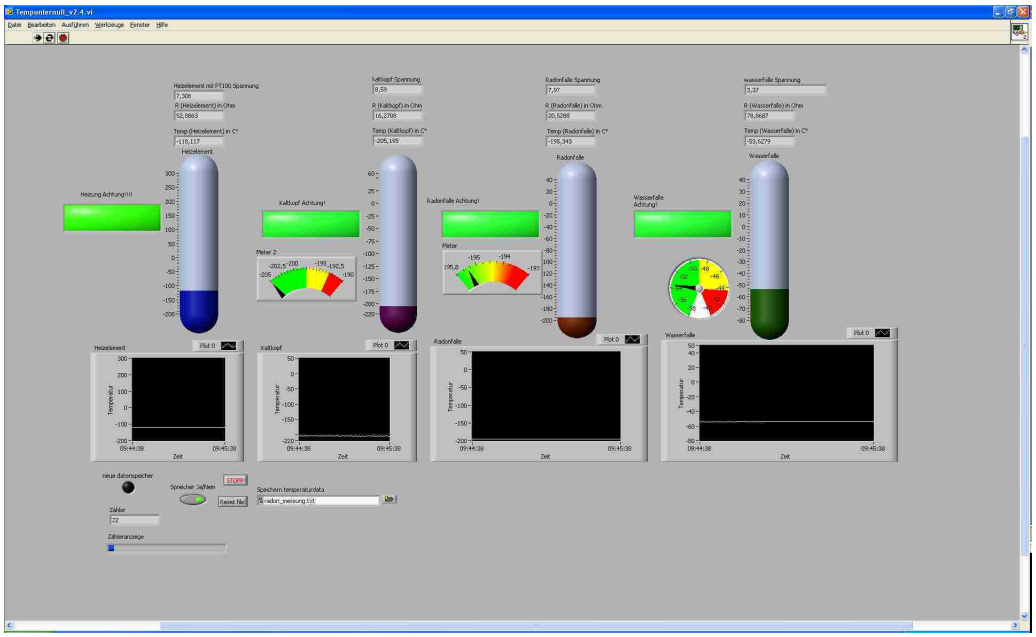

Figure 3.25.: New program Temperature version 2.5: In the picture a capture of the program operating during the cooling down has been shown. The program implement some indicators to operate in the optimal temperature range. Four thermometers to show dynamical temperature evolution in the heat cartridge, water trap, radon trap and cold head have been placed, as well as temperature in time. The program show voltage, resistance, and temperature with numerical value.

The new software to control the temperature range is the program *Temperature V 2.5*. This program has the finality to do easy a measurement as well as control the temperature operation range in every cryo-devices with accuracy.
The program dispose four thermometers with alarm when the temperature isn't in the optimal range. Temperature is showed in a minute range on life thanks to the dynamical monitors. Numerical values of voltage, resistance and conversion in temperature have been implemented. The program also disposes the possibility to save all data in a file, the temperature will be saved in four columns in the next order: heat cartridge, cold head, radon trap and water trap. Due to overflow the program is automatic reseted every 600 s and a new file is created. For this reason finished the measurement all files must be collected in only one file. To do a script code in UNIX has been realized.

4. Calibration and radon air sample

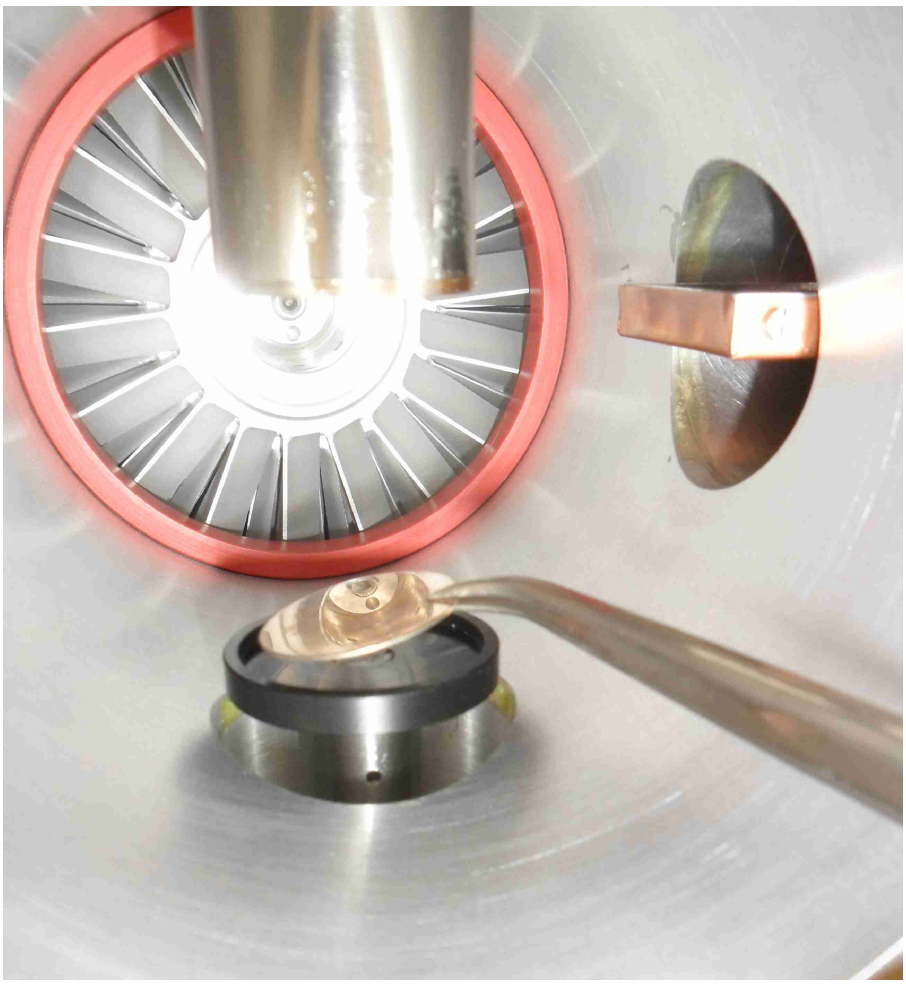

4.1. Calibration

Calibration is the process aimed at obtaining a relation between the channel and energy in the spectra. For this process, it is necessary to use a calibration source with peaks and energy well defined. The program *Maestro* [Orta] provides the possibility to implement linear and polynomial calibration. The calibration process can take from two to five hours if one wants to simulate the experimental condition as in a radon measurement. A resume how to realize a calibration measurement can be found in the appendix C.1.

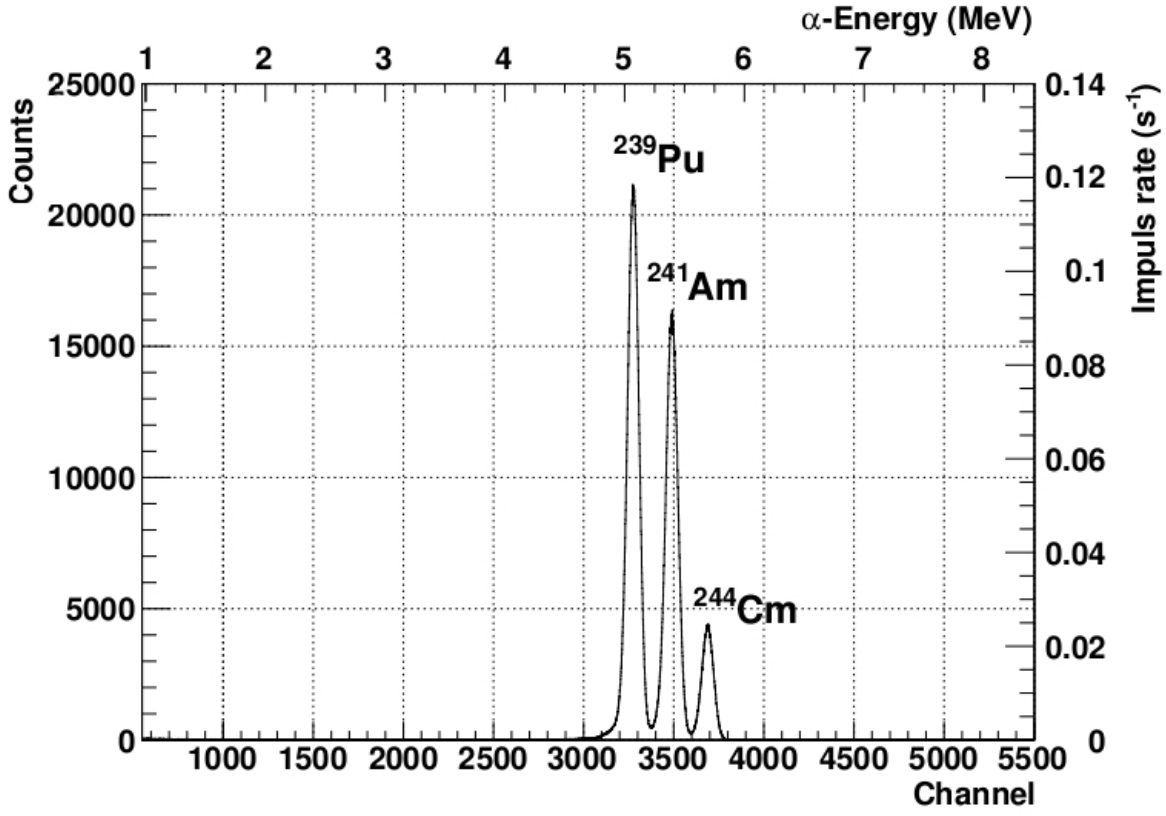

Figure 4.1.: Calibration using "Mixquelle 38". Life-time: 8149 s, a=10 mm, date: 25.06.2012

In Figure 4.1 a calibration is showed. Thanks to these measurements the energy axis is calibrated for the radon air measurements. The calibration parameters are

directly obtained by the program *Maestro* [Orta] and a linear calibration is attached in every radon measurement. To realize a calibration equation 4.1 will be used:

$$E(c) = E_0 + \{\frac{(E_2 - E_1)}{(c_2 - c_1)}\}c. \tag{4.1}$$

where c is the channel and E the energy of the alpha particle.
Parameters like as E_0 and $\{\frac{(E_2-E_1)}{(c_2-c_1)}\}$ can be obtained directly after the calibration measurement from the output data using *Maestro* [Orta].

4.1.1. Calibration source

The radioactive source used in a calibration was a solid mix source with the nuclei: ^{239}Pu, ^{241}Am and ^{244}Cm.
As has been shown in Figure 4.1 the peaks correspond to the most probable transitions. In this case to achieve a linear calibration the data from the table 4.1 can be used. For the linear fit it is necessary to use two peaks, in this case the most probable transitions are: $^{239}_{94}Pu \rightarrow ^{235}_{92}U$ with 70.77% and $^{241}_{95}Am \rightarrow ^{237}_{93}Np$ with 84.8%

Nucleus $T_{1/2}$	α-Energy(keV)	P_α(%)	Daughter
$^{239}_{94}Pu$ (24110 ± 30)y	5105.5 ± 0.8	11.94 ± 0.07	$^{235}_{92}U$
$^{239}_{94}Pu$	5144.3 ± 0.8	17.11 ± 0.14	$^{235}_{92}U$
$^{239}_{94}Pu$	5156.6 ± 0.1	70.77 ± 0.14	$^{235}_{92}U$
$^{241}_{95}Am$ (432.6 ± 0.6)y	5388	1.66 ± 0.02	$^{237}_{93}Np$
$^{241}_{95}Am$	5442.80 ± 0.13	13.1 ± 0.3	$^{237}_{93}Np$
$^{241}_{95}Am$	5485.56 ± 0.12	84.8 ± 0.5	$^{237}_{93}Np$
$^{244}_{96}Cm$ (18.11 ± 0.03)y	5762.64 ± 0.03	23.1 ± 0.1	$^{240}_{94}Pu$
$^{244}_{96}Cm$	5804.77 ± 0.05	76.9 ± 0.1	$^{240}_{94}Pu$

Table 4.1.: α-decays of the calibrated source. All decays have been included with half-life, energy and probabilty. Source: [Lab]

4.1.2. Calibration test

During the calibration process the sample table must be used to support the solid radioactive source. The elevation of the sample must be 10 mm from the detector (Position 10). The reason is explained in [Nus11], basically if a measurement with a distance smaller than 10 mm is done the detector will be saturated and the spectra will be deformed. However if the distance is higher than 10 mm a spectrum will be obtained but not with the optimal number of counts.
All measurements shown in Figures A.1, A.2, A.3, A.4, A.5 and A.6 were done under the same experimental conditions. The measuring time was approximately 60 min.
In these measurements different distances a were used and one could see that the optimal distance is $a = 10\,\text{mm}$. It is independent of the modifications done. A test of calibrations were done with distances $a = 5\,\text{mm}$, $a = 10\,\text{mm}$, $a = 15\,\text{mm}$, $a = 20\,\text{mm}$, $a = 25\,\text{mm}$ and $a = 30\,\text{mm}$. (see Apendix A.1)

4.2. The radioactive source

To obtain a radon gas sample a calibrated ^{226}Ra source was used. This source was prepared by M.Nettebrock [Net94]. The radioactive source is a radium solution prepared with an electrolytic method and inserted into a Titan-Backing cylinder [Net94], [Nus11]. (see Figure 4.2)

The activity of this source was determined in $2750 \pm 74\,\text{Bq}$ by [Net94] using electrolytic methods and as reference nuclei ^{222}Rn, ^{218}Po, ^{214}Po and ^{210}Po. In [Nus11] the activity of the sample was determined one more time using the probe table with different values of a. In [Nus11] the last value of the activity can be found as:

$$A_{Ra,0} = (2604 \pm 6)\,\text{Bq} \tag{4.2}$$

For the efficiency measurements the value determined in formula 4.2 was assumed. To determine the activity of a decay product formula 2.14 can be used, but in practical measurements formula 2.14 must be corrected with the *emanation factor*.

Figure 4.2.: Titan-Backing cylinder with the calibrated source ^{226}Ra. The radium source is the disc fixed in the central point. The radon gas will be contained into the cylinder. The cylinder disposes two valves to connect the air pump and plastic bag. Photo obtained by: [Nus11]

The *emanation factor* describes the exhalation of the radium source. The last value of this factor was determinated in [Nus11]:

$$(1 - \frac{A_{Rn}}{A_{Ra}}) = (0.382 \pm 0.016) \tag{4.3}$$

With this correction the Radon activity in a air sample can be calculated using the model of formula 2.14 but with the new correction.[1]

$$A_{Rn(air)} = \frac{\lambda_{Rn}}{\lambda_{Rn} - \lambda_{Ra}} A_{Rn,0}(e^{-\lambda_{Ra} t_{\text{enr}}} - e^{-\lambda_{Rn} t_{\text{enr}}})(1 - \frac{A_{Rn}}{A_{Ra}}) \tag{4.4}$$

4.2.1. Working with the radioactive source

As radon is a gas, to build a radioactive probe, air has to be pumped through the cylindrical container of the radium source. The radon will be distributed in the $10l$ that the plastic gas bag contains (see Figure: 4.3). To create a radon probe sample, the air pump and the plastic bag will be placed and fixed in the Titan-Backing cylinder. All valves will be closed before start pumping. First the valve of the plastic bag will be opened, second valves of the cylinder will be opened simultaneously. Air will be pumped through the cylinder enriching the air of radon. When the plastic bag will reach the maximal capacity, valves will be closed in the next order: First

[1] Formula used in[Nus11] and [Net94]

plastic bag, valve between plastic bag and cylinder and finally the last valve. The setup will be disassembled and the plastic bag will be placed in the experimental setup.

The time between two injections of radon air samples has to be written down, it is called "enrichment time". The time correction using the enrichment time will be used to calculate the final sample activity. The "time" must be written down in the moment of start to pumping, because it will be used to calculate the "enrichment time". To automate the calculation process a excel code sheet for calculate the en-

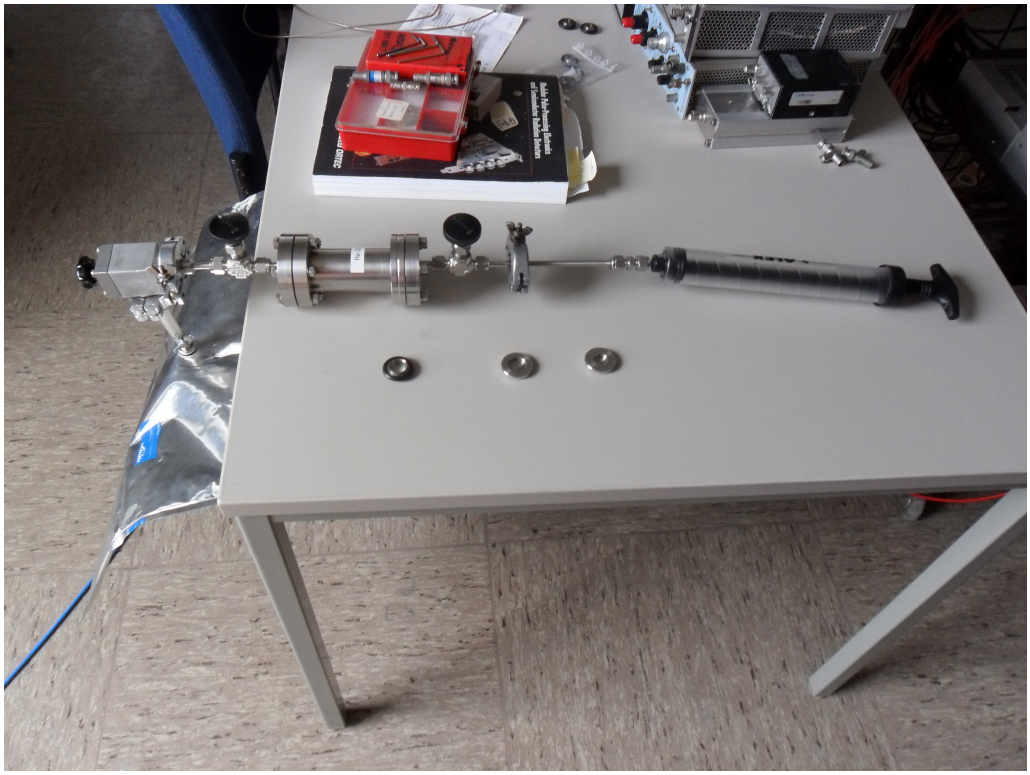

Figure 4.3.: ^{226}Ra source, pump and plastic bag. It is advisable operate the valves in the order indicated, and don't reach the maximal pressure in the plastic bag. The plastic bag dispose a valve in the input. This valve will be remained always opened (turn left). To control the pressure in the plastic bag the valve after the tube will be used.

richment time between two dates has been developed. To correct the radon activity, two things will be considered: The time between the creation of two radon air samples and the time between creating a radon sample and starting the measurement.

5. Modifications of the setup and results

In this section, the setup modifications realized during this master thesis will be described.
Section 5.1 will describe the original setup with disadvantages and reasons to change the setup, it was the initial point. Section 5.2 will deal with the setup used in the first part of the master thesis and the conclusion obtained of this setup. These results will be the reasons for modifications oriented to improve the system efficiency. In the last section 5.3 the final installed configuration setup will be explained as well as result of the final efficiency will be shown.
In the following, the various versions from M. Nettebrock [Net94], A. Nustede [Nus11] and this master thesis will be labeled $V1.0$, $V2.0$ and $V3.0$.

5.1. Radon in detection system V 2.0

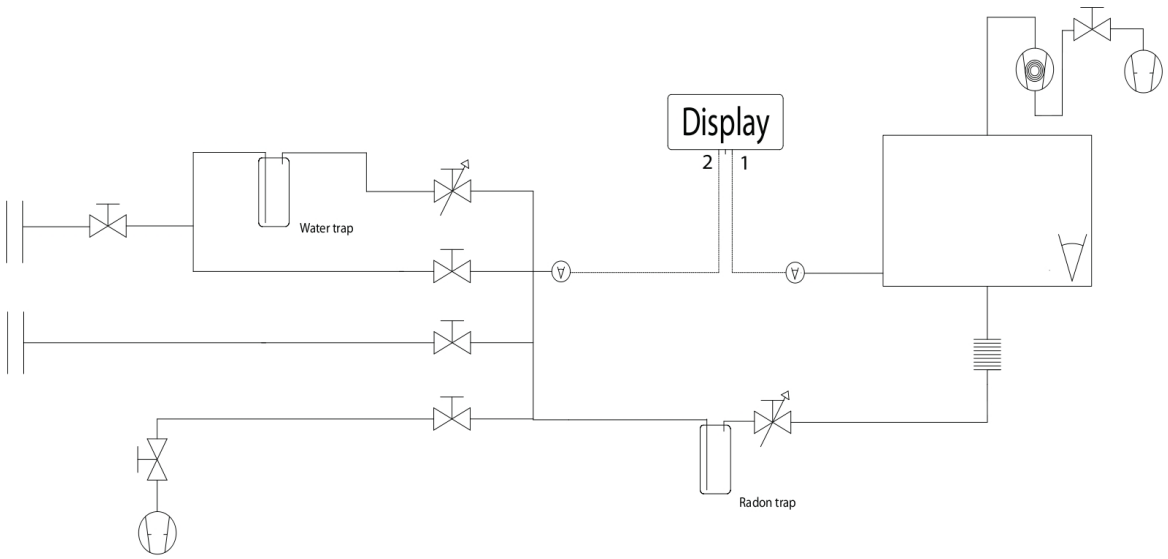

Figure 5.1.: Version 2.0 of the radon air system: Scheme obtained as adaptation of scheme in [Nus11]. This setup was the original configuration used before this master thesis, the system disposes the same cryo-devices but the principal difference is the cooling down of the radon. In this setup the gas after cooling down in the radon trap was evacuated using the detection chamber.

In the present section a brief overview of the first version used to realize radon air measurements before this master thesis will be shown.
The gas system consisted of a primary vacuum pump *Alcatel*, four gas valves *Swagelok MS-01-38*, two precision valves *Leybold Heraeus 28338B2*, a vacuum gauge *Leybold Thermovac TTR91* in the gas system, another *Leybold Penninvac PTR 90* and finally a turbo pump *Leybold Turbovac SL 300* in the vacuum chamber were installed. In this version of the setup, one calibration measurement has been done per week. The disadvantage of the original setup is that a calibration needed the same time to a normal measurement. In Figure 5.1 a scheme of the original setup can be observed.
The principal disadvantage of this configuration was the working time if a background measurement want to be obtained. At the beginning, the background measurements were not relevant and only a background measurement per week was done.
It was discovered that leftovers of the last measurements on the cold head can be

remained and a background measurement for each radon air measurement will be required. In this configuration the radon air sample was cooled down using the vacuum chamber. It means first the radon air concentration passes through the water trap, in the second step radon was catched by the radon trap and the rest of the gas was evacuated by the turbo pump in the vacuum chamber. A background measurement with the old configuration was not possible to do in the same day, due to the working time of a regular measurement is approximately 8 h, for this reason some changes needed to be applied.
In the last work realized on this experimental setup, the global efficiency of the setup was determinated in [Nus11]. Measurements data of the original setup was written in Appendix: G.1 and showed in Figure 5.2

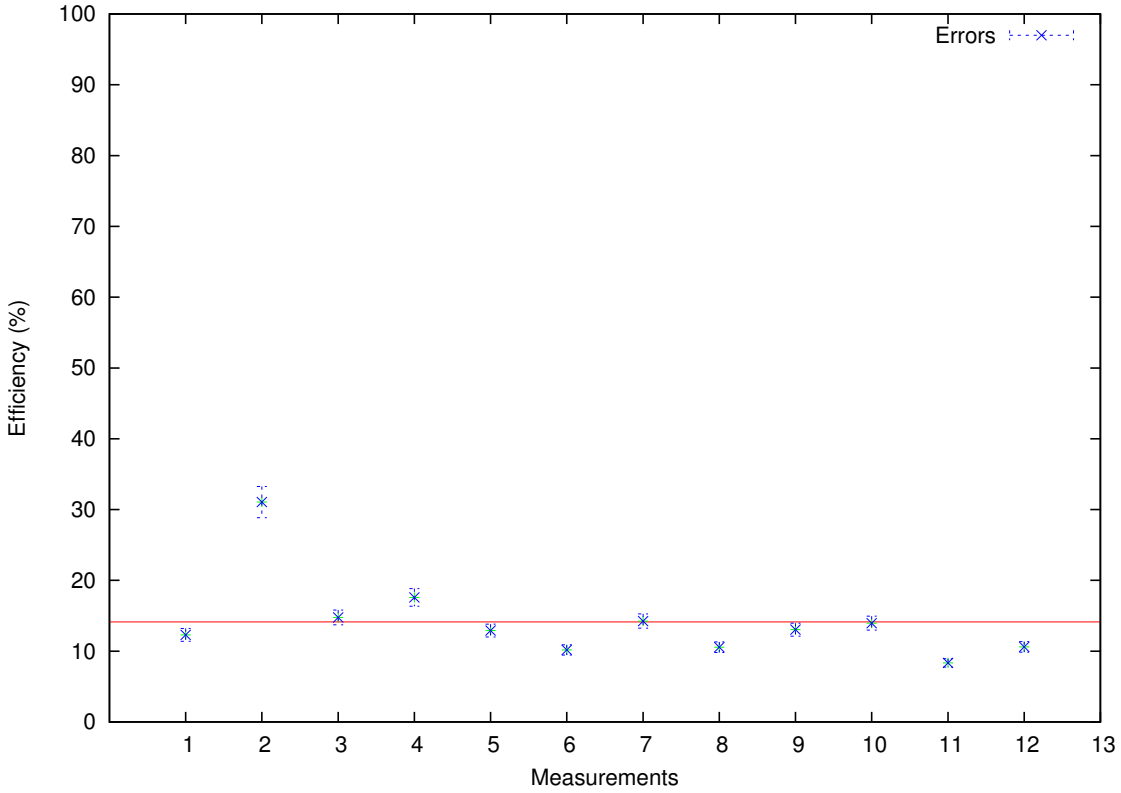

Figure 5.2.: Efficiency data: This diagram was obtained of the original thesis [Nus11]. In the picture the result of 12 measurements to determinate the efficiency have been plotted. Every measurement has been drawn with the statistic error of the experimental measurement. The red line indicates the mean value of the calculation. By [Nus11].

Figure 5.2 shows the conclusion of [Nus11] and start point of this master thesis. Efficiency was determined in $(12.59 \pm 0.78)\%$. One can be observed in the Figure 5.2 that the value of $\frac{\chi^2}{ndf}$ will be a high value, in this case the efficiency result will be conditioned by the guarantee given by $\frac{\chi^2}{ndf}$. It means that deviations between the measurements are bigger that the statistical uncertainty or explained with other words: the reproducibility of the efficiency measurements has to be improved. In this point this master thesis started with the followings points advised by A.Nustede in [Nus11]:

• Implementation of a background measurement for each radon air measurement and improvement of the working time.
• Subtraction of the background at every radon air measurement .
• Cleaning of the cold head with isopropanol before the next radon measurement.
• Efficiency determination of the radon air setup and improvements.
• Additional uncertainty which is not yet considered.

5.2. Radon in detection system V3.1

The first modification of the setup wants to improve the measuring time doing a background measurement per radon measurement (see Figure 5.3).
The task is: during the cooling down of the radon, it must be possible realize a parallel background measurement on the cold head. To realize it, a T divisor and two new valves were used after the flow control valve (8) (valves (10) and (11) see Figure 5.5). The new valve (10) has the task to isolate the vacuum chamber and the valve (11) to connect with the gas system. In this configuration the control flow is controlled by valve (8). A photo of the experimental setup can be observed in Figure 5.4. The new valve (11) is only accessible under the table, the return tube was connected using a T union connecting the gas system and the rotary pump of the gas system. Additionally the turbo pump was equipped with a cooling system for long term measurements of more than 24 h.

With this setup, the optimization were:

• It was possible to do a background measurement for every radon measurement.
• It was possible to correct the fit thanks to a modification in the fit program.
• It was possible to realize a large number of measurements to determine the efficiency.

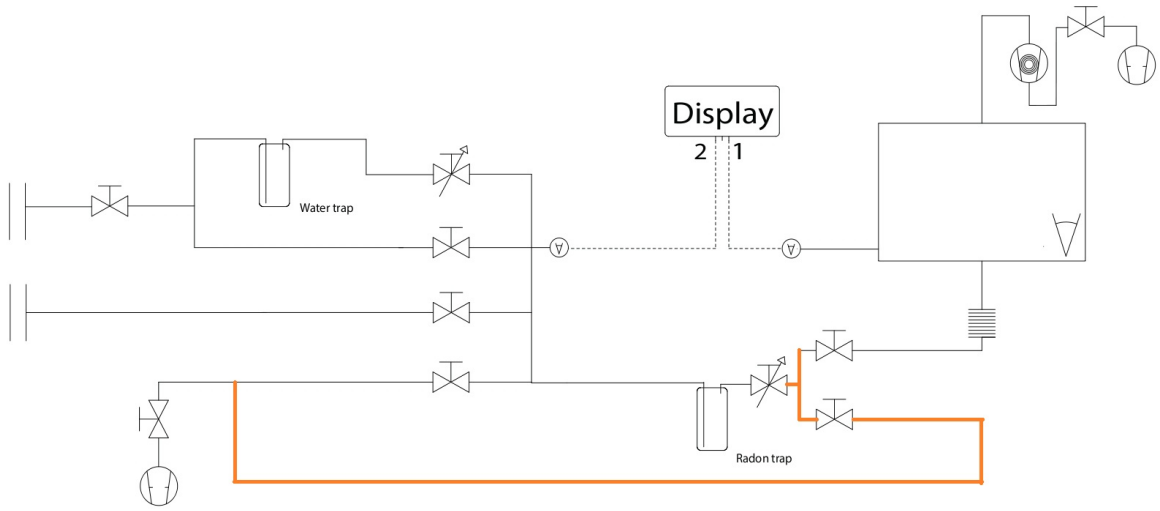

Figure 5.3.: Version 3.1 radon air system: In this picture a scheme of the new configuration has been shown, the orange line indicates the new tube implemented in the system, after the radon trap there is a regulator valve and two new valves have been settled. During the cooling down of the radon, the gas passes through the radon trap and is evacuated by the gas system. In this case the vacuum chamber during the cooling down of the radon is used to realize a background measurement.

Using the experimental setup V 3.1 a large number of measurements have been measured. During 4 months, 44 measurements could be measured (a normal measurement required around 8 h to be realized) with the objective of determinate a value of the global efficiency of the setup.

Measurements have been shown in Figure 5.6, this plot was the first result of collect all measurements and plot into a diagram. A calculation of the mean value of the efficiency was tried, but the value was rejected for the next arguments, in total 13 of 44 measurements were rejected. The causes were:
→ Measurement 1 was rejected because a lost of pressure was found during the first measurements with the new setup V 3.1.
→ Measurements 8 and 33 were wrong results of a high value of efficiency. A mistake detected in the program used to calculate the enrichment time was the key to found the calculation error and these points were rejected.
→ Measurements 17 and 19 were rejected for not maintain temperature and other parameters in the optimal range. Some problems with valves during the measurement were the reason to find a too low efficiency.

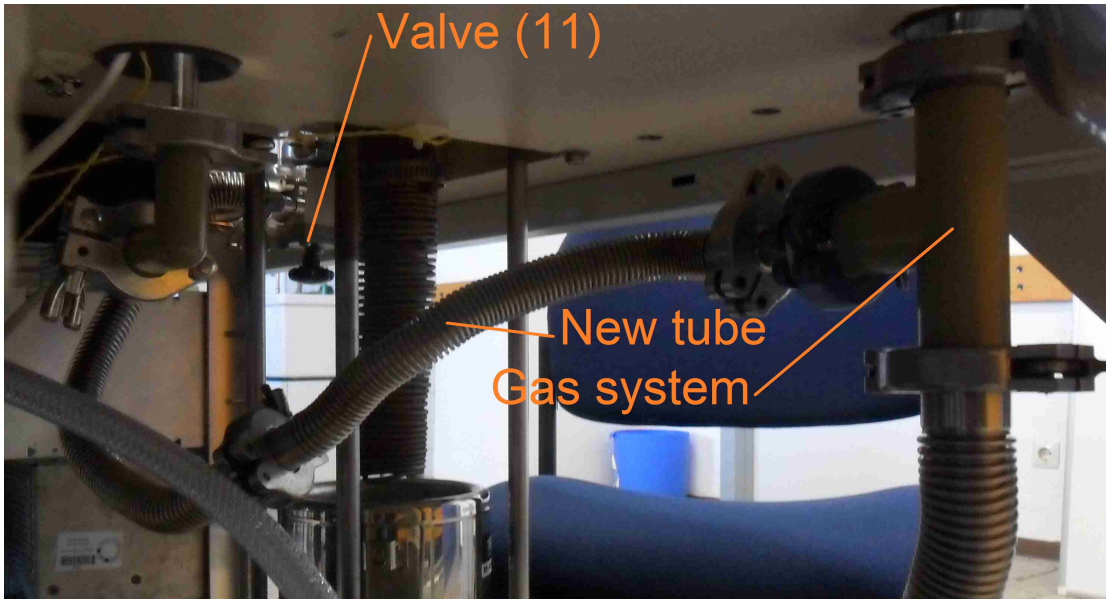

Figure 5.4.: Return tube installed in the V 3.1 radon air setup: In the picture the new tube as well as the new valve and the connection with the gas system have been shown. The valve (11) is only attainable under the table.

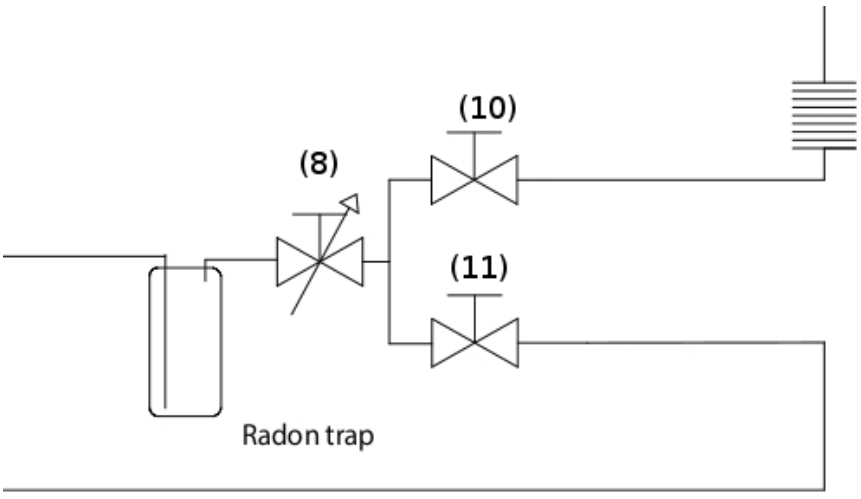

Figure 5.5.: Zoom of the Figure 5.3: In this picture a zoom of the last scheme was done. The flow control is governed by the valve (8), valve (10) connect with the vacuum chamber and the valve (11) connect with the gas system.

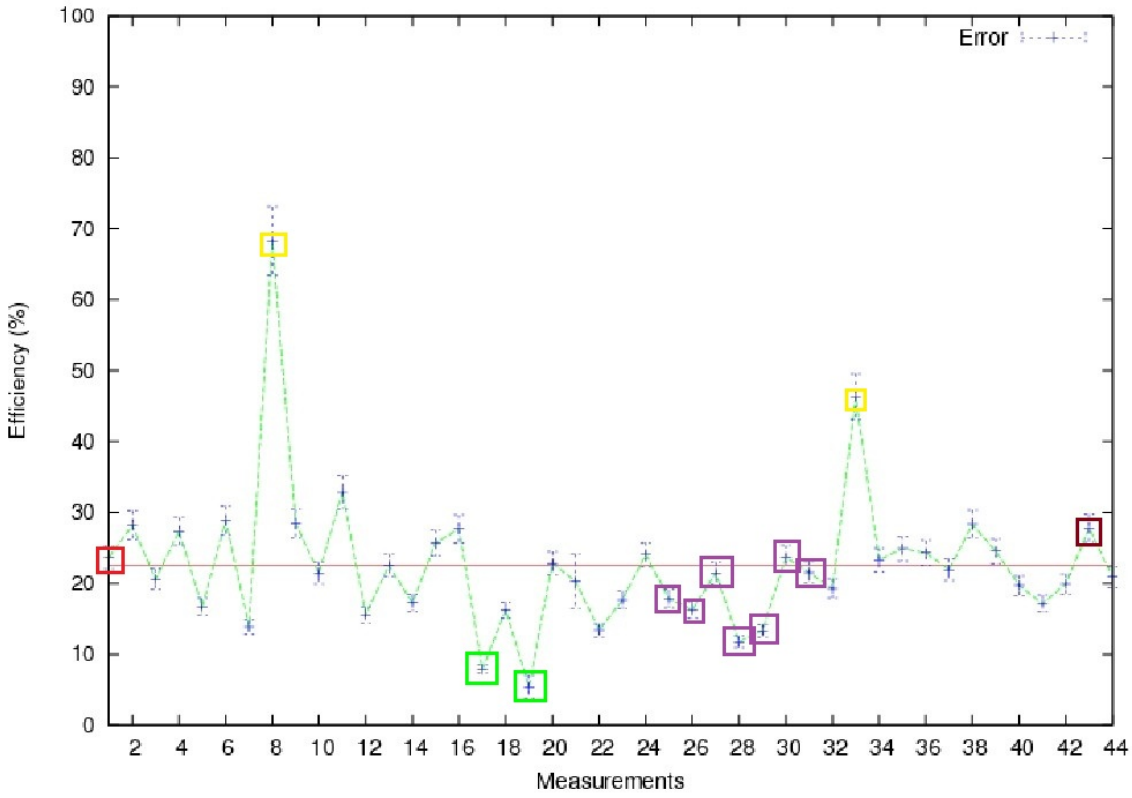

Figure 5.6.: Measurements setup V 3.1: In the figure all measurement realized to determinate the efficiency have been plotted. In blue color the statistic error has been indicated, the green color indicates the order of the measurements, the red line indicates the first attempt to obtain a value of the efficiency. The colored boxes indicate measurements which were excluded for the final efficiency determination. Details are given in the text. The red box indicates the measurement 1. The yellow box indicates measurements 8 and 33. The green box indicates measurements 17 and 19. The violet box indicates measurements 25, 26, 27, 28, 29 30 and 31. Finally the brown box indicates the measurement 43.

→ Measurements 25, 26, 27, 28, 29, 30, 31 were rejected to found instabilities problems with the pump of the gas system and because a hole in the plastic bag was found after a measurement sequence.
→ Finally the measurement 43 was rejected because electric noise in the background was increased and it was impossible to reach the convergence with the fit program, making reject this measurement.
In every measurement the background was subtracted with a background measurement before the radon measurement. Eliminated the measurements explained, difficult to calculated a mean value of the efficiency were found one more time. Deviations between the measurements and the statistical uncertainty were appeared. To solve it, a new strategy was developed: It consists on eliminate outliers values with known explication, it was explained in the last point and apply the absolute and relative scaling of the uncertainty.
The algorithm to apply the absolute and relative corrections can be found in the appendix B. The absolute and relative scaling of the uncertainty consists on adding a constant value u_{absolute} in the uncertainty of every measurements $u_i^{'} = \sqrt{u_i^2 + u_{\text{absolute}}^2}$ (absolute scaling) or a relative value u_{relative} in the uncertainty of the measurements $u_i^{'} = \sqrt{u_i^2 + (\frac{u_{\text{relative}}}{100} y_i)^2}$ (relative scaling, where y_i is the measurement value) making the value of $\frac{\chi^2}{ndf} = 1$. The new values of the error of all measurements will be bigger than original case, but in this case 68% of all measurements should cut the mean value. The absolute scaling gives an anomaly of an offset of the setup, it means an error that always is doing with the same frequency during the measurements. The relative scaling gives the correction weighted with the value of the measurement. It means that error will come from a proportion of the measurement.

Absolute correction

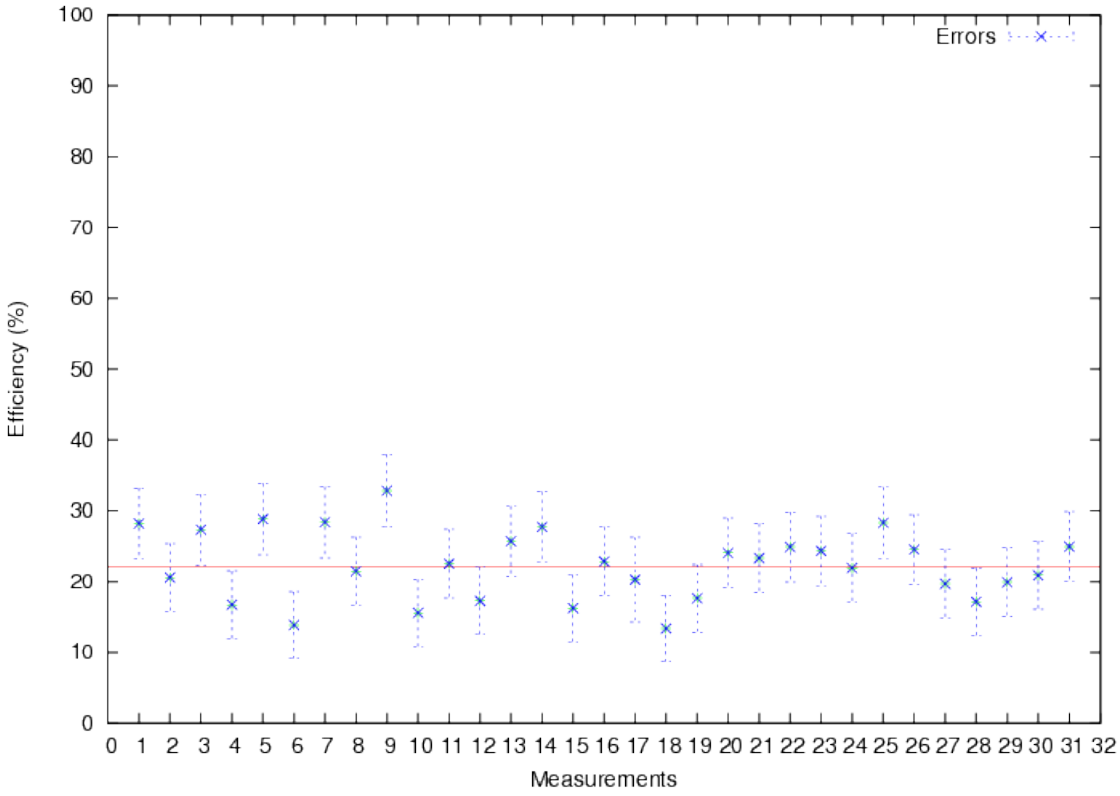

Figure 5.7.: Absolute correction measurements V 3.1: In this plot 31 renumbered measurements to determinate the mean value of the efficiency have been used. The order of the measurement corresponds to the measurements showed in tables of G.2, G.3, G.4, G.5, G.6, G.7. The new error calculated with the absolute scaling of the uncertainty has been drawn with blue color. The red line indicates the new mean value weighted by the absolute scaling.

Figure 5.7 shows the result of applying the absolute correction. With this method, the mean value of the efficiency with the statistical error has been fixed in:

$$\text{Efficiency} = (0.221 \pm 0.009) \tag{5.1}$$

The absolute scaling of the uncertainty was fixed into $u_{\text{absolute}} = \pm 0.046$. With the newly introduced uncertainty one gets a total uncertainty in the efficiency of ± 0.046 for the new independent measurements.

Relative correction

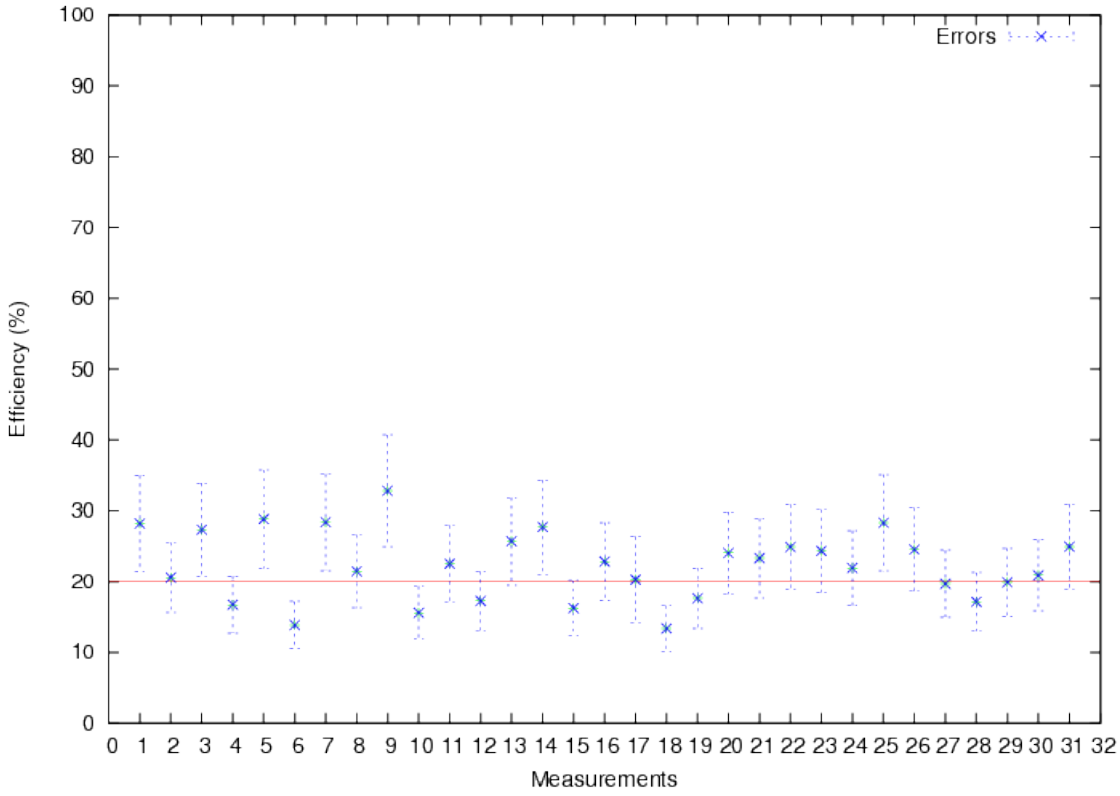

Figure 5.8.: Relative correction measurements V 3.1: Using the relative scaling 31 renumbered measurements to determinate the mean value of the efficiency have been used. The order of the measurement corresponds to the measurements showed in tables of G.2, G.3, G.4, G.5, G.6, G.7. The new error calculated with the relative scaling of the uncertainty has been drawn with blue color. The red line indicates the new mean value weighted by the relative scaling.

Figure 5.8 shows the result of apply the relative correction. With this method, the mean value of the efficiency with the statistical error has been fixed in:

$$\text{Efficiency} = (0.201 \pm 0.009) \tag{5.2}$$

The relative scaling of the uncertainty was fixed into $u_{\text{relative}} = \pm 23\%$. In this case, with the newly introduced relative uncertainty one gets a relative uncertainty of $\pm 23\%$ for the new measurements of the efficiency.

In this case, comparing the methods, one can observe that the difference between the result is $\Delta\varepsilon_{\text{efficiency}} = 0.02 \approx 2\sigma$. Obtained first values of the global efficiency the next step was apply challenges related with the operation mode. The conclusion of the measurements for this configuration were:

- It was difficult to maintain a stable temperature in the water and radon trap.
- The vacuum pump *Alcatel* showed instabilities.
- The temperature read out in the heater cartridge was limited to 50 °C
- The radon gas is expanded through the gas system before the injection.
- The efficiency value was low and unstable.

These points led to a new modification of the radon air setup: the version $V3.2$.

5.3. Radon in detection system V 3.2

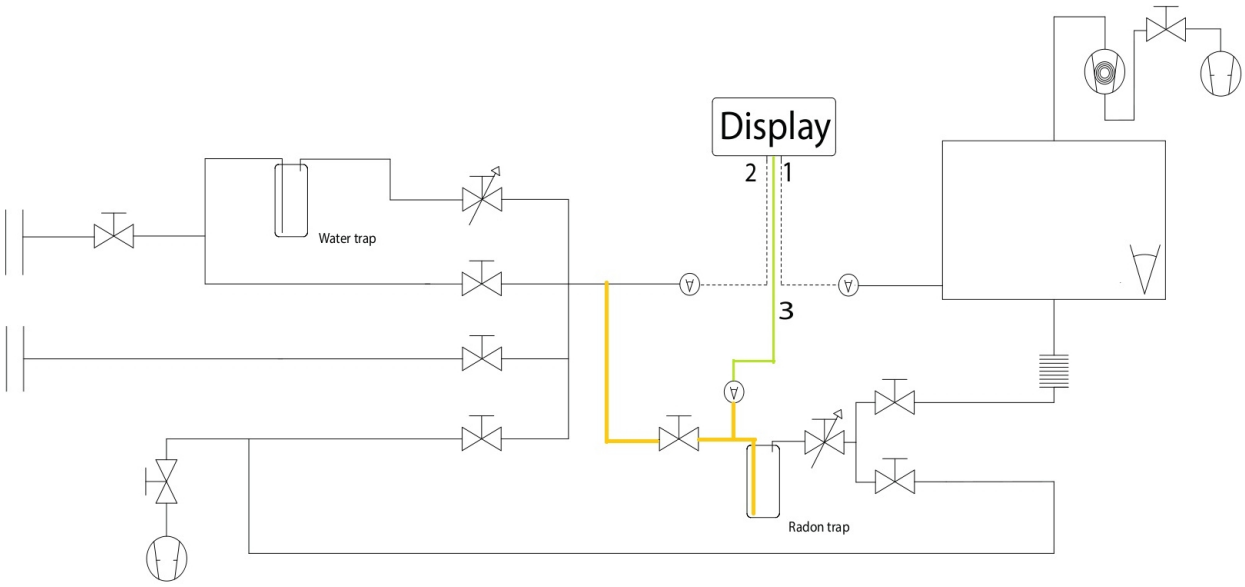

Figure 5.9.: Version 3.2 radon air system: Final version of the radon detection system. In the picture the new tube installed in the gas system has been shown in yellow color. The green cable indicates the new vacuum gauge used and connected to the vacuum system. A new valve settled before the radon trap has been installed. This new valve is used during the heating up of the radon concentration to isolate the radon in the radon trap.

The second modification of the radon air detection system has the objective of respond all problems observed in the last configuration and resolve them. To resume it, the ideas were:

• Avoid the expansion of the radon air concentration after cooled down and before the injection on the cool head
• Avoid excess temperature on the heater cartridge and monitoring the temperature exceeded 50 °C
• Precision Control on the temperatures to avoid lost radon
• Improve the instabilities in the gas system due to a poor vacuum

Every point will be treated in the next sections as well as the final efficiency of the experimental setup will be shown. During the next lines every modification of the system will be explained in a sub-section explaining reasons and improvements realized.

5.3.1. New tube system with new valve and vacuum sensor

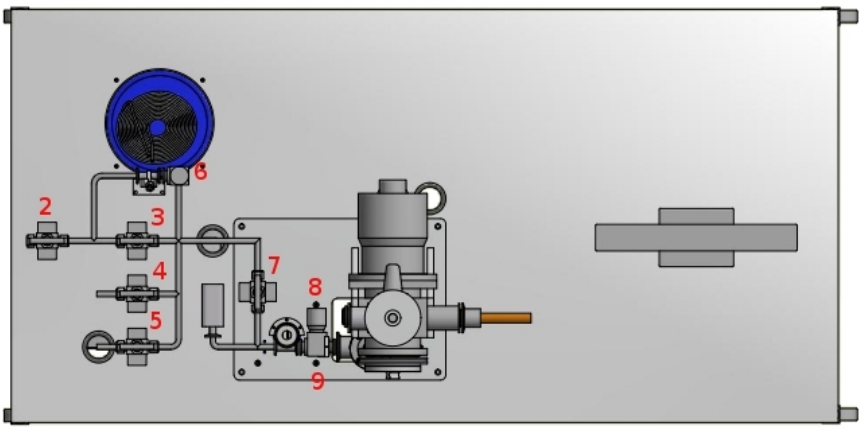

Figure 5.10.: CAD-Picture of new tube system. In this case, valves have been labeled with the numbers of the scheme V 3.2. In this scheme the water trap has been showed in blue color and the measurement chamber can be observed in the central point of the picture. The object on the right part of the picture is a illustration of the computer used in the experimental setup. By D. Bonaventura

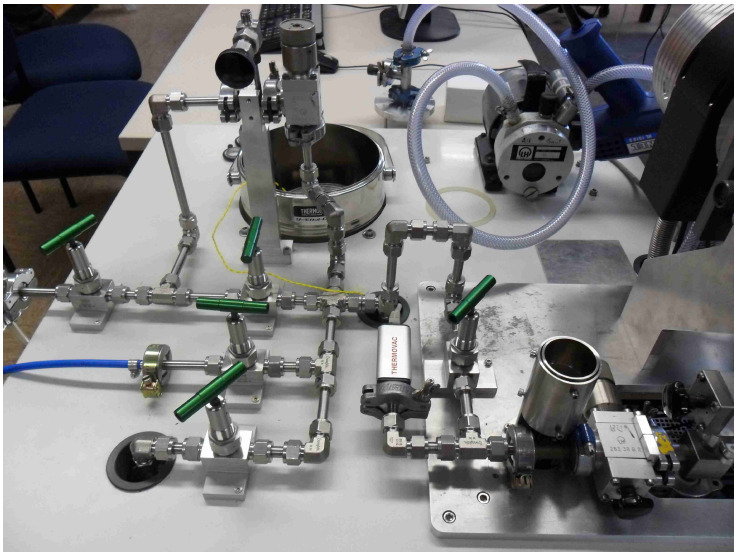

Figure 5.11.: Photo of the new tube system. In the central part of the photo the new vacuum gauge and the valve (7) can be observed. The new vacuum gauge is a model *Thermovac transmitter TTR 91* and the new valve is the same model that the other ones: *Leybold Heraeus 28228B2*.

The new tube configuration has the finality to concentrate the radon concentration in a short zone of the gas system and avoid the expansion before cooling down the gas sample and before the injection. A CAD-Picture can be observed in Figure 5.10 as well as in the Figure 5.11 a photo of the final experimental setup has been shown. During the radon preparation when plastic bag will be empty the next step is close all valves of the gas system and evacuate the gas of the radon trap[1]. With the new tube system the valve (7) is closed and the heater gun can be switched on to heat up the radon in the trap. Thanks to the new valve 7 the high radon concentration is kept in the radon trap. On the other hand with the valve (7), one can clean the gas system doing vacuum and getting into gas N_2 pressure in the tube before the injection. The difference explained can be understood looking at the Figures 5.12 and 5.13. With the new vacuum gauge the vacuum during this process can be monitored. The pressure in the radon trap before heating up the radon must be approximately 10^{-2} mbar and after heating up 12 mbar. With this new tube configuration the first result has been a reduction of the background, due to rest of the gas can be eliminated before the injection. Only the gas kept in the radon

[1]The radon gas remains at $-193\,^{\circ}$C in the radon trap

trap will be injected. The pressure control before and after the injection shows that similar volume of gas has been injected on the cold head.

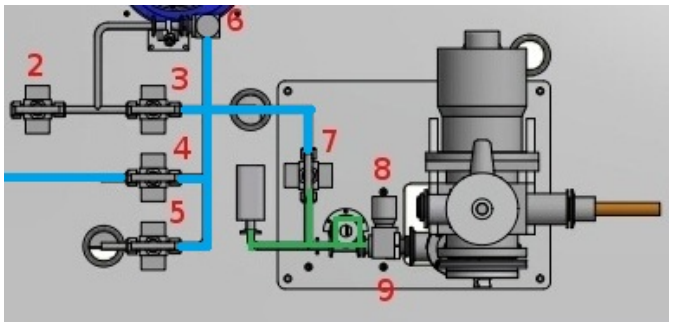

Figure 5.12.: New tube system before injection. In this scheme the radon concentration has been shown in green color and the carrier gas N_2 in blue. Valve (7) has been used to isolate the radon concentration and will be the last valve opened to start the injection. Before the injection the gas system (blue tube) can be cleaned making vacuum and injecting gas N_2 thanks to valve (7) remains closed.

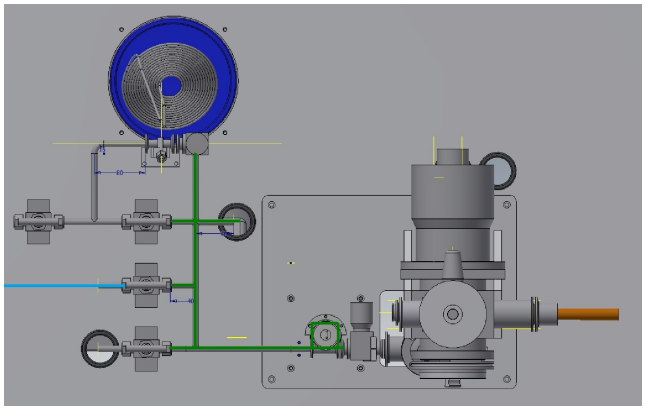

Figure 5.13.: Old tube system before the injection. Similar to the Figure 5.12, radon concentration has been shown in green color and the carrier gas N_2 in blue. The carrier gas come in over the valve (4) and valve (9) start the injection. In this case gas before heating up is expanded over all gas system.

5.3.2. Temperature card modification

An experimental problem detected during the heating up of the cold head was: It was not possible monitoring the temperature of the heater cartridge exceeded 50 °C. To measure temperatures the setup disposes 4 resistance thermometers type PT100 [nIDE] assisted by a preamplifier system developed in the electronic workshop and a reader card type[2] *NI USB-6008/6009*.

The temperature module was developed with 8 channels[3], in every channel the amplifier factor was ×83.5. The temperature module impose a DC current of 1 mA and multiplier the voltage by the factor indicated.
The input voltage of the card *NI USB-6008/6009* is limited in +10 V when it is connected in mode RSE with *floating signal sources*. Due to the factor ×83.5 when the temperature in any resistance thermometers gets over 50 °C the preamplifier card multiplier the voltage in a value higher than +10 V and the reader card *NI USB-6008/6009* will get in saturation mode.
To solve this problem, the amplifier factor of the output number[4] 3 was changed for ×46.2. This number was chosen to reach a maximal temperature of 300 °C, but due to overheating it was recommended to not exceed 100 °C when the heater cartridge is working.

In Figures 5.14 and 5.15 the electrical scheme of the output number 3 and the new resistors to change the amplification value have been shown.

5.3.3. Temperature control with Temp V2.5

The program *Temp V 2.5* was developed to have a better control of the temperatures (see Figure 5.16). The program adds the working ranges in every cryogenic system, at the same time there are four visuals alarms and four graphics monitors to maintain temperatures in the optimal ranges. The program incorporate a function to save all data and to analyze it posteriorly.

Due to the new amplifier factor, a new calibration of every resistor thermometer was developed. Taking experimental data of voltages and resistances linear fits have been done. To do it, one was used a variable resistor set on the place of every PT100

[2] Assistant guide in [ni]
[3] Every channel correspond a pair of cables, it is possible measure 8 temperature simultaneously. To find more information about the original cart go to [Nus11]
[4] Correspond with the resistance thermometers integrated in the heater cartridge.

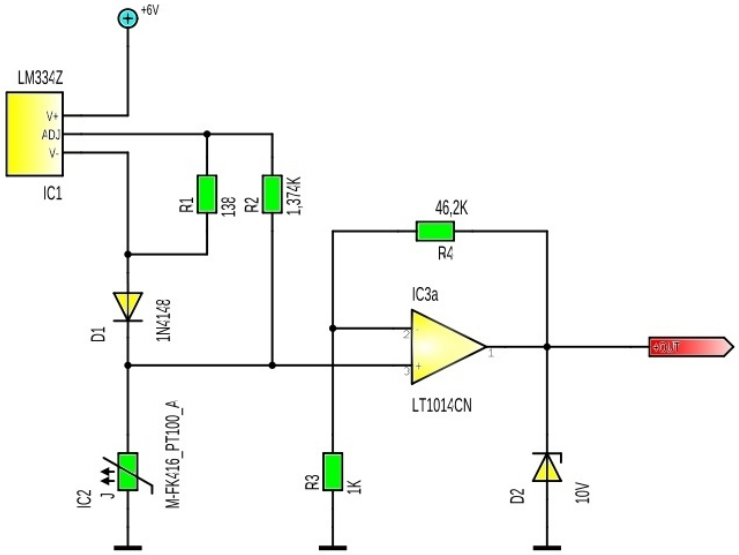

Figure 5.14.: New scheme using the amplifier factor $\times 46.2$. In this new scheme respect the resistor *R4* has been modified. In this case the new value is $46.2k\,\Omega$, it means that amplifier factor will be in this case $\times 46.2$ because the resistor *R3* has a value of $1k\,\Omega$. The scheme corresponds of an op-amp with negative feedback

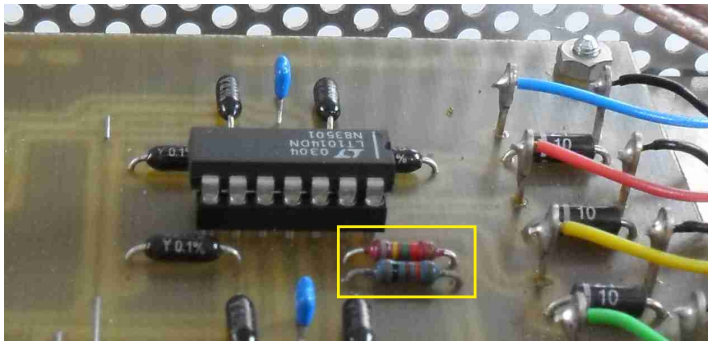

Figure 5.15.: New parallel resistors. In this photo the new resistors can be observed in a yellow box. To obtain a total resistor of $46.2k\,\Omega$ two parallel resistors have been implemented. In the scheme this two resistors are the resistor number *R4*. By R. Berendes.

resistor and an Ohmmeter was used to know the value of the resistors. It was taken a data serial of resistance measurements with the Ohmmeter and measurements of voltage with the program Labview has been done. Finally the calibrations indicates in the section 3.2.2 have been written in the temperature program *Temp V 2.5* .

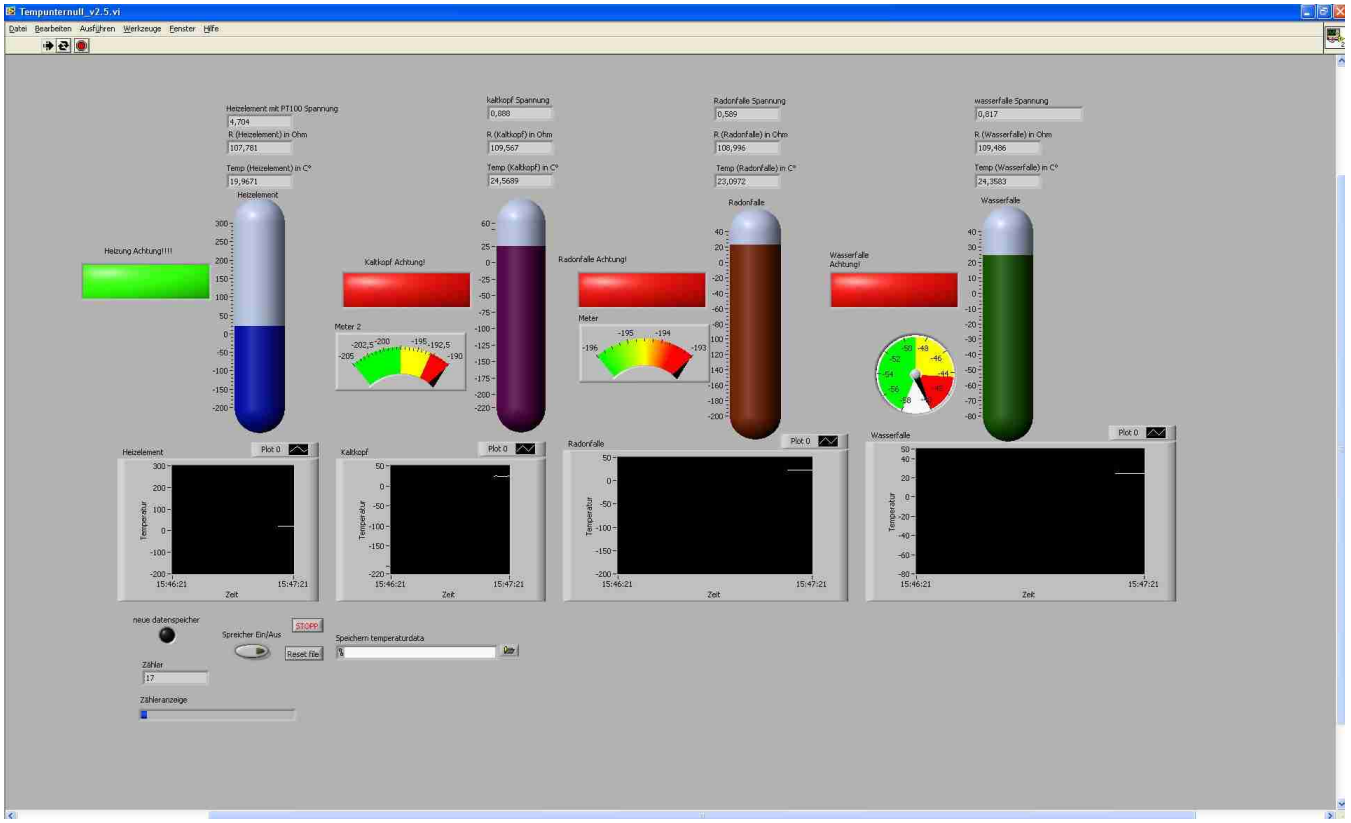

Figure 5.16.: Program temp V2.5. A capture of the program before starting the cooling down of the radon has been shown. The program incorporate four thermometers and four graphics monitors to show temperatures. Every thermometer has three numerical indicators with voltage, resistance and temperature. An alarm has been implemented in every thermometer to indicate that temperatures are not in the optimal range and three extra indicators have been placed in cold head, radon trap and water trap to maintain the temperature in the optimal range. The program creates a new file every 600 s due to data overflow, when a new file is created the yellow light is running. The program create a data file with four columns in the next order: heater cartridge, cold head, radon trap and water trap.

5.3.4. Exchange of a vacuum pump in the gas system

Figure 5.17.: Alcatel pump was the original pump of the gas system. The Alcatel pump is a rotary oil pump used to do vacuum in the gas system. A original point of this master thesis was checking the global efficiency of the system using this pump. But due to mechanical problems as well as blocking and lost of oil the pump was replaced for the Leybold pump.

Originally the system was composed by a rotary pump *Alcatel* in the gas system (see Figure 5.17). Vibrations observed in the ammeter of the detector made to change the pump out of the carriage. The problem was eliminated during a period of time but again the pump showed instabilities and finally it was blocked. The *Alcatel* pump was repaired but instabilities problems made replace the original pump by the pump *Leybold* (see Figure 5.18) The first instability was a high background detected. It was increased by lost oil by the pump *Alcatel* and threw into the gas system. The second problem was electric noise showed in the current of the detector created by pump *Leybold*. The pump was used to make some measurements, but measurements

Figure 5.18.: Leybold pump. This pump was used to realize vacuum in the gas system after used the Alcatel pump. Leybold pump is a rotary pump with a pumping speed of 16.5 m^3/h and an ultimate pressure of 2×10^{-3} mbar. This pump disposes a output without filter, so for this reason the output of this pump was redirect to the filter used by the other primary pump.

have been discarded due to these instabilities.
Thanks to the new pump, the global system won stability during the radon preparation and it was translated in a stability of the efficiency. Background was decreased thanks to the cleaning of the gas system realized before the injection.
The new pump *Leybold* with a higher pumping speed of 16.5 m^3/h and an ultimate pressure of 2×10^{-3} mbar has been installed out of the carriage due to this pump is bigger than the last one. An output tube has been installed because the new pump doesn't dispose output filter.

Efficiency calculation

The final results will be shown in the next lines. One more time, the result was calculated with both methods. It indicates that problems were not fully eliminate but one will see that in this case the system has reached a good point of stability. Due to the limited time in thesis the same number of measurements to determine the efficiency were not possible, but with the data showed the improvements of the system can be observed. The conclusions of the new setup and the final efficiency calculated will be discussed at the end of this section. The efficiency result will be used in the next section to calculate the quantity of radon in the basement and floor measurements.

Absolute correction

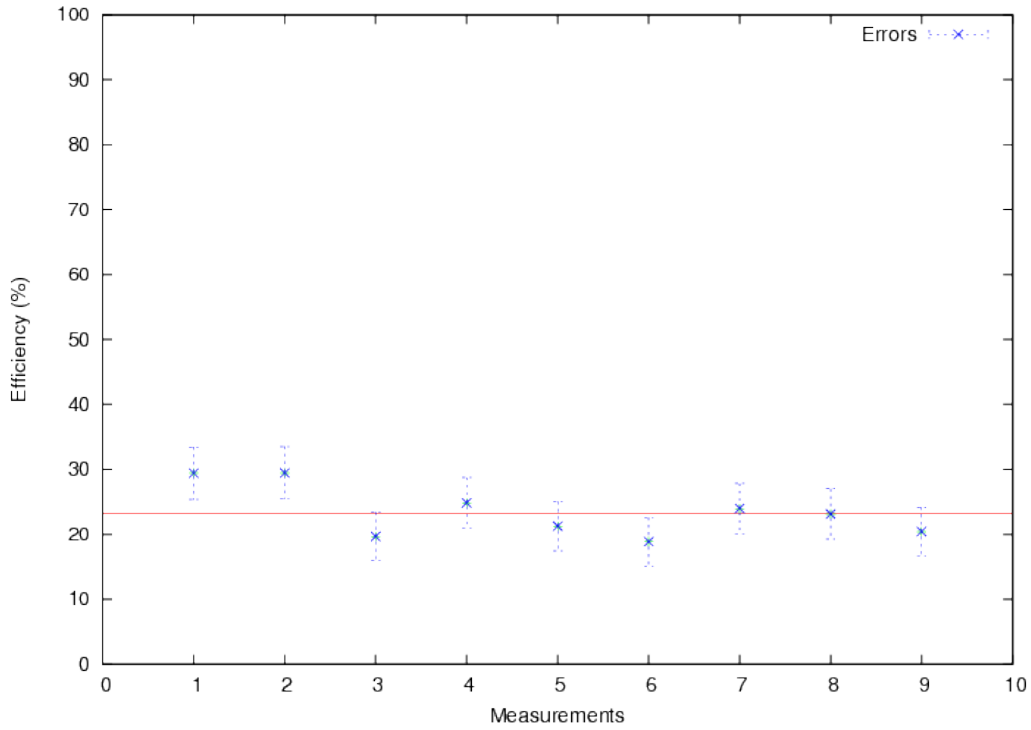

Figure 5.19.: Absolute correction measurements V 3.2: In this case 9 measurements have been used to calculate the finally efficiency. The new error calculated with the absolute scaling has been represented with blue color in the vertical axis. The red line indicates the mean value weighted by the absolute value.

Figure 5.19 shows the final efficiency corrected with the absolute scaling. In this case nine measurements have been measured to determinate the efficiency. The calculation shows that the mean value of the efficiency with the statistical error has been fixed in:

$$\text{Efficiency} = (0.232 \pm 0.013) \tag{5.3}$$

In this result the value of the absolute error was calculated in $u_{\text{absolute}} = \pm 0.035$. Using the same method for the last calculation, the uncertainty of ± 0.035 will give the uncertainty for the new measurements.

The new value of the efficiency is more stable in the new setup. The argument of the low efficiency proposed here is: The creation of the film on the cool head. The problem could be that the film on the cold head hasn't all quantity of cooled radon. During the injection 76.8% of the radon is lost by reflection of the radon particles on the cold head . Although a good point of this result is: The value of the efficiency reduction is constant and the measurements can be corrected.

Relative correction

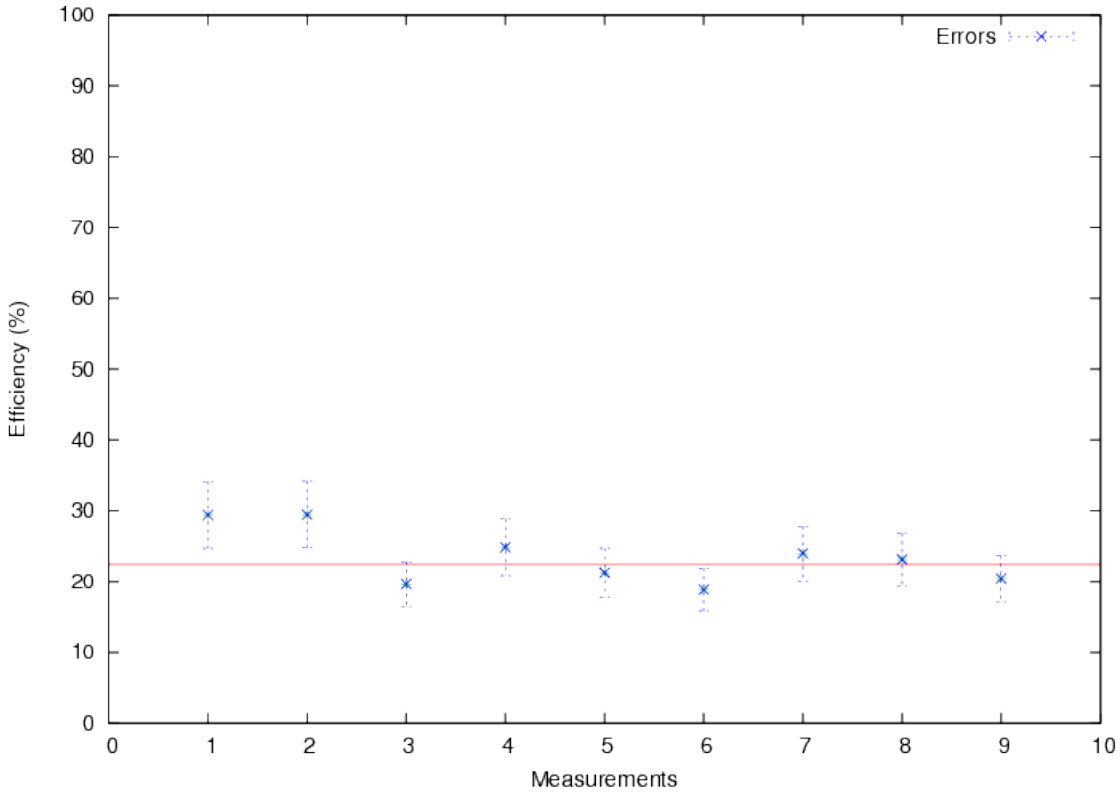

Figure 5.20.: Relative correction measurements V 3.2: In this case the same nine measurements have been used. The relative scaling of the error was written with blue color in the vertical axis. The red line indicates the mean value one more time. In this case six of nine measurements cut the mean value, it is the similar case that Figure 5.19.

Figure 5.20 shows the finally efficiency corrected with the relative scaling. The calculation shows that mean value of the efficiency with the statistical error has been fixed in:

$$\text{Efficiency} = (0.224 \pm 0.012) \tag{5.4}$$

In this result the value of the extra relative error was calculated in $u_{\text{relative}} = \pm 14\%$. Here with the newly introduced relative uncertainty one gets an total uncertainty of $\pm 14\%$ relative of the new measurement.

In this point the results 5.3 and 5.4 need to be compared. Comparing the methods, one can observe that the difference between the result is $\Delta\varepsilon_{\text{efficiency}} = 0.008$.
One can be observed that both results independent of the method used to calculate have similar values. If the two corrections give a similar value , it indicates that on the one hand the cause of the low efficiency is a constant, independently of the measurement because the value of the efficiency in this calculation is approximately similar that in the last calculation. On the other hand the system has won stability due to the value of u_{relative} has been reduced.

Conclusion of the lasts measurements, V 3.2

In this point the final result of the radon air measurement will be present.
A similar value of the efficiency result with both methods give a certain of the efficiency value. More important that reach a high efficiency is the stability point. It has been shown that the global efficiency of the system has improved around 10% more than the original setup, it is a good point.
Values 5.3 and 5.4 have error compatible, it means that the correct value of the efficiency will be a number between them, however the value 5.3 will be chosen. The reasons to choose this value is because the most important problem of the setup is the cryo-adsorption of the cold head. Eliminated the possibility to lost radon during the cooling down the only possibility is that the 76.8% of the cooled radon is lost during the injection by reflection of the particles on the cold head.
To finalize this paragraph the final efficiency of the radon air detection system will be given: [5]

$$\text{Efficiency: } \varepsilon_{\text{system}} = 0.232 \pm 0.013 \tag{5.5}$$

[5]This date will be used to calculate the radon air concentration in the experimental measurements

6. Radon measurements

In this chapter measurements of the basement, floors and background of the laboratory in the building of physics will be presented. The chapter will be started with an introduction of the equations used to calculate the radon air concentration. Finished the determination of the global efficiency in the last chapter, this parameter will be used during the next sections to correct the measurement. In the next sections six radon air measurement in the basement of the physics building have been performed, it will be shown in the section 6.2. Normally, one will expected that a radon air concentration will be obtained in a basement because in a non-ventilated room could accumulate a detectable radon concentration. The next section 6.3 will treat floor measurements. In total seven measurements of every floor in the physics building have been done. In this case one will appreciate a smaller radon concentration compared with the last section. Finally to close this chapter two measurements of the air in the laboratory will be performed, see section 6.4. These measurements will be used as background and to show that there is any radon concentration in a ventilated room.

6.1. Calculation of radon concentration in air

Concentration of a radon measurement will be obtained as a modification of a equation developed in [Nus11] and [Net94]. With this new setup in every radon measurement a background measurement is performed. A background correction is executed by the fit program ROOT during the calculation of the area of the radon peak. The activity of a radioactive element in an air sample is defined as:

$$C_A = \frac{A}{V}(\mathrm{Bq/m^3}). \tag{6.1}$$

Using the definition 6.1, the efficiency 5.5, the formula 2.63 and the correction by t_{diff} 2.64 one finds:

$$C_{A,Rn} = \frac{1}{\varepsilon_{\mathrm{system}}} \cdot (\frac{Area_{^{222}Rn}}{t_{\mathrm{life}}}) \cdot (\frac{1000(\mathrm{l/m^3})}{V_{\mathrm{Plas.\ bag}}}) \cdot (\frac{4\pi}{\Omega}) \cdot (\frac{1}{P_\alpha}) \cdot e^{+\lambda_{Rn} t_{diff}}. \tag{6.2}$$

Where
*ε_{system} is the value determined in value 5.5
*$V_{\mathrm{Plas.\ bag}}$ is 10 l, the capacity of the plastic air bag
*$\Omega = (4.23 \pm 0.1)\,\mathrm{Sr}$ (see Value 2.61)

The radon concentration can be calculated with the area of the daughter peaks. The next formula will be used to obtain a value of the radon concentration using the family peaks of ^{222}Rn, applying the Bateman equations 2.16.

$$^{222}Rn \xrightarrow{\lambda_{^{222}Rn}} {}^{218}Po \xrightarrow{\lambda_{^{218}Po}} {}^{214}Pb \xrightarrow{\lambda_{^{214}Pb}} {}^{214}Bi \xrightarrow{\lambda_{^{214}Bi}} {}^{214}Po \xrightarrow{\lambda_{^{214}Po}} {}^{210}Pb$$

Making use of the Bateman equation for the activity of ^{218}Po and ^{214}Po[1]:

$$A_{^{218}Po} = A_{^{222}Rn} \sum_{i=1}^{2} C_i e^{-\lambda_i t} \Rightarrow A_{^{222}Rn} = \frac{A_{^{218}Po}}{\sum_{i=1}^{2} C_i e^{-\lambda_i t}}. \tag{6.3}$$

$$A_{^{214}Po} = A_{^{222}Rn} \sum_{i=1}^{5} C_i e^{-\lambda_i t} \Rightarrow A_{^{222}Rn} = \frac{A_{^{214}Po}}{\sum_{i=1}^{5} C_i e^{-\lambda_i t}}. \tag{6.4}$$

[1]The method was developed in [Net94] and [Nus11]

The Bateman coefficients are given by [Nus11]:
$^{*}c_1 = 1.009$
$^{*}c_2 = -0.024$
$^{*}c_3 = -4.413$
$^{*}c_4 = 3.428$
$^{*}c_5 = 1.2 \times 10^{-20}$

6.2. Measurements of basement samples

In the measurements of the basement, six measurements in the basement of the institute of nuclear physics have been developed. All radon air concentration will be calculated with the equation 6.2. The peaks ^{218}Po and ^{214}Po will be used as well as the equation to calculate these peaks can be found in 6.3 and 6.4. Normally in a measurement of radon air a low radon concentration will be expected. In this case the uncertainty of the measurement will be high. A example of basement sample can be observed in Figure 6.1, the rest of basements measurements have been included in the appendix of this master thesis, see appendix: A.47, A.48, A.49, A.50, A.51, A.52. The too low quantity of impulses gives a measurement with a high uncertainty. It can be observed in all of results here obtained during the measurements of the basement samples. In all measurements, the uncertainty here expressed comes from the fit program used to fit the spectra using the fit function 2.48. In the peak ^{222}Rn normally, the radon concentration should have the minimal uncertainty because the concentration is calculated direct using the equation 6.2. In the case of the peaks ^{218}Po and ^{214}Po the radon concentration is calculated using the equations 6.3 and 6.4. It should show a higher uncertainty due to a littler rate counts than the peak ^{222}Rn.
In every measurement, values of the sum of counts for the peaks ^{222}Rn, ^{218}Po and ^{214}Po will be shown, as well as the final radon concentration calculated with the uncertainty. In some measurements due to the too low counts a result of the concentration has not given. The too low number of counts made impossible fit the spectra.

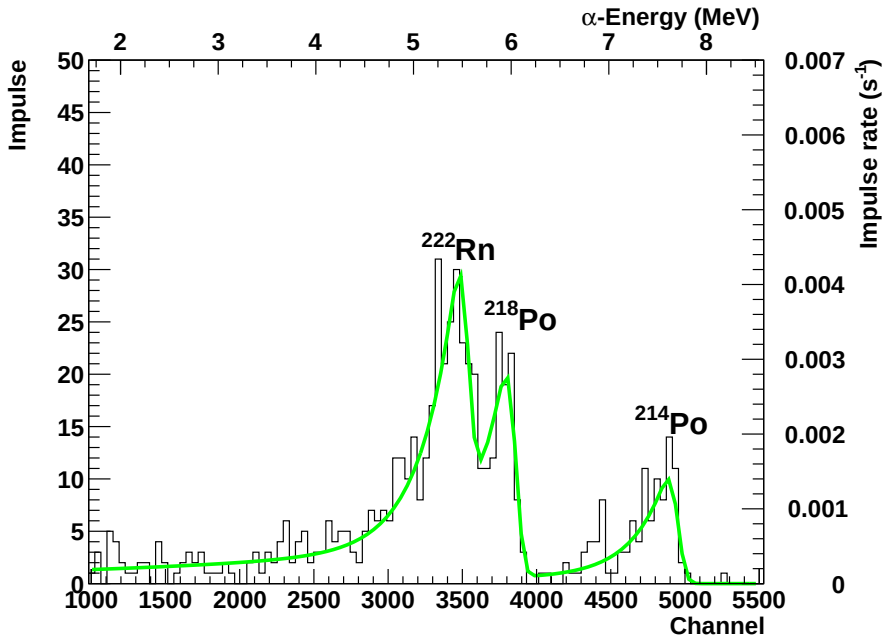

Figure 6.1.: Measurement of the basement: N°1, date: 16.07.2012. In this plot one of the six measurements has been shown. This measurement is a example of a low impulse counts. It indicates that the fit of the spectra will present a high uncertainty. The uncertainty of the result is obtained using the fit program.

Measurement of basement 16.07.2012, N°1

Nucleus	^{222}Rn	^{218}Po	^{214}Po
Counts	58 ± 12	49 ± 12	25 ± 5

Radon air concentration obtained by the peaks.

- $C_{A,222Rn} = (10.5 \pm 2.7)\text{Bq/m}^3$ obtained by the ^{222}Rn-peaks.
- $C_{A,222Rn} = (9.1 \pm 2.6)\text{Bq/m}^3$ obtained by the ^{218}Po-peaks.
- $C_{A,222Rn} = (4.7 \pm 1.2)\text{Bq/m}^3$ obtained by the ^{214}Po-peaks.

Measurement of basement 17.07.2012, N°2

Nucleus	^{222}Rn	^{218}Po	^{214}Po
Counts	N.A	89 ± 21	46 ± 9

Radon air concentration obtained by the peaks.

- $C_{A,222Rn}$ =(N.A) Bq/m^3 obtained by the ^{222}Rn-peaks[2].
- $C_{A,222Rn} = (16.3 \pm 4.7)$ Bq/m^3 obtained by the ^{218}Po-peaks.
- $C_{A,222Rn} = (8.7 \pm 2.2)$ Bq/m^3 obtained by the ^{214}Po-peak.

Measurement of basement 18.07.2012, N°3

Nucleus	^{222}Rn	^{218}Po	^{214}Po
Counts	26 ± 7	34 ± 7	21 ± 4

Radon air concentration obtained by the peaks.

- $C_{A,222Rn} = (4.5 \pm 1.4)$ Bq/m^3 obtained by the ^{222}Rn-peaks.
- $C_{A,222Rn} = (6.0 \pm 1.6)$ Bq/m^3 obtained by the ^{218}Po-peaks.
- $C_{A,222Rn} = (3.8 \pm 0.9)$ Bq/m^3 obtained by the ^{214}Po-peak.

Measurement of basement 19.07.2012, N°4

Nucleus	^{222}Rn	^{218}Po	^{214}Po
Counts	51 ± 22	35 ± 17	32 ± 17

Radon air concentration obtained by the peaks.

- $C_{A,222Rn} = (8.8 \pm 4.1)$(Bq/m^3) obtained by the ^{222}Rn-peaks.
- $C_{A,222Rn} = (6.1 \pm 3.1)$(Bq/m^3) obtained by the ^{218}Po-peaks.
- $C_{A,222Rn} = (5.9 \pm 3.2)$(Bq/m^3) obtained by the ^{214}Po-peaks.

[2]Not Available. In this case the uncertainty is higher than the measurement

Measurement of basement 20.07.2012, N°5

Nucleus	^{222}Rn	^{218}Po	^{214}Po
Counts	80 ± 19	43 ± 1	41 ± 10

Radon air concentration obtained by the peaks.

- $C_{A,222Rn} = (14.6 \pm 4.2)(\mathrm{Bq/m^3})$ obtained by the ^{222}Rn-peaks.
- $C_{A,222Rn} = (8.0 \pm 1.3)(\mathrm{Bq/m^3})$ obtained by the ^{218}Po-peaks.
- $C_{A,222Rn} = (7.9 \pm 2.3)(\mathrm{Bq/m^3})$ obtained by the ^{214}Po-peaks.

Measurement of basement 23.07.2012, N°6

Nucleus	^{222}Rn	^{218}Po	^{214}Po
Counts	90 ± 67	69 ± 52	34 ± 26

Radon air concentration obtained by the peaks.

- $C_{A,222Rn} = (16.4 \pm 12.5)(\mathrm{Bq/m^3})$ obtained by the ^{222}Rn-peaks.
- $C_{A,222Rn} = (12.7 \pm 9.9)(\mathrm{Bq/m^3})$ obtained by the ^{218}Po-peaks.
- $C_{A,222Rn} = (6.5 \pm 5.0)(\mathrm{Bq/m^3})$ obtained by the ^{214}Po-peaks.

To conclude the section of basement measurement, a normal radon concentration has been found. Maybe a low radon concentration but it is normal value for a non-ventilated room.

6.3. Measurements of floor samples

In this section a smaller radon concentration than the last measurements will be expected. The reason is because normally in a good ventilated room there is not radon concentration. All measurement will present in floor order. One will expect a little concentration in the basement floor and it will decrease. In this section seven measurements correspondent to the floor: -1, 0, +1, +2, +3, +4, +5 will be presented. An example of measurement in the floor number 2 has been shown in Figure 6.2. The rest of plots can be found in the appendix of this master thesis: A.53, A.54, A.55, A.56, A.57, A.58, A.59. In this plot, it can observed the low count. The uncertainty of the measurements will be calculated using the fit program with the fit function 2.48. The result will be presented in the next lines showing the counts measured for every peaks and the uncertainty proportionated by the fit program.

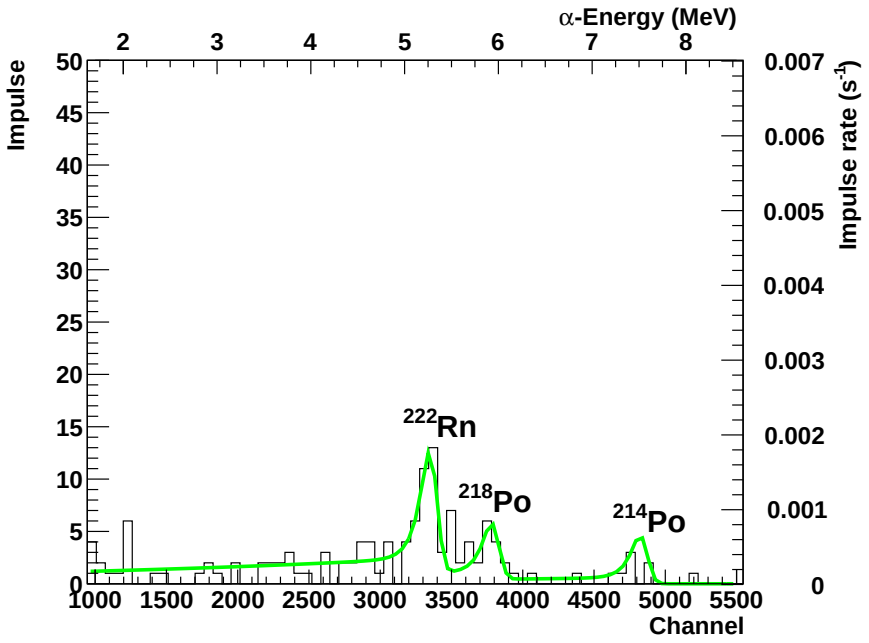

Figure 6.2.: Measurement of the floor: (2). This plot is an example of the measurements performed on the floors of the institute of nuclear physics. In this plot a low count of detected particles has been shown. The low count will make difficult realize a good fit of the peaks, for this reason an uncertainty in the measurements will be expected.

Measurement of floor (-1) 24.07.2012, N°1

Nucleus	^{222}Rn	^{218}Po	^{214}Po
Counts	65 ± 18	61 ± 13	43 ± 10

Radon air concentration obtained by the peaks.

- $C_{A,222Rn} = (11.8 \pm 3.8)(\mathrm{Bq/m^3})$ obtained by the ^{222}Rn-peaks.
- $C_{A,222Rn} = (11.3 \pm 3.1)(\mathrm{Bq/m^3})$ obtained by the ^{218}Po-peaks.
- $C_{A,222Rn} = (8.1 \pm 2.4)(\mathrm{Bq/m^3})$ obtained by the ^{214}Po-peaks.

Measurement of floor (0) 25.07.2012, N°2

Nucleus	^{222}Rn	^{218}Po	^{214}Po
Counts	32 ± 5	19 ± 4	5 ± 2

Radon air concentration obtained by the peaks.

- $C_{A,222Rn} = (5.9 \pm 1.3)(\mathrm{Bq/m^3})$ obtained by the ^{222}Rn-peaks.
- $C_{A,222Rn} = (3.6 \pm 0.9)(\mathrm{Bq/m^3})$ obtained by the ^{218}Po-peaks.
- $C_{A,222Rn} = (1.0 \pm 0.4)(\mathrm{Bq/m^3})$ obtained by the ^{214}Po-peaks.

Measurement of floor (+1) 26.07.2012, N°3

Nucleus	^{222}Rn	^{218}Po	^{214}Po
Counts	25 ± 22	10 ± 6	N.A

Radon air concentration obtained by the peaks.

- $C_{A,222Rn} = (4.6 \pm 4.0)(\mathrm{Bq/m^3})$ obtained by the ^{222}Rn-peaks.
- $C_{A,222Rn} = (1.9 \pm 1.1)(\mathrm{Bq/m^3})$ obtained by the ^{218}Po-peaks.
- $C_{A,222Rn} = (\mathrm{N.A})(\mathrm{Bq/m^3})$ obtained by the ^{214}Po-peaks.

Measurement of floor (+2) 27.07.2012, N°4

Nucleus	^{222}Rn	^{218}Po	^{214}Po
Counts	50 ± 27	23 ± 13	20 ± 10

Radon air concentration obtained by the peaks.

- $C_{A,222Rn} = (9.2 \pm 5.1)(\mathrm{Bq/m^3})$ obtained by the ^{222}Rn-peaks.
- $C_{A,222Rn} = (4.3 \pm 2.5)(\mathrm{Bq/m^3})$ obtained by the ^{218}Po-peaks.
- $C_{A,222Rn} = (3.8 \pm 2.1)(\mathrm{Bq/m^3})$ obtained by the ^{214}Po-peaks.

Measurement of floor (+3) 30.07.2012, N°5

Nucleus	^{222}Rn	^{218}Po	^{214}Po
Counts	10 ± 3	N.A	N.A

Radon air concentration obtained by the peaks.

- $C_{A,222Rn} = (1.8 \pm 0.7)(\mathrm{Bq/m^3})$ obtained by the ^{222}Rn-peaks.
- $C_{A,222Rn} =$(N.A) obtained by the ^{218}Po-peaks.
- $C_{A,222Rn} =$(N.A) obtained by the ^{214}Po-peaks.

Measurement of floor (+4) 28.08.2012, N°6

Nucleus	^{222}Rn	^{218}Po	^{214}Po
Counts	30 ± 15	22 ± 10	17 ± 7

Radon air concentration obtained by the peaks.

- $C_{A,222Rn} = (5.5 \pm 2.8)(\mathrm{Bq/m^3})$ obtained by the ^{222}Rn-peaks.
- $C_{A,222Rn} = (4.1 \pm 2.0)(\mathrm{Bq/m^3})$ obtained by the ^{218}Po-peaks.
- $C_{A,222Rn} = (3.2 \pm 1.5)(\mathrm{Bq/m^3})$ obtained by the ^{214}Po-peaks.

Measurement of floor (+5) 29.08.2012, N°7

Nucleus	^{222}Rn	^{218}Po	^{214}Po
Counts	47 ± 6	21 ± 5	10 ± 3

Radon air concentration obtained by the peaks.

- $C_{A,222Rn} = (8.5 \pm 1.8)(\mathrm{Bq/m^3})$ obtained by the ^{222}Rn-peaks.
- $C_{A,222Rn} = (3.9 \pm 1.1)(\mathrm{Bq/m^3})$ obtained by the ^{218}Po-peaks.
- $C_{A,222Rn} = (1.8 \pm 0.6)(\mathrm{Bq/m^3})$ obtained by the ^{214}Po-peaks.

In general in measurements where radon air concentration is less than $5\,\mathrm{Bq/m^3}$ determinate the radon air concentration is a difficult task. In this case the uncertainty is too high to give a result.

6.4. Measurements of background samples

In this section the background measurements of the laboratory will be exposed. The background measurements correspond of two measurements of the air in the laboratory done. Two probes with different waiting times have been measured. The first one (measured: 13.07.2012) was 269 days, 3 hours and 14 minutes in the case of the second one (measured: 18.09.2012) was 66 days 20 hours and 23 minutes. For these air tests no radon concentration will be expected. The idea is to measure an air probe without radon concentration, look at the spectra and compare with a normal spectra. These measurements will be considered the background of the system. The radon half-life is 3.8 days, it is easy to suppose that in these samples any radon air concentration will be found. In the next lines the results and a finally commentary will be attached. In Figures 6.3 and 6.4 the measurements performed have been shown and calculation of the radon concentration with the uncertainty have been performed.

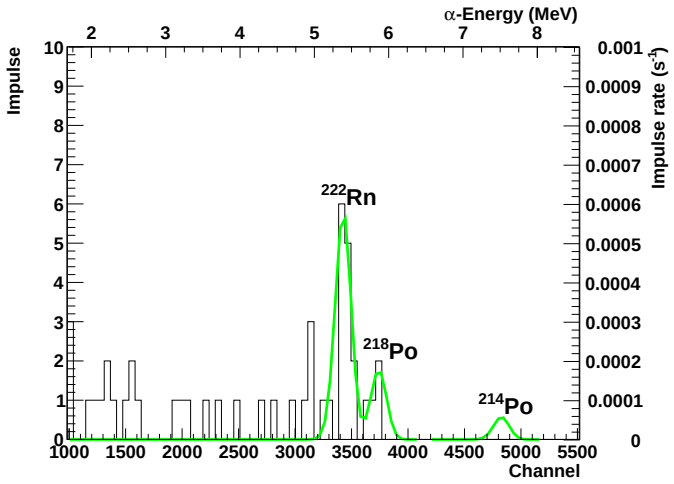

Figure 6.3.: Background measurement of the laboratory air: 13.07.2012. The waiting time was 269 days, 3 hours and 14 minutes.

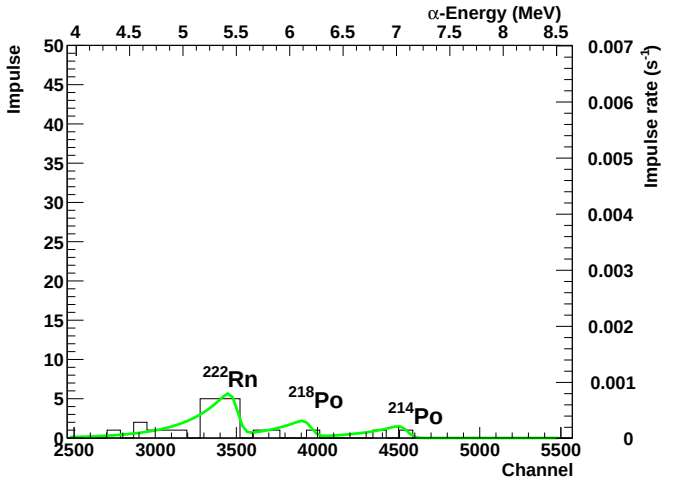

Figure 6.4.: Background measurement of the laboratory air: 18.09.2012. The waiting time was 66 days 20 hours and 23 minutes.

Background measurement in laboratory 13.07.2012

Nucleus	^{222}Rn	^{218}Po	^{214}Po
Counts	7 ± 2	2 ± 1	1 ± 1

Radon air concentration obtained by the peaks.

- $C_{A,222Rn} = (1.2 \pm 0.4)(\mathrm{Bq/m^3})$ obtained by the ^{222}Rn-peaks.
- $C_{A,222Rn}$=(N.A) obtained by the ^{218}Po-peaks[3].
- $C_{A,222Rn}$=(N.A) obtained by the ^{214}Po-peaks.

Background measurement in laboratory 18.09.2012

Nucleus	^{222}Rn	^{218}Po	^{214}Po
Counts	17 ± 2	7 ± 1	5 ± 1

Radon air concentration obtained by the peaks.

- $C_{A,222Rn} = (3.1 \pm 0.6)(\mathrm{Bq/m^3})$ obtained by the ^{222}Rn-peaks.
- $C_{A,222Rn} = (1.2 \pm 0.3)(\mathrm{Bq/m^3})$ obtained by the ^{218}Po-peaks.
- $C_{A,222Rn}$= (N.A) obtained by the ^{214}Po-peaks.

In both measurements, determinate the radon concentration with a low impulse rate were a difficult tasks. If the radon concentration is less than $5\,\mathrm{Bq/m^3}$, it can insure that no radon concentration is present in the air.

[3]Not Available. In this case the error is higher than the measurement

7. Conclusions

To finish this master thesis the most important results will be summarized.
At the start of the master thesis the original intentions were to determine the actual conditions of the setup, to perform systematic measurements, to determine the global efficiency of the setup and as the most important objective, to optimize the system in order to achieve a better efficiency.

During the first part of the work of this thesis, firstly a good number of measurements have been done. Thanks to a high number of measurements all instabilities of the system could be discovered. A first value of the efficiency of 22.1% was calculated, but with a high uncertainty. The most important sources of error at this moment were: The control of the temperature in the cryogenic systems, the expansion of the gas before the injection and the vacuum losses due to the *Alcatel* pump.

Studied the setup, the second part of this master thesis were improvements of the system: The first difficulty was solved with the program *Temp V 2.5*, a better control of temperature eliminated the possibility of radon losses in the cryogenic modules and made it easy to perform systematic measurements.
Secondly to avoid radon losses before the injection an isolator gas system was developed. During the heating up of the radon the gas was expanding into the whole system, what was solved with the new valve system. Thirdly exchanging the original pump for the new pump *Leybold*, the background was reduced and the system won stability.

The result of all modifications were: On the one hand a better efficiency of the global system has been reached. The finally efficiency was established at 23.2%. On the other hand a better stability of the system has been found. This indicates that the system works now with repeatability.

Finished all improvements of the experimental setup, measurements of air samples have been done: Six measurements in the basement and six measurements of the floors in the institute of nuclear physics were performed. The results were the expected radon concentration for closed places, always values below $100\,\mathrm{Bq/m^3}$. In some cases the radon air concentration could not be measured due to the low quantity of radon in air $< 2\,\mathrm{Bq/m^3}$.

Outlook

In the end, some tips for future improvements are given in the following.
To solve instabilities in the gas system it would be optimal to buy a new pump similar to the actual *TRIVAC D16B* with a pumping speed of $16.5\,\mathrm{m^3/h}$ or more, as the actual pump belongs to a pumping station.
Another important aspect is the absorption of the radon on the cold head. With a vacuum of almost $10^{-6}\,\mathrm{mbar}$ the MFP[1] lies in the range from 10 cm to 1 km. This means that during the injection particles could be caught by the cool head or reflected. One solution can be to build an interchangeable cold head. It could be a cold head composed of a different material or design.
One could use a different carrier gas, for example He, H_2 or O_2. The central point is to check the cryogenic adsorption of the radon on the cold head during the injection. It will be a good point to check the length of the radon trap. An efficiency test could be to test another length of the radon trap. Because of using a pump with a higher pumping speed, efficiency has been increased. It could be a possibility that the length of the radon trap is excessive.

[1]MFP (Mean Free Path) [fmt]

A. Plots

A.1. Calibrations

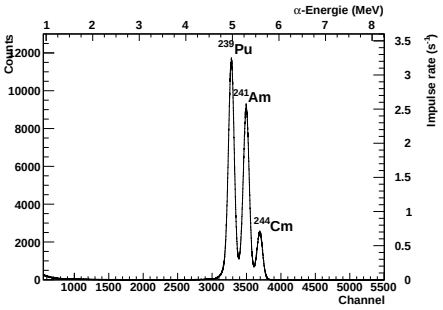

Figure A.1.: Calibration with $a = 5\,\mathrm{mm}$

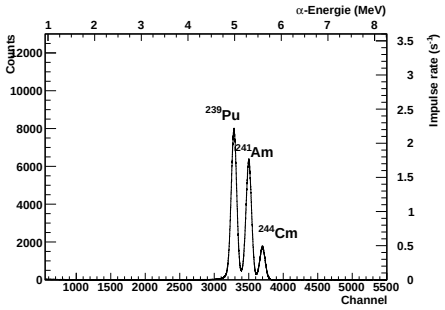

Figure A.2.: Calibration with $a = 10\,\mathrm{mm}$

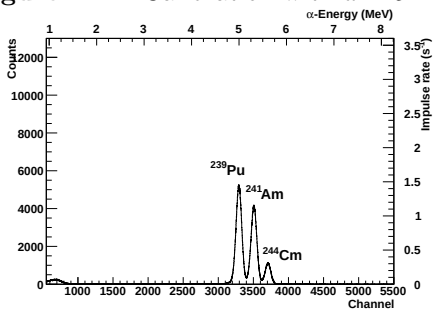

Figure A.3.: Calibration with $a = 15\,\mathrm{mm}$

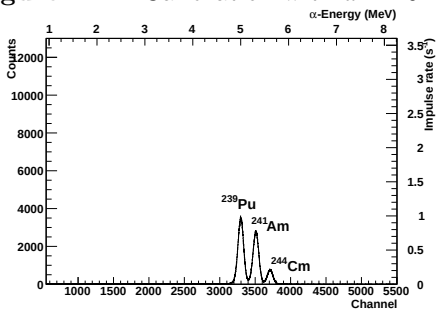

Figure A.4.: Calibration with $a = 20\,\mathrm{mm}$

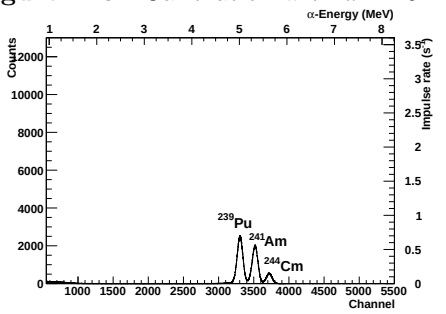

Figure A.5.: Calibration with $a = 25\,\mathrm{mm}$

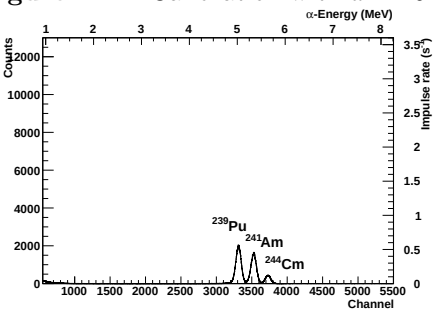

Figure A.6.: Calibration with $a = 30\,\mathrm{mm}$

A.2. Measurements with setup V3.1

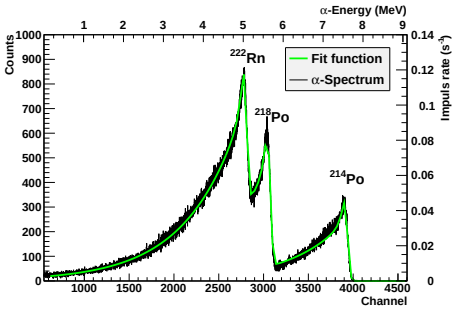

Figure A.7.: Efficiency measurement 30.09.2011, N°1

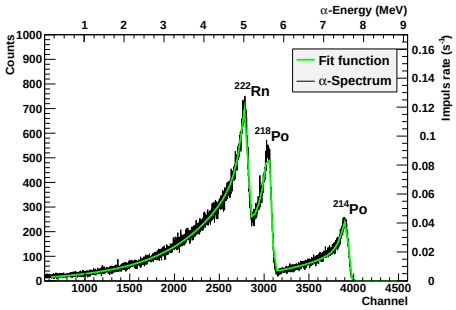

Figure A.8.: Efficiency measurement 04.10.2011, N°2

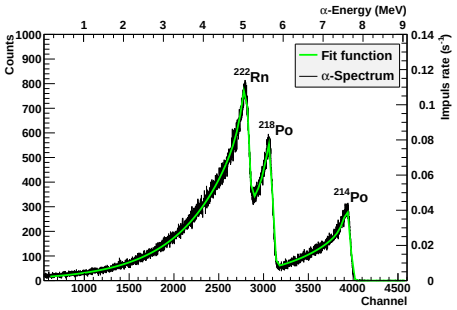

Figure A.9.: Efficiency measurement 07.10.2011, N°3

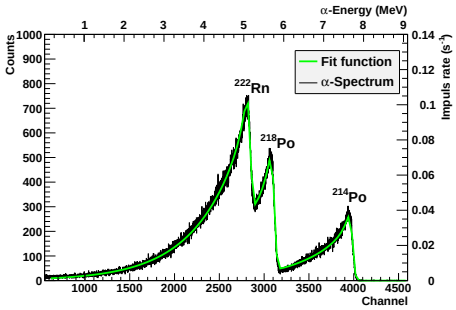

Figure A.10.: Efficiency measurement 12.10.2011, N°4

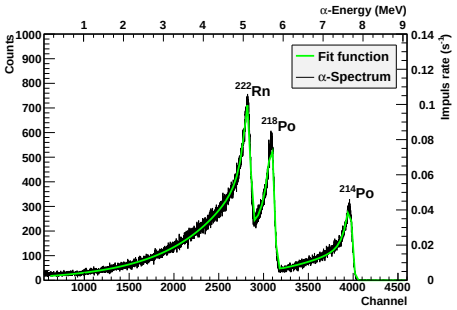

Figure A.11.: Efficiency measurement 14.10.2011, N°5

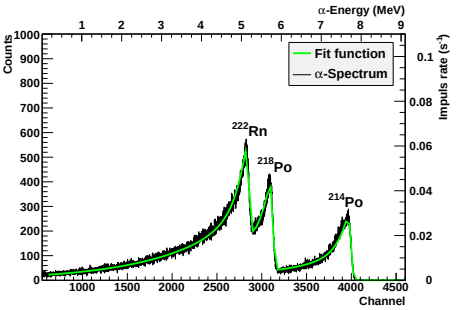

Figure A.12.: Efficiency measurement 17.10.2011, N°6

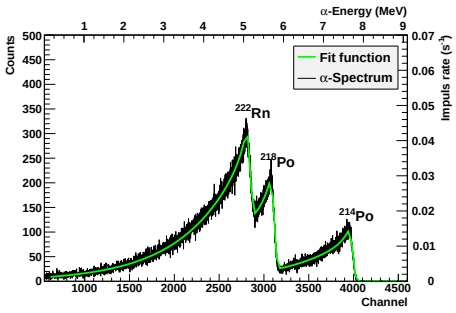

Figure A.13.: Efficiency measurement 19.10.2011, N°7

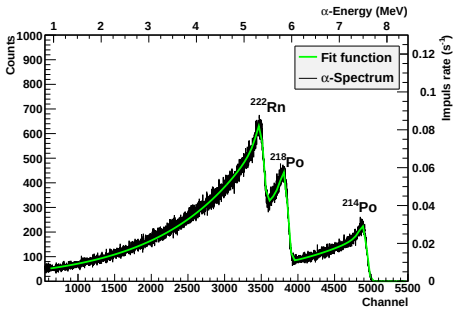

Figure A.14.: Efficiency measurement 25.10.2011, N°8

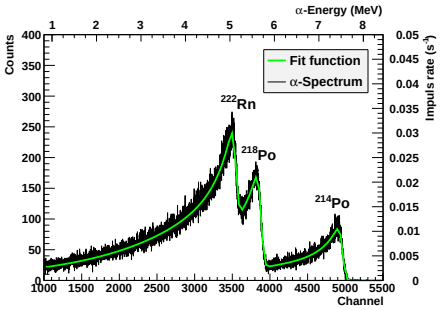

Figure A.15.: Efficiency measurement 26.10.2011, N°9

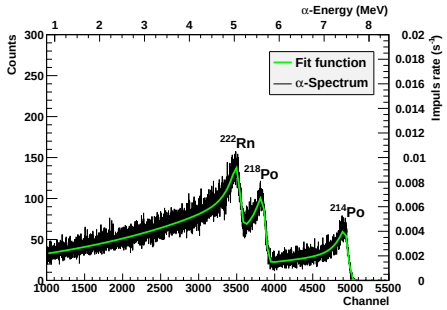

Figure A.16.: Efficiency measurement 27.10.2011, N°10

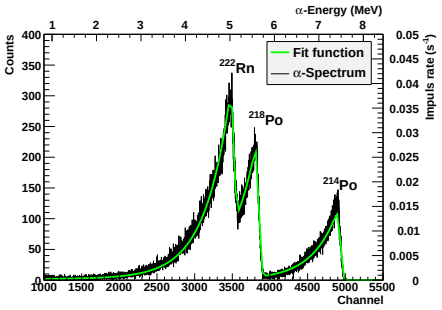

Figure A.17.: Efficiency measurement 28.10.2011, N°11

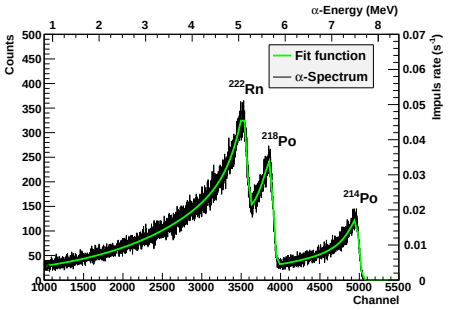

Figure A.18.: Efficiency measurement 31.10.2011, N°12

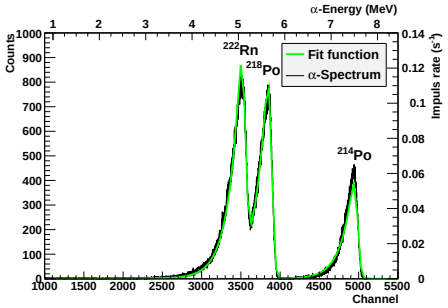

Figure A.19.: Efficiency measurement 02.11.2011, N°13

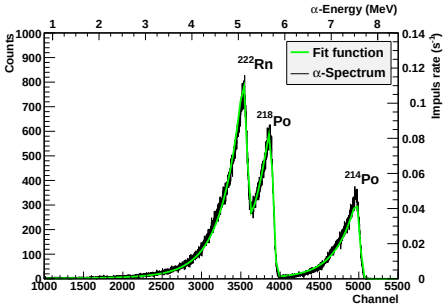

Figure A.20.: Efficiency measurement 04.11.2011, N°14

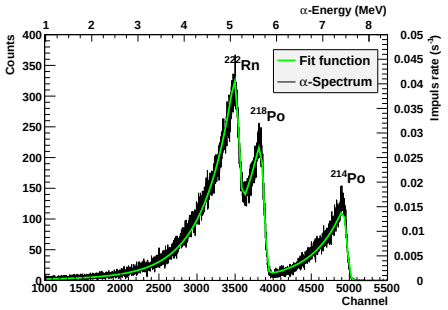

Figure A.21.: Efficiency measurement 09.11.2011, N°15

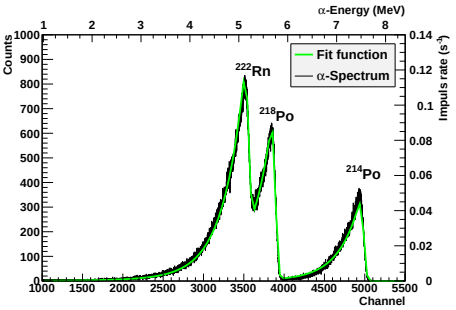

Figure A.22.: Efficiency measurement 14.11.2011, N°16

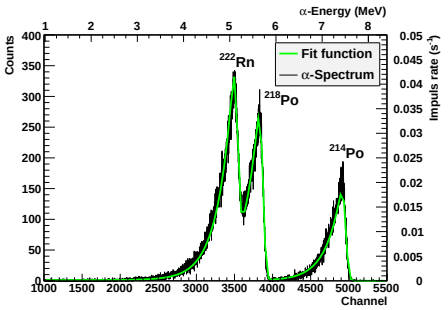

Figure A.23.: Efficiency measurement 15.11.2011, N°17

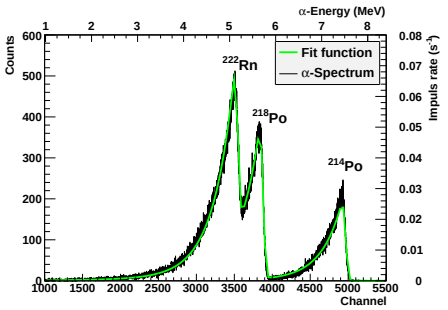

Figure A.24.: Efficiency measurement 18.11.2011, N°18

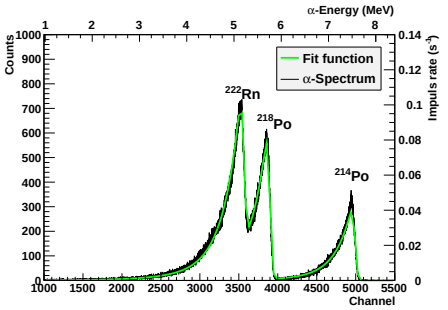

Figure A.25.: Efficiency measurement 21.11.2011, N°19

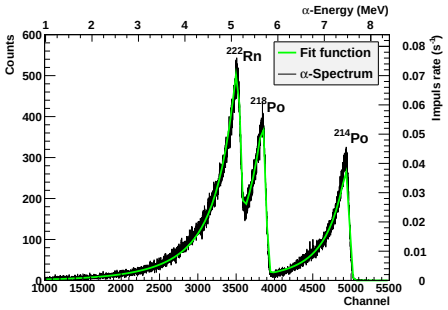

Figure A.26.: Efficiency measurement 22.11.2011, N°20

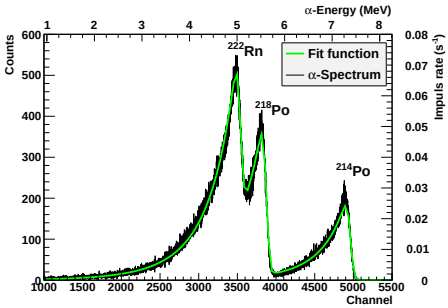

Figure A.27.: Efficiency measurement 18.01.2011, N°21

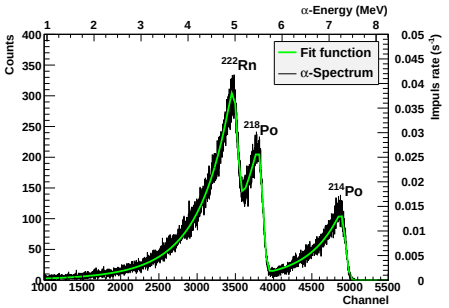

Figure A.28.: Efficiency measurement 19.01.2011, N°22

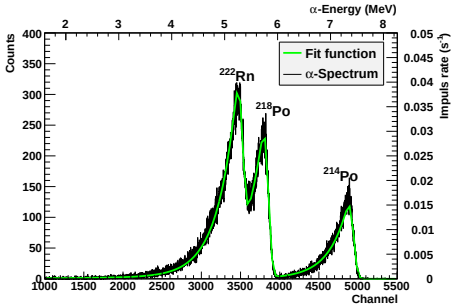

Figure A.29.: Efficiency measurement 20.01.2012, N°23

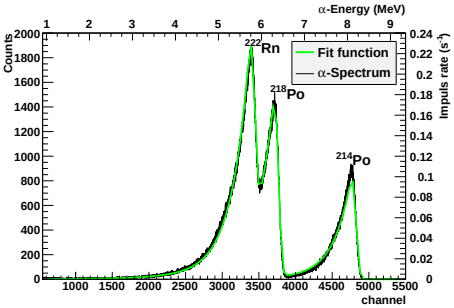

Figure A.30.: Efficiency measurement 31.01.2012, N°24

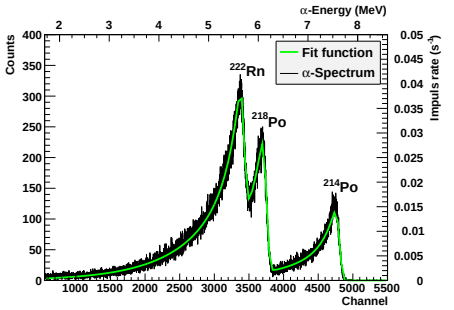

Figure A.31.: Efficiency measurement 01.02.2012, N°25

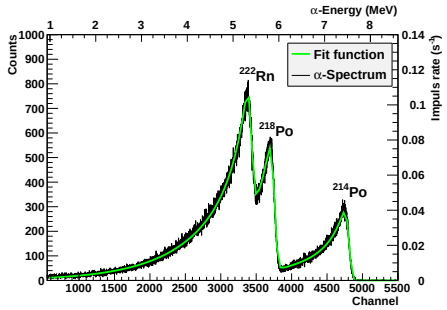

Figure A.32.: Efficiency measurement 07.02.2012, N°26

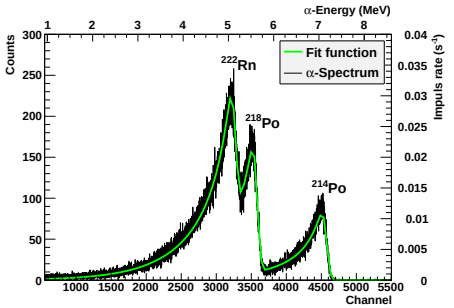

Figure A.33.: Efficiency measurement 08.02.2012, N°27

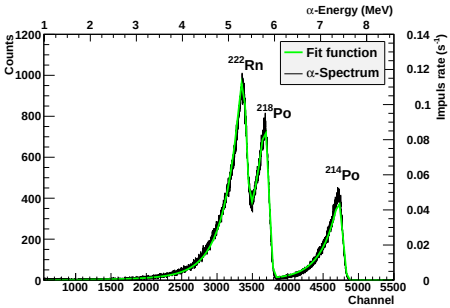

Figure A.34.: Efficiency measurement 13.02.2012, N°28

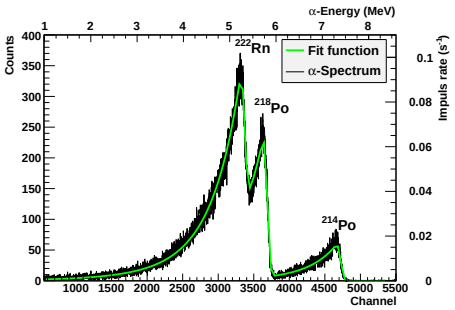

Figure A.35.: Efficiency measurement 17.02.2012, N°29

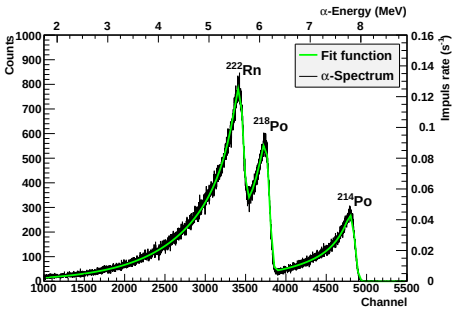

Figure A.36.: Efficiency measurement 27.02.2012, N°30

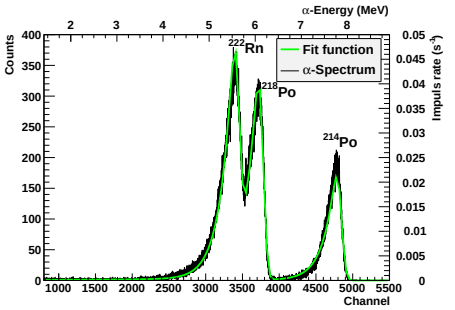

Figure A.37.: Efficiency measurement 28.02.2012, N°31

A.3. Measurements with setup V3.2

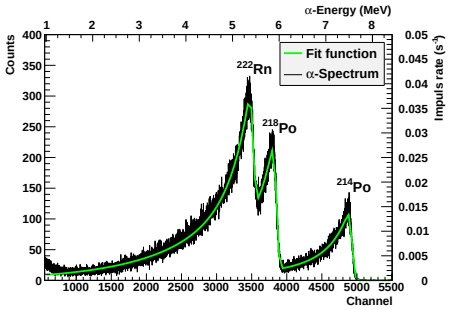

Figure A.38.: Efficiency measurement 16.06.2012, N°1

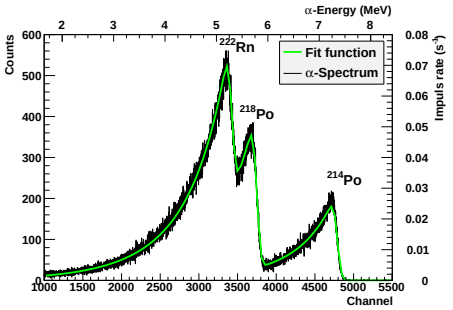

Figure A.39.: Efficiency measurement 18.06.2012, N°2

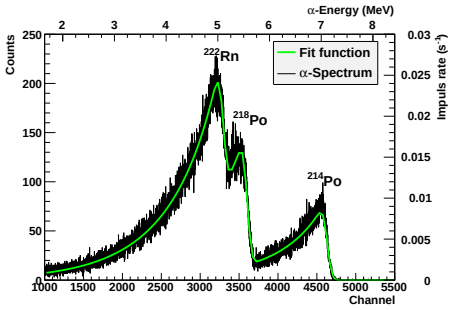

Figure A.40.: Efficiency measurement 20.06.2012, N°3

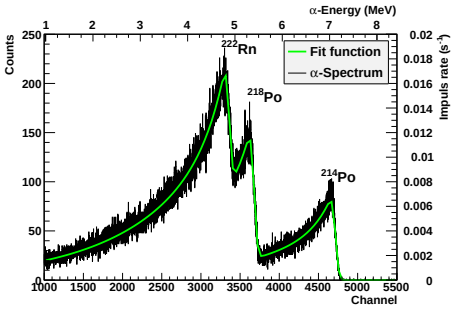

Figure A.41.: Efficiency measurement 21.06.2012, N°4

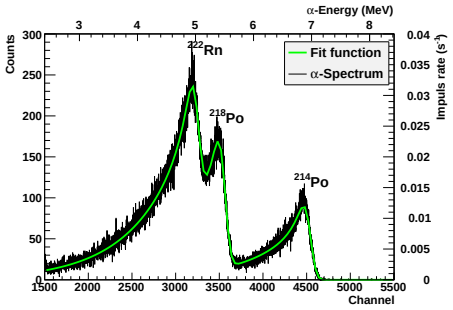

Figure A.42.: Efficiency measurement 22.06.2012, N°5

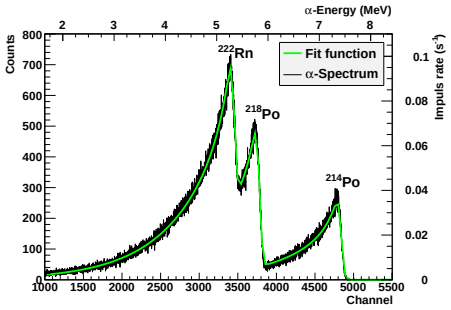

Figure A.43.: Efficiency measurement 27.06.2012, N°6

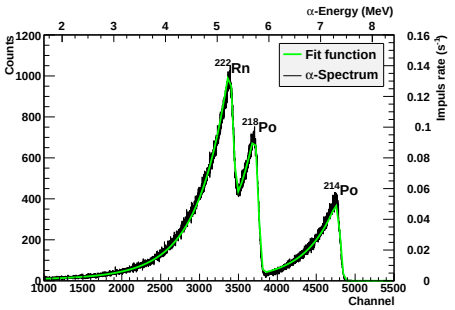

Figure A.44.: Efficiency measurement 02.07.2012, N°7

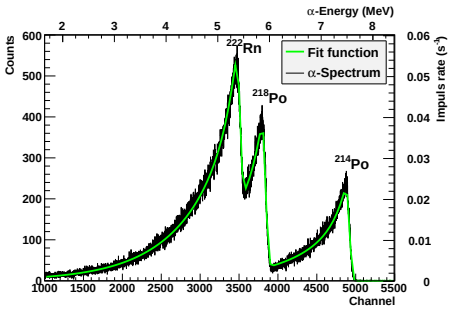

Figure A.45.: Efficiency measurement 04.07.2012, N°8

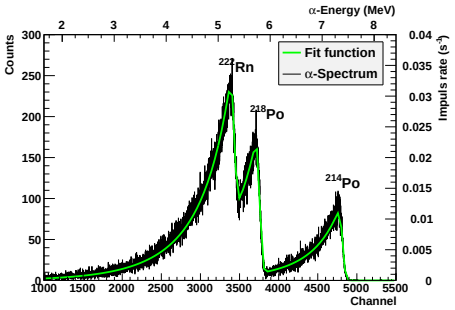

Figure A.46.: Efficiency measurement 05.07.2012, N°9

A.4. Measurements of basement samples

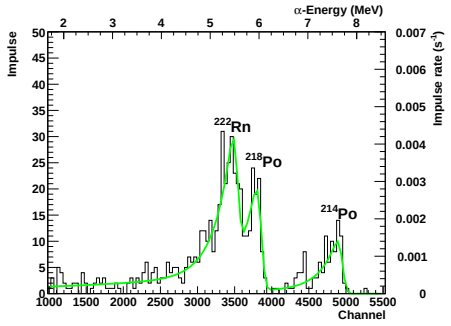

Figure A.47.: Basement measurement 16.07.2012, N°1

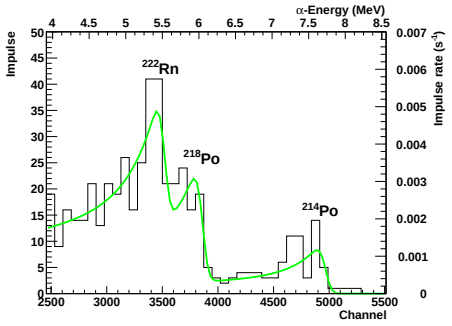

Figure A.48.: Basement measurement 17.07.2012, N°2

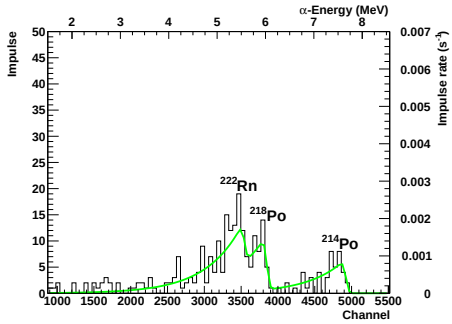

Figure A.49.: Basement measurement 18.07.2012, N°3

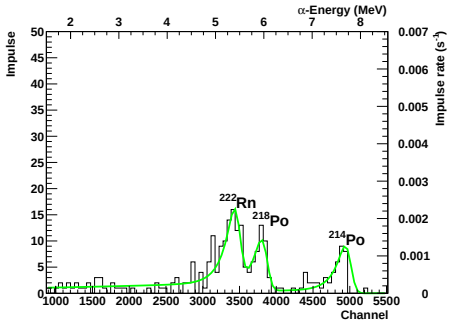

Figure A.50.: Basement measurement 19.07.2012, N°4

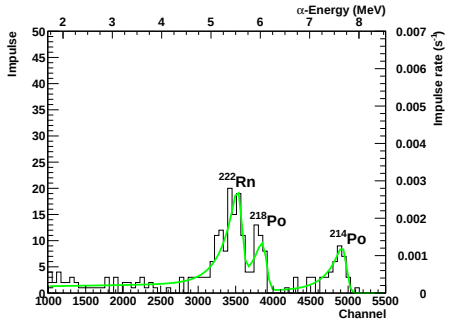

Figure A.51.: Basement measurement 20.07.2012, N°5

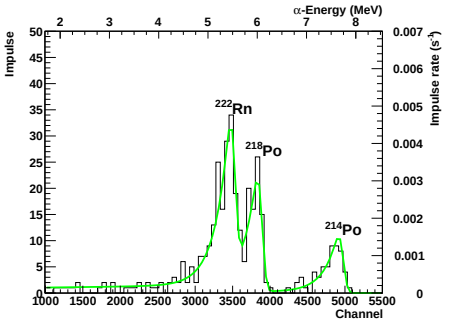

Figure A.52.: Basement measurement 23.07.2012, N°6

A.5. Measurements of floor samples

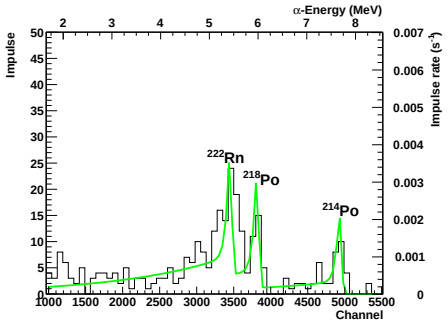

Figure A.53.: Floor (-1) 24.07.2012

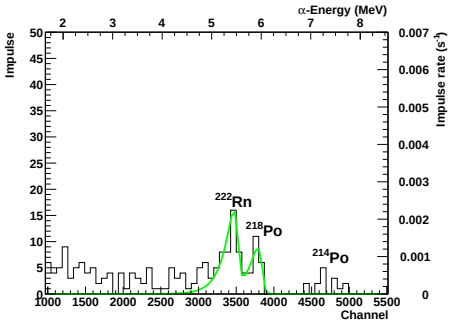

Figure A.54.: Floor (0) 25.07.2012

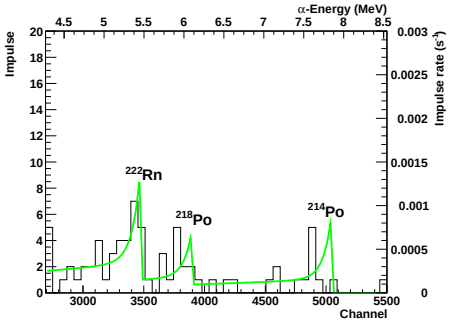

Figure A.55.: Floor (1) 26.07.2012

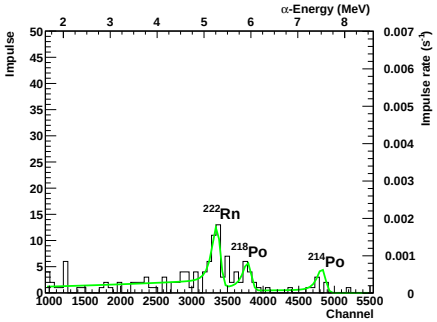

Figure A.56.: Floor (2) 27.07.2012

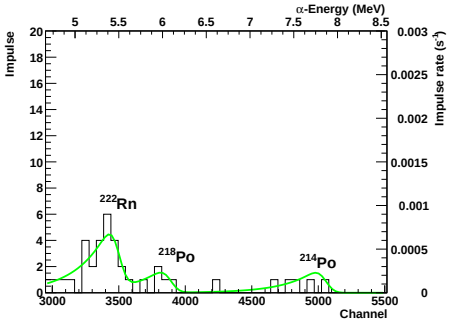

Figure A.57.: Floor (3) 30.07.2012

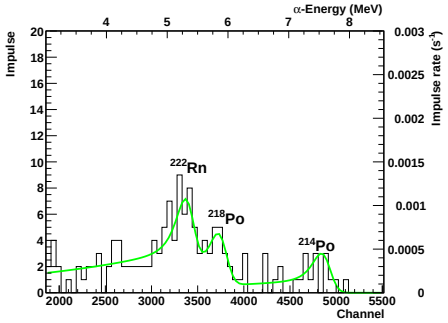

Figure A.58.: Floor (4) 28.08.2012

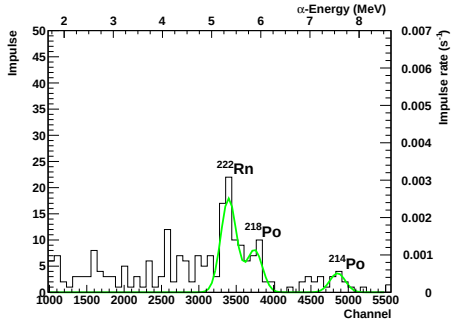

Figure A.59.: Floor (5) 29.08.2012

A.6. Measurements of background samples

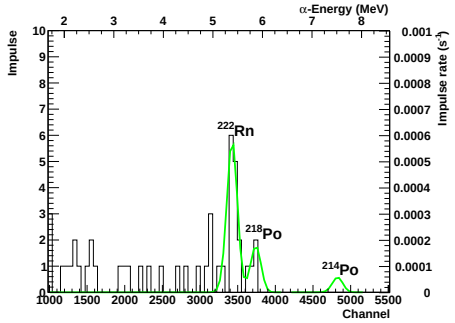

Figure A.60.: Background measurement in laboratory 13.07.2012

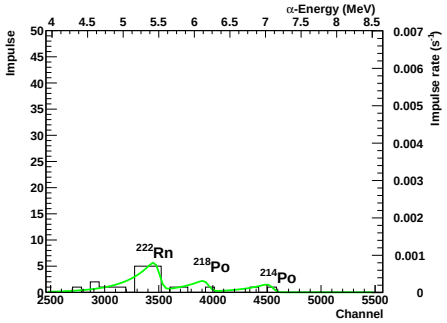

Figure A.61.: Background measurement in laboratory 18.09.2012

B. Relative and absolute corrections

B.1. Absolute correction

The absolute correction consists on introduction of a constant unknown error in the uncertainty of every measurement. Normally it is the case where a constant problem independent of the number of measurements can be detected. Absolute correction can be used to give a quantity of the problem. Source [Tä12] and [esc]
The Operation is:
There are data x_i with its error Δx_i. n is the number of data.

$$\{x_i\} \text{ and } \{\Delta x_i\} \text{ with } ; i = 1...n \tag{B.1}$$

A new error in the uncertain of every measurements will be added. It is called ε_{abs}

$$\begin{aligned} &x_1 \pm \Delta x_1 \pm \varepsilon_{abs} \\ &x_2 \pm \Delta x_2 \pm \varepsilon_{abs} \\ &x_3 \pm \Delta x_3 \pm \varepsilon_{abs} \\ &\vdots \end{aligned} \tag{B.2}$$

The new error is added like a squared error.

$$\Delta x_i' = \sqrt{(\Delta x_1)^2 + (\varepsilon_{abs})^2} \tag{B.3}$$

So, the new data are:

$$\begin{aligned} &x_1 \pm \Delta x_1' \\ &x_2 \pm \Delta x_2' \\ &x_3 \pm \Delta x_3' \\ &\vdots \end{aligned} \tag{B.4}$$

Now the new mean value and the error will be calculated with:

$$\overline{x} = \frac{\sum_{i=1}^{n} \frac{x_i}{(\Delta x_i')^2}}{\sum_{i=1}^{n} \frac{1}{(\Delta x_i')^2}} \tag{B.5}$$

$$\Delta\overline{x} = \sqrt{\frac{1}{\sum_{i=1}^{n} \frac{1}{(\Delta x_i')^2}}} \tag{B.6}$$

Finally the quality of the fit will be given by:

$$\frac{\chi^2}{ndf} = \frac{1}{n-1} \sum_{i=1}^{n} \frac{(x_i - \overline{x})^2}{(\Delta x_i')^2} \tag{B.7}$$

The algorithm will be running to converge the value of $\frac{\chi^2}{ndf} = 1$. In every running the value of ε_{abs} will be changed. Finally the value of ε_{abs} gives the constant error of the system in every measurement.

B.2. Relative correction

The relative error consists on an extra percent unknown error from the measurement value added . The difference with the last method is that in this case the error depends on the measurement. In a measurement not always all parameters has the same value. This correction gives information about the stability of the system and the repetition of the experimental condition in every case. Source [Tä12] and [esc]
The algorithm is similar:

There are data x_i with its error Δx_i. n is the number of data.

$$\{x_i\}; \{\Delta x_i\}; i = 1...n \tag{B.8}$$

An unknown percent of every measurement as unknown error will be added. It will be called $\varepsilon_{rel}(\%)$

$$\begin{aligned} &x_1 \pm \Delta x_1 \pm (\tfrac{\varepsilon_{rel}}{100}) \cdot x_1 \\ &x_2 \pm \Delta x_2 \pm (\tfrac{\varepsilon_{rel}}{100}) \cdot x_2 \\ &x_3 \pm \Delta x_3 \pm (\tfrac{\varepsilon_{rel}}{100}) \cdot x_3 \\ &\vdots \end{aligned} \tag{B.9}$$

Like a the last method, the new error will be added as quadratic error:

$$\Delta x_i' = \sqrt{(\Delta x_i)^2 + ((\frac{\varepsilon_{rel}}{100}) \cdot x_i)^2} \tag{B.10}$$

Now, the new data are:

$$\begin{aligned} &x_1 \pm \Delta x_1' \\ &x_2 \pm \Delta x_2' \\ &x_3 \pm \Delta x_3' \\ &\vdots \end{aligned} \tag{B.11}$$

The new mean value and the error of the mean value will be calculated with:

$$\overline{x} = \frac{\sum_{i=1}^{n} \frac{x_i}{(\Delta x_i')^2}}{\sum_{i=1}^{n} \frac{1}{(\Delta x_i')^2}} \tag{B.12}$$

$$\Delta\overline{x} = \sqrt{\frac{1}{\sum_{i=1}^{n} \frac{1}{(\Delta x_i')^2}}} \tag{B.13}$$

The quality of the fit will be given by:

$$\frac{\chi^2}{ndf} = \frac{1}{n-1} \sum_{i=1}^{n} \frac{(x_i - \overline{x})^2}{(\Delta x_i')^2} \tag{B.14}$$

The algorithm will be executed changing the value of $\varepsilon_{rel}(\%)$ to obtain a value of $\frac{\chi^2}{ndf} = 1$. The result will give the percent of the data must be corrected. This data ε_{rel} gives the stability of the system.

C. Measurement protocol V3.2

C.1. Calibration protocol

In this appendix a protocol to realize the energy-channel calibration will be described. The radioactive source used to do a calibration is the *MIXQUELLE 38* (see chapter 4.1).

1 Start the electronic of the setup, the computer and the oscilloscope. Switch on the "Leiste" 2 and 3. The number 1 is always running.

2 Both valves of the principal rotary vane pumps must to be closed (see Figures C.1 and C.2). Then both pumps can be started. Wait approximately 30 min before using the pumps.

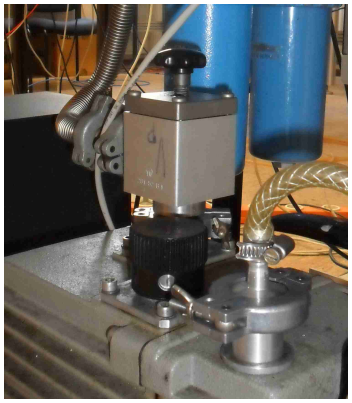

Figure C.1.: Valve of primary pump vacuum chamber

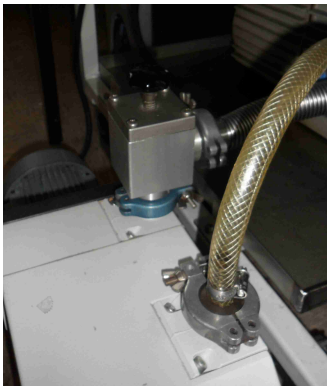

Figure C.2.: Valve of gas system vacuum pump

3 Open the principal chamber (see Figure C.4), disassemble the gas injector (see Figure C.3), assemble the measurement table, clean the vacuum chamber with isopropanol, put the radioactive source in the central position of the measure table and close it (see Figure C.6). Finally the detector will put in the calibration mode and put the bolt (see Figure C.5).

Figure C.3.: Injector, measurement table and other components.

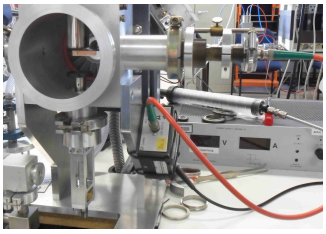

Figure C.4.: Calibration configuration setup

Figure C.5.: Detector in calibration position

Figure C.6.: To put the radioactive source MIXQUELLE 38 in the middle of the measure table

4 Realize vacuum in the principal chamber. The first step is open the valve of the primary pump (see Figure C.7). Wait until the vacuum will be approximately $10^{-1}mbar$ and then start the turbo pump (see Figure C.8). One will wait until the vacuum will be $10^{-5}mbar$.

Figure C.7.: Primary vacuum pump of the principal chamber

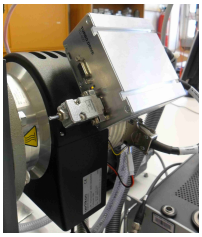

Figure C.8.: Turbo pump, principal chamber

5 Initiate the program *temp 2.5* to control the temperature. If a high number of radon measurement will be done, it would be appropriate to do a long calibration. Cooling down to cold head simulates the experimental conditions of a real measurement (the calibration will last 2 or 3 hours). When the vacuum becomes $10^{-5}mbar$

liquid N_2into the dewar vessel will be added. Wait until the temperature go down to $-180°C$, with this temperature the dewar glass will be closed (see Figure C.9) and the rotary vane pump(LEYBOLD) will be started (see Figure C.10). The temperature will be stable at $-204°C$

Figure C.9.: Closing the dewar vessel

Figure C.10.: rotary vane pump

6 Put the detector on the source (try to put in the middle see Figure C.11), elevate the measurement table to 10 mm. Switch on the power supply and reach 65 V at the detector number 3 (see Figure C.12).

Figure C.11.: Detector in calibration position and measure table

Figure C.12.: Power supply

7 Start the program Maestro and begin the count capture. The capture process will be last around 2 hours or 7200 s.

8 For the calibration process first the measurement must be stopped, with the spectra in screen:

8.1 calculate $\longrightarrow$ calibration $\longrightarrow$ Destroy calibration

8.2 The first peak is the $^{239}_{94}Pu$ peak, select a big part of the peak, do the right click and select (MARK ROE), the peak will be full filled with red color.

8.3 calculate $\longrightarrow$ calibration. Introduce the energy of the $^{239}_{94}Pu$ in keV, it is: 5156.59 keV [1]

8.4 Select the peak number two. The $^{241}_{95}Am$ peak will be selected, after do the right click and select (MARK ROE), the peak will be full filled with red color.

8.5 calculate $\longrightarrow$ calibration. We introduce the energy of the $^{241}_{95}Am$ in kev, it is: 5485.56

8.6 Finally select keV of a unit and press "ok" to finish the calibration.

Figure C.13.: Calibration dialog

[1] Use in the program . and not , for decimal numbers

9 Switch off the rotary vane pump (LEYBOLD) and open the valve of the dewar glass, star the voltage-current supply to heat up the heater cartridge (see Figure C.14). Select the maximal voltage of 45 V and a current of 2.5 A. If the temperature exceed 90 °C on the ""Heizelement" go down quickly the voltage. Work with a maximal temperature of 90 °C in the Heizelement. There is a red alarm when the temperature in the Heizelement exceed of 70 °C (see Figure C.15).
Progressively temperature in the cold head "kaltkopf" will reach 0 °C, go down the voltage to not exceed 70 °C in the heizelement.

Figure C.14.: Voltage-current heater cartridge power source

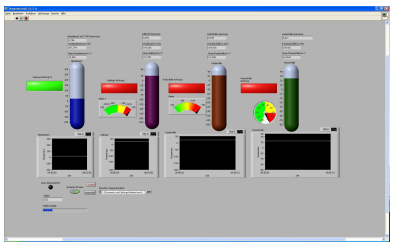

Figure C.15.: Program Temp 2.5

10 When temperature in the cold head will reach 20 °C, take off the vacuum. Close the valve of the principal pump of the camera (see Figure C.16), then switch off the turbo pump and the principal vacuum pump [2]. The pressure will go up to 10^{-1} mbar, when the chamber reach this pressure, open the valve of the chamber and reach the atmospheric press (see Figure C.17).

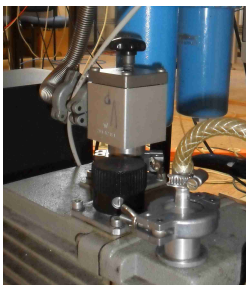

Figure C.16.: Valve principal pump for the principal chamber

Figure C.17.: Valve principal chamber

[2] Don't forget the right order to switch off the pumps

11 Finally save all dates, switch off the NIM crate and “Leiste” 2, 3.

C.2. Radon air measurement protocol

In this section the process to realize ordinary radon gas measurement can be found. The practical exercise can be last approximately 8 hours. It is necessary realize the cleaning of the principal chamber because it was confirmed in [Nus11] that there could be leftovers of the last measurement on the cold head.

1 Start the electronic of the setup and start the computer. Switch on the "Leiste" 2 and 3, (the number 1 is always running), the oscilloscope, the NIM crate and the power supply to feed the detector (but don't apply voltage)[3].

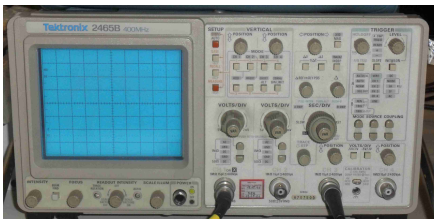

Figure C.18.: The oscilloscope

Figure C.19.: NIM crate

Figure C.20.: Power source

[3]The power supply need around 30 min to operate in stable mode, it can be dangerous switch on the power supply and apply voltage on the detector

2 Valves of the principal pumps must to be closed (see Figures C.21 and C.22). Switch on both pumps and wait approximately 30 min before using the pumps.

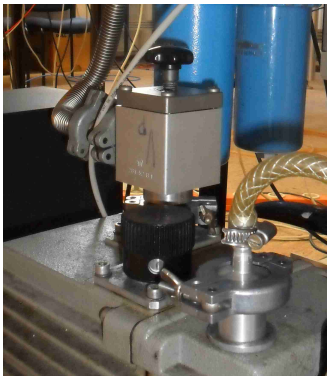

Figure C.21.: Valve Primary pump vacuum chamber

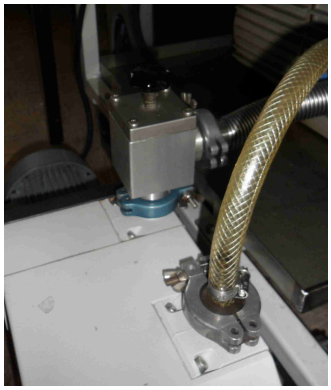

Figure C.22.: Valve Gas system vacuum pump

3 Assemble the injector to realize a gas measurement. After cleaning the principal chamber with "isopropanol" and close it (see Figure C.23). Be sure that the bolt holds the detector before doing vacuum (see Figure C.24).

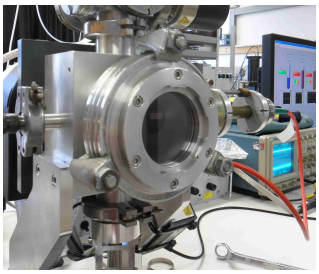

Figure C.23.: Principal chamber assembled

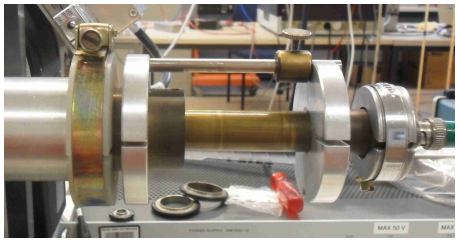

Figure C.24.: Security Bolt

4 First step: close all valves. The second step: clean the gas system.
Close the valves (1),(4) and (10) and open the valves: (2), (3), (5), (6), (7), (8), (9) and (11). Open the valves of the principal vacuum pumps and realize a first vacuum in the chamber and the gas system (see Figures C.25 and C.26).

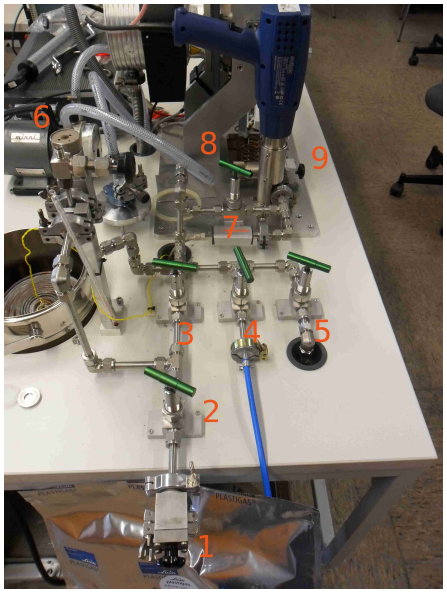

Figure C.25.: Gas system valves

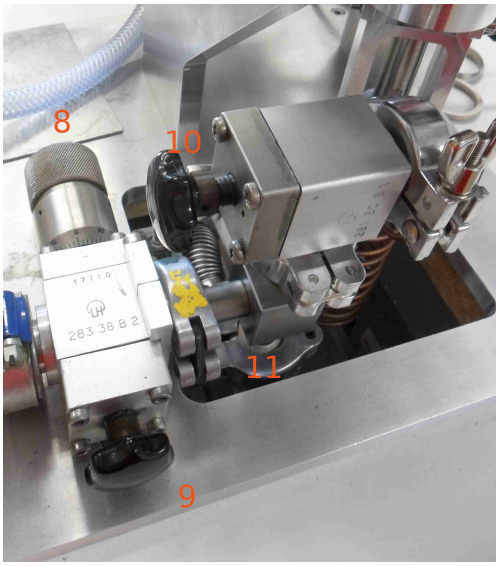

Figure C.26.: Injection valves

5 Open the valve (12), (14) and slowly the valve (13) to getting a pressure of 1.0 bar in the second barometer (see Figure C.27).

Figure C.27.: N_2 bottle

6 To realize the cleaning process:

a Start with vacuum in the gas system

b Close valves (11) and (5)

c Open valve (4), reach atmospheric pressure in the gas system

d Close valve (4) and open valve (5)

e Repeat the process three or four times

f Finally close the valve (4) and open the (5). Continue doing vacuum in the gas system.

g Close the valves in the next order: (14), (12), (13), (3), (6), (2), (8), (9), (10), (11). The valve (7) muss be open.

7 A vacuum approximately of 10^{-1} mbar in the principal chamber will be reached. Check if valve (10) is closed and switch on the turbo pump (see Figure C.28).

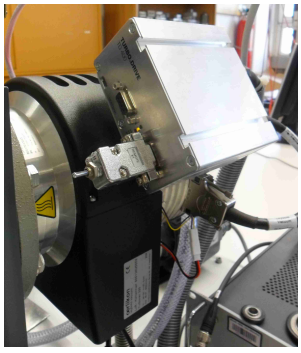

Figure C.28.: Turbo pump principal chamber

8 Prepare the radioactive probe (radon air probe) and put it in at valve (1) (see Figure C.29). Instructions to do a radioactive probe can be found in section 4.2.1. Switch on the power supply, but don't apply voltage[4] (see Figure C.30).

Figure C.29.: Radon air probe

Figure C.30.: Detector power source

9 Radon air cools down.

First is to initiate the program Temp 2.5 to check the temperature. Second is to fill in liquid N_2 at the radon trap (see Figure C.31), the water trap (see Figure C.33) and the dewar vessel (see Figure C.32). The radon trap must go below the liquid N_2, the temperature of the radon trap will be stabilized at $-195\,°C$. The red alarm shows that replace liquid N_2 must to be done, because temperature is too high and it is necessary to cool down the radon trap. In the case of the cold head when the temperature reach at $-175\,°C$, the cold head dewar vessel will be closed and switch on rotary vane pump (LEYBOLD). Wait until the temperature reach to $-203\,°C$. Exceeding $-200\,°C$ a green light in the cold head thermometer can be observed (see Figure C.34). In the case of the water trap to stabilize the temperature between $-40\,°C$ and $-60\,°C$, before starting preparation of the radon gas sample. The optimal working temperature of the water trap is between $-49\,°C$ and $-58\,°C$ (green range in the program Temp 2.5).

[4]It is necessary to start the power supply some minutes before begin the measurement to reduce the electric noise

Figure C.31.: Radon trap

Figure C.32.: Cold head dewar vessel

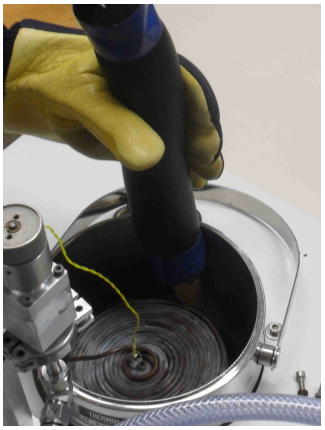

Figure C.33.: Watter trap

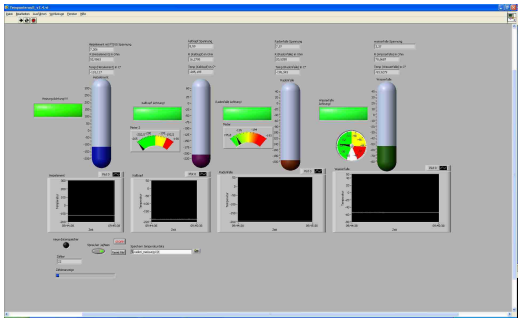

Figure C.34.: Stable temperature before start the radon air preparation

10 When all temperatures are in stable range, start the background measurement and the radon air preparation. These processes should be executed at the same time in parallel. The reason is because both processes last 2 hours (7200 s). Before starting the underground measurement the power source must have worked 30 minutes (without applying voltage), place the detector under the cold head in the measurement position and increases the voltage of the detector up to 65 V (see Figure C.35).

Figure C.35.: Detector in measurement position

11 Before starting the radon air preparation, check all temperatures again and start with the radon air preparation[5]:

11.1 All valves are in the position of step (6.g), that means:
Opened: (5), (7)
Closed: (1), (2), (3), (4), (6), (8), (9), (10), (11), (12), (13) and (14)

11.2 Close valve (5)

11.3 Open valve (1)

11.4 Open valve (2)

11.5 Open valve (6), up to 7 lines (see Figure C.36).

11.6 Open valve (8), up to 2 lines (see Figure C.37)

11.7 Open valve (9).

11.8 Open valve (11).

[5]It is important to open all valves in the indicated order

Figure C.36.: Valve (6)

Figure C.37.: Valve (8)

11.9 The pressure in the vacuum detector 2 and 3 will increase to 1000 mbar, but slowly.

12 Start the background measurement with the program *Maestro*

13 During the radon air preparation it is necessary to replace liquid N_2 in the water trap and radon trap. In the case of the water trap only tip out liquid N_2 and the case of the radon trap it must be executed quickly (see Figure C.38). See the procedure here.

13.1 Close valve (9).

13.2 Go down the radon trap vessel.

13.3 Fill the dewar vessel with N_2.

13.4 Lift the radon trap dewar.

13.5 Don't forget to open valve (9).

14 When the measurement has exceeded 7200 s in the background measurement, the counting process will be stopped, save the results in a folder with the format (.Spe) and clean the obtained spectra .

15 Decrease the detector voltage to zero, but don't switch off the power supply.

Figure C.38.: Filling in

16 Return the detector at the rest position

17 Check the plastic bag if it is empty and start the close valve process if there is a bit gas some minutes will be waited.

18 Close the valves in the order[6]:
(1), (2), (6), (8), (9) and (11)

19 Open valve (5) and evacuate the gas system. When the vacuum is approximately 10^{-2} mbar in the detector 2 and 3, close the valve (7). Continue evacuating the gas system and one minute after close the valve (5).

20 Close valve of the primary pump of the gas system and switch off the pump.

[6]Don't let down the radon trap

21 Go up the injector in the principal chamber to a distance 0 mm (see Figures C.39 and C.40).

Figure C.39.: Go up to 0mm

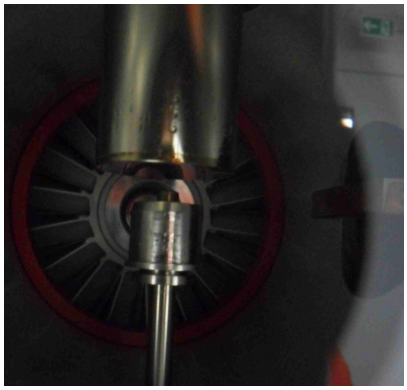

Figure C.40.: Injector and cold head

22 Open the next valves:

Figure C.41.: N_2 bottle

22.1 (12) and (14) (see Figure C.41).

22.2 Valve number (13) will be opened slowly to get the pressure of 0.6 bar in the barometer.

23 The next point will be the injection of the radon concentration. It is necessary to execute this procedure in the order indicated.

23.1 Starting with low pressure in the detector 2 and 3. Around 10^{-1} mbar.

23.2 Open valve (4), detector 2 will show a pressure of 1000 mbar but a low pressure in the detector 3 must be shown.[7].

23.3 Let down the radon trap vessel and switch on the hot air gun. The temperature of the radon trap must reach 10 °C. Use the hot air gun carefully because the increase of the temperature must be progressive (see Figure C.42).

Figure C.42.: Hot air gun

23.4 When temperature will reach approximately 10 °C in the radon trap, open valve (8) in 0.70, valve (10)[8].

23.5 Finally open valves (7) and (9) at the same time. Wait 6 minutes, the stopwatch to controller the time will be required.

23.6 Exceeded 6 min, close all valves: (10), (12), (13), (14), (8), (9) and (4). Valve (7) can stay opened.

[7]Because valve (7) is closed
[8]Don't forget that valve number (11) must be closed!

24 Let the injector to the position 35 mm down, put the detector under the cold head, close the window of the chamber and increase the voltage of the detector to 65 V.

25 Start the measurement with the program *Maestro*. The measurement time of a radon air probe is 7200s.

26 To finish the measurement the capture of counts will be stopped and the spectra with the format (.Spe) will be saved.

27 Decrease the detector voltage, and switch off the power supply. Detector will go back to the rest position (see Figure C.43).

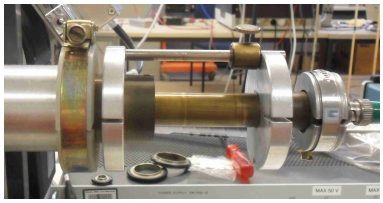

Figure C.43.: Rest position of detector

28 Open valve of the cold head dewar and switch off the rotary vane (LEYBOLD).

29 Switch on the power supply of the heater cartridge settled on the cold head. Apply a voltage of 45 V and a current of 2.5 A. Temperature of the cold head will increase, when temperature of the Heizelement reach to 90 °C, decrease the voltage. Try[9] to keep the temperature of the Heizelement around 70 °C[10].

Figure C.44.: Rest position of detector

[9]Not exceed 90 °C in the heater cartridge
[10]Defrost process could last 2 hours

30 When the temperature of the cold head reaches to 20 °C, switch off the power source and close valve of the pump of the chamber, switch off the turbo pump and the principal pump.

31 Remove the vacuum in the principal chamber and save all dates. Close all programs, switch off the NIM crate, the power supply of the heater cartridge, the detector power supply, the oscilloscope and to finally the “Leiste” 2 and 3.

D. CAD-drawings

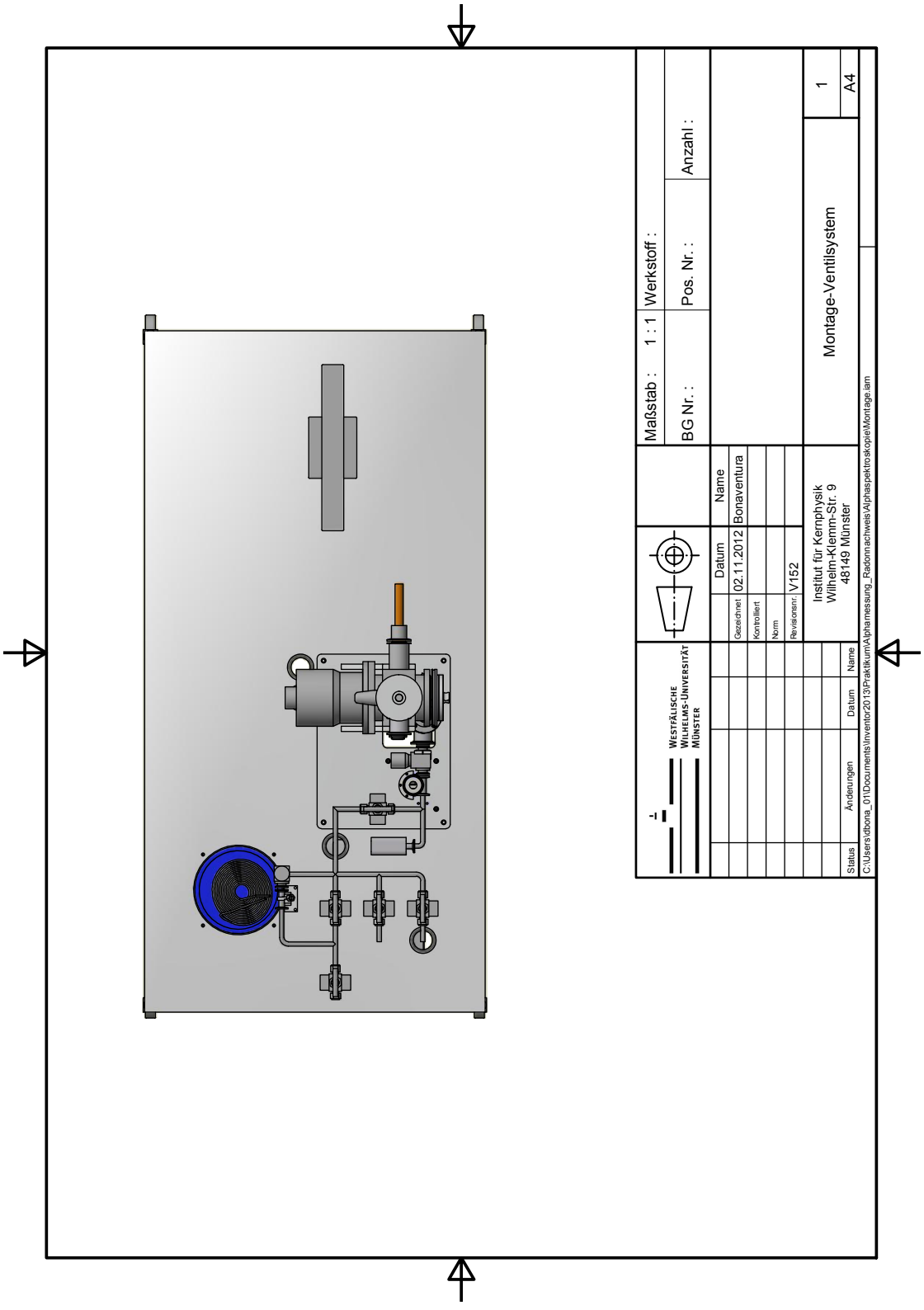

Figure D.1.: Valve system Version 3.2.

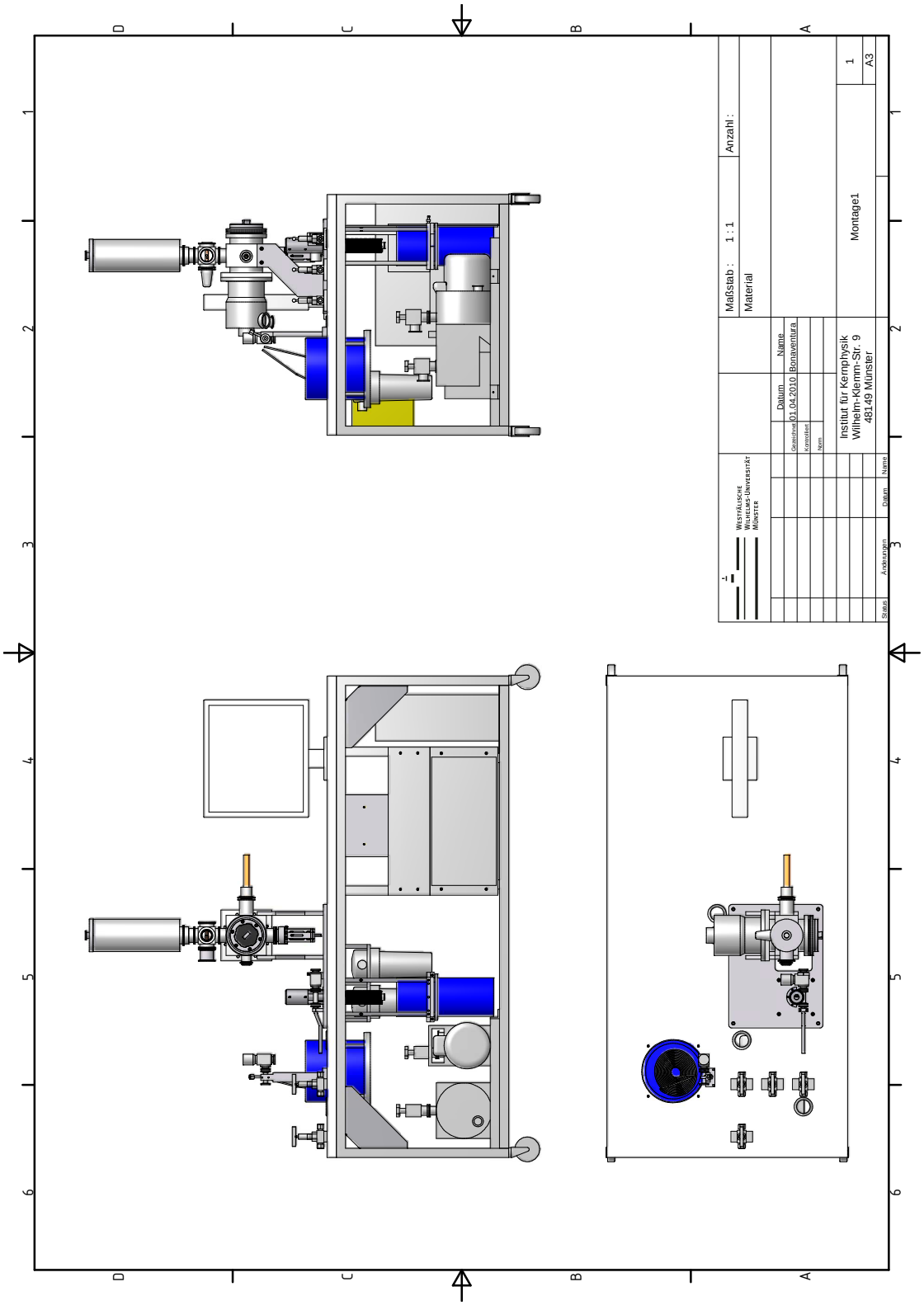

Figure D.2.: Valve system Version 2.0

E. Electronic diagrams

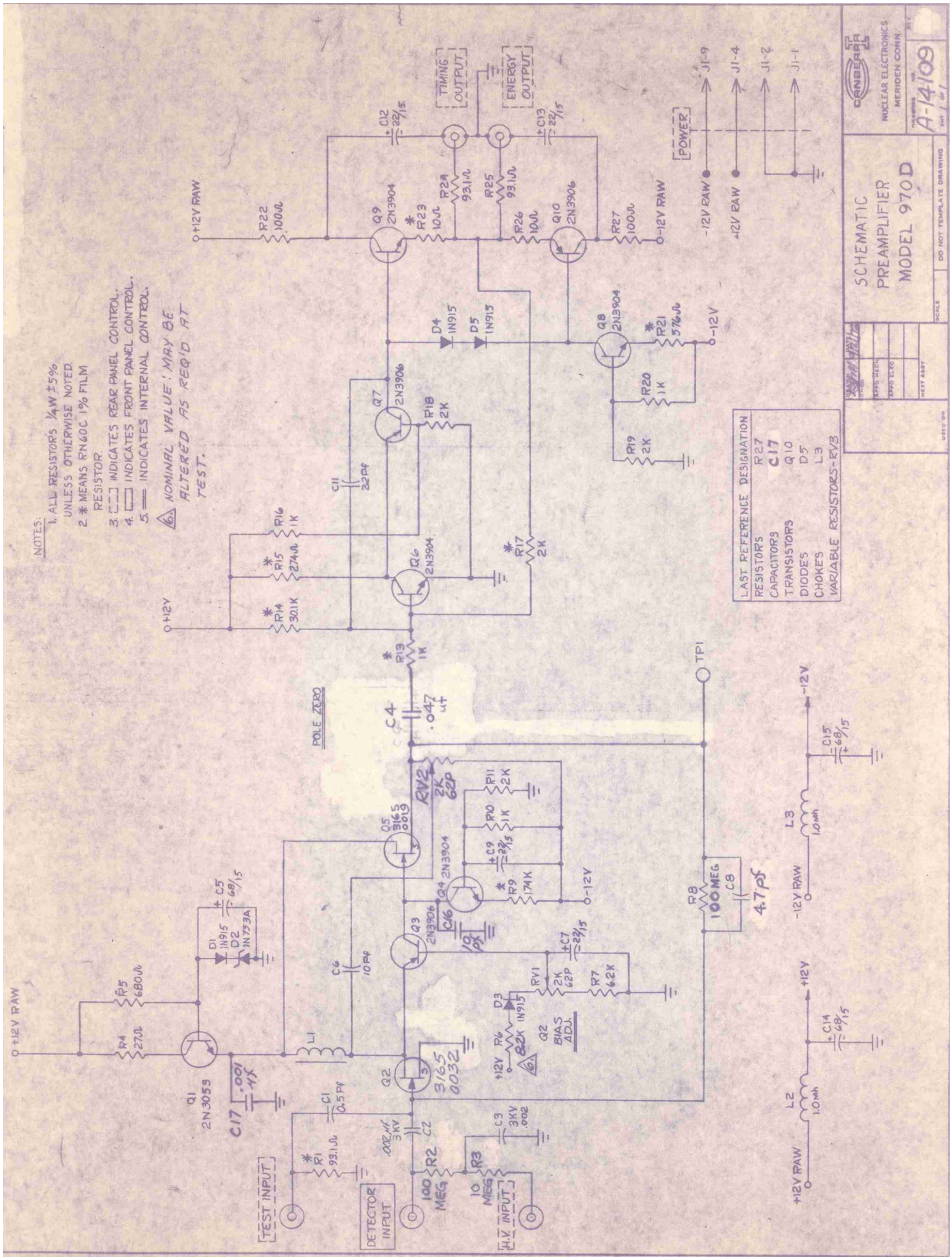

Figure E.1.: Scheme preamplifier Canberra 970D [Ind]

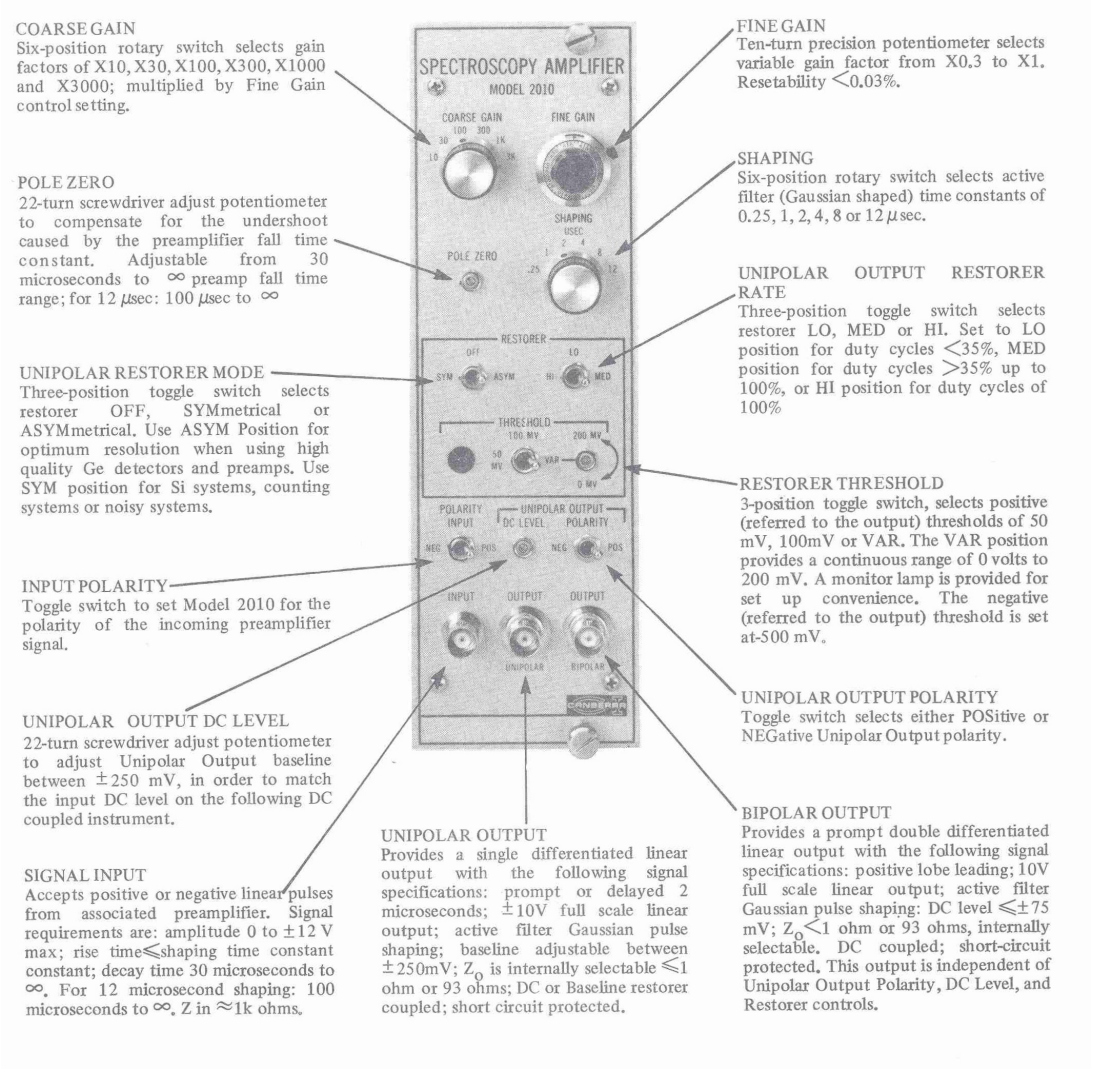

Figure E.2.: Spectroscopy Preamplifier Model 2010, front panel [Ind76]

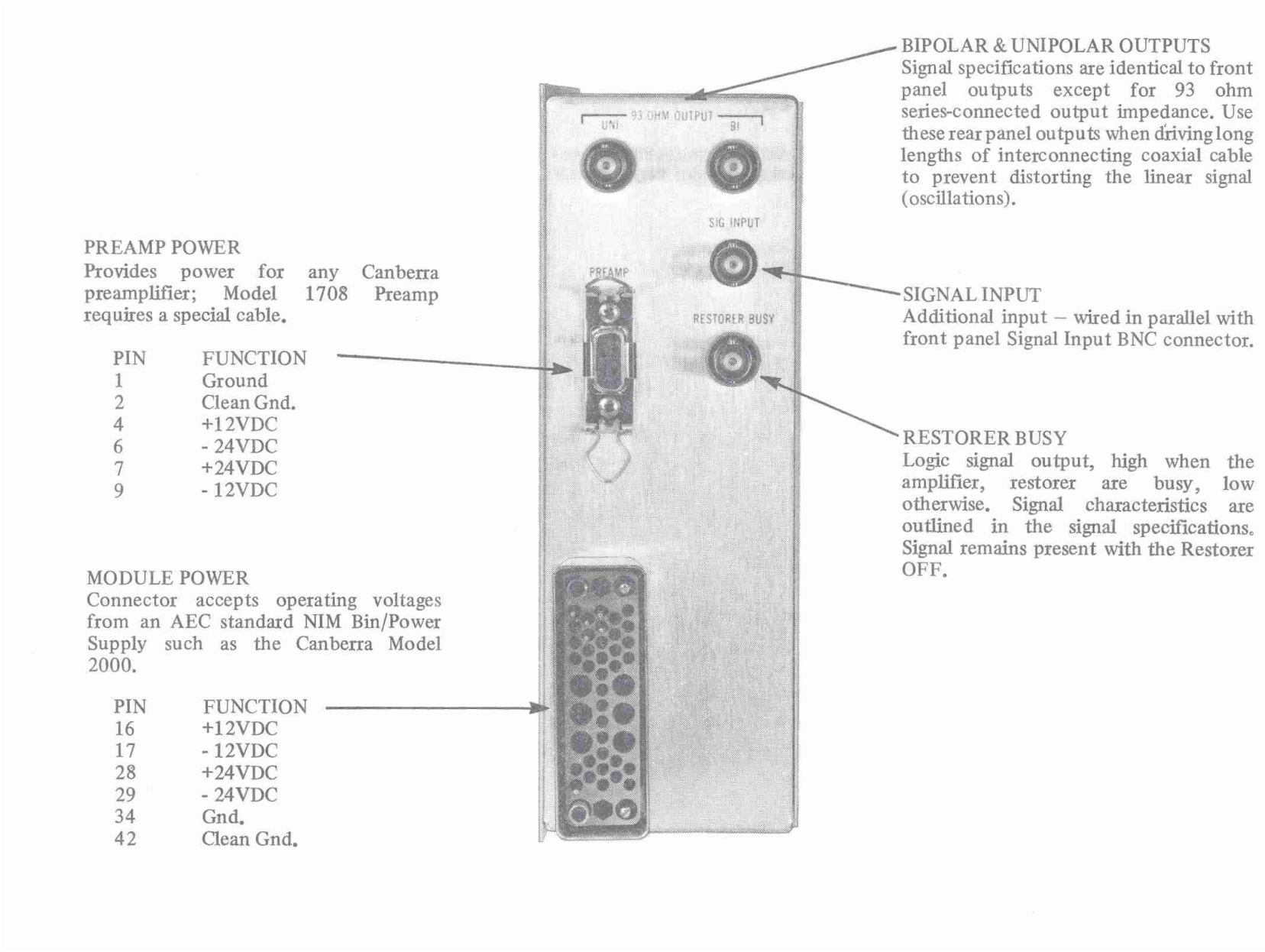

Figure E.3.: Spectroscopy Preamplifier Model 2010, rear panel [Ind76]

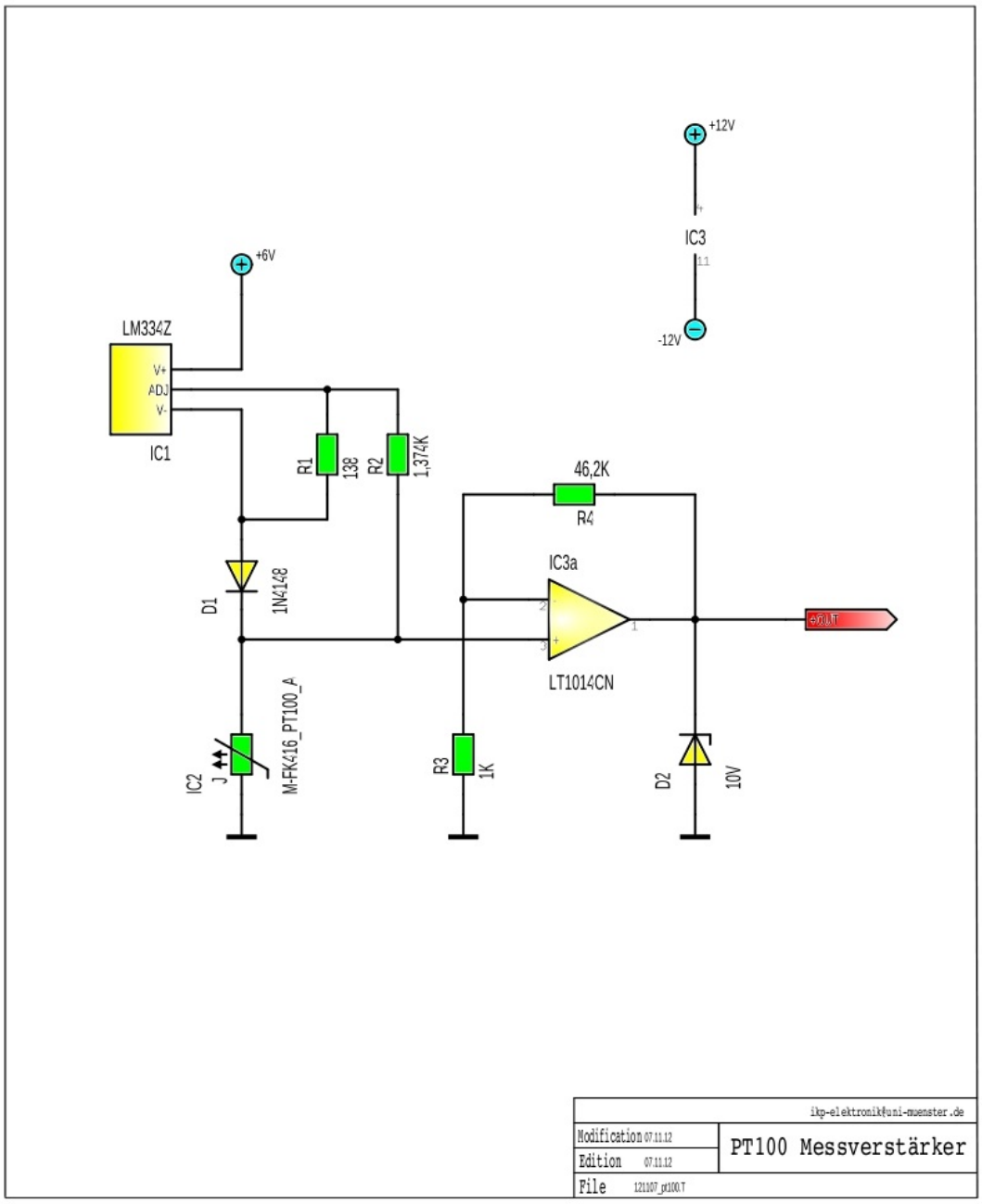

Figure E.4.: Scheme of the preamplifier card, output 3 by R. Berendes

F. Radon properties and extra information

Properties	**Radon**
Appearance	Colorless,odorless and tasteless gas. When cooled below its freezing point it brightly phosphoresces
Category	Noble Gas
Group,Period, Block	18, 6, p
Standard atomic weight	222
Atomic Radius ($\AA$)	1.34
Atomic Volume (cm^3/mol)	50.5
Cross Section(Thermal Neutron Capture) (σ_a/barns)	0.72
Crystal Structure	Cubic face centered
Electron Configuration	$1s^2$;$2s^2p^6$;$3s^2p^6d^{10}$;$4s^2p^6d^{10}f^{14}$;$5s^2p^6d^{10}$;$6s^2p^6$
Electrons per Energy Level	2,8,18,32,18,8
Filling Orbital	$6p^6$
Number of Electrons (no charge)	86
Number of Neutrons (stable nuclide)	136
Number of Protons	86
Oxidation States	0
Valence Electrons	$6s^2p^6$
Heat of Fusion (kJ/mol)	2.89
Ionization Potential (1°) (eV)	10.748
Atomic Mass Average	222
Thermal conductivity (W/cmK)	0.0000364

Table F.1.: Physical properties of Radon [Bar]

Properties	Radon
Boiling Point (K), (°C)	211, -62°
Melting point (K), (°C)	202, −71°
Critical point	377K, 6.28MPa
Density(273K;1atm) (g/l)	9.73
Enthalpy of Fusion (kJ/mol)	2.89
Enthalpy of Vaporization (kJ/mol)	16.4
Molar Volume (m^3/mol)	50.5
Physical State (at 20°C; 1atm)	Gas
Specific Heat (J/gK)	0.09
Abundance in seawater (p.p.m)	10^{-14}
Abundance in atmosphere (p.p.m)	10^{-15}
Discoverer	Fredrich Ernst Dorn
Discovery Location	Halle, Germany
Discovery Year	1900

Table F.2.: Physical properties of Radon [Bar]

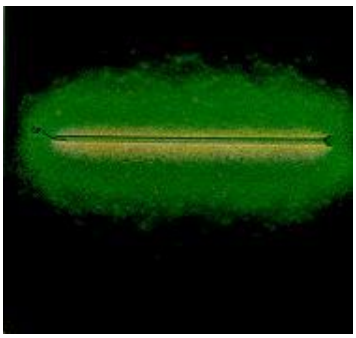

Figure F.1.: Cooled radon [Lap65]

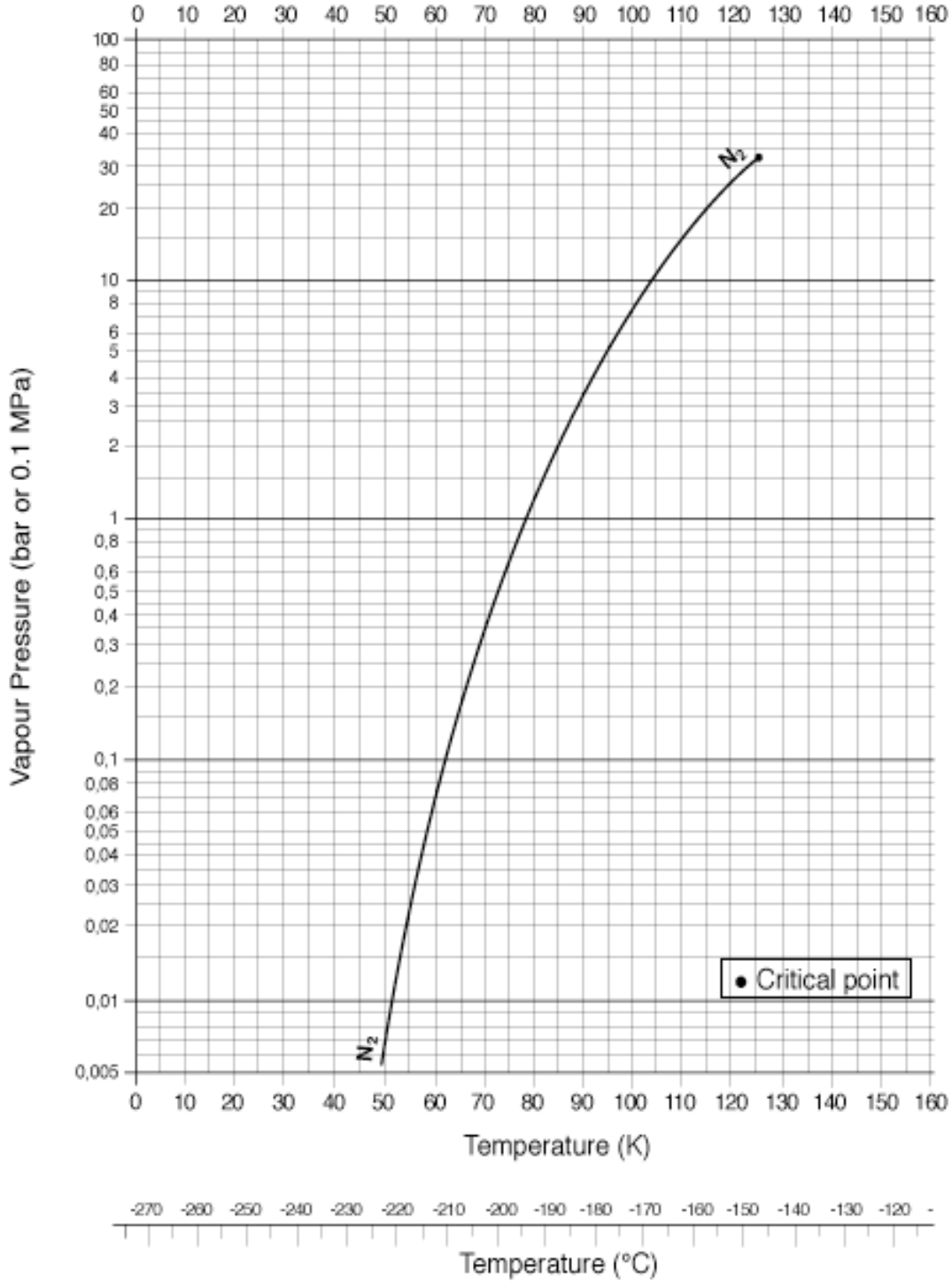

Figure F.2.: Nitrogen curve, Pressure vs Temperature [liq]

G. Tables

G.1. Measurements with setup V2.0

Measurement	222-Rn Activity (Bq)	Enrichment time	time life (s)	Experimental Activity (Bq)	Efficient (%)
1	974±41	138d23h21min	7339	120±7	12.3±0.9
2	163±7	0d24h18min	9362	51±3	31.1±2.2
3	648±27	6d1h42min	7522	96±5	14.8±1.0
4	157±7	0d23h16min	7693	28.0±2.0	17.6±1.2
5	153±6	0d22h43min	7550	20±1	12.9±0.9
6	509±21	4d01h55min	7599	52±3	10.2±0.7
7	153±6	0d22h37min	7629	22±1	14.3±1.0
8	162±7	1d00h02min	8187	17±1	10.6±0.7
9	158±7	0d23h29min	9386	21±1	13.0±1.0
10	417±18	3d2h00min	6650	58±3	14.0±0.9
11	968±41	28d21h54min	7204	81±5	8.3±0.6
12	950±40	21d00h10min	7620	101±6	10.6±0.7

Table G.1.: Original radon measurements [Nus11], Pag.96

G.2. Measurements with setup V3.1

Measure	File name	Date air Probe	Enrichement time	Enrichement time in (s)	Radon air probe activity (Bq)
1	30_09_2011_Radon.spe	09:08	2d23h32min	257520	415 ± 17
2	04_10_2011_Radon.Spe	12:26	4d03h18min	357480	525 ± 22
3	07_10_2011_Radon.Spe	10:09	2d21h43min	250980	407 ± 17
4	12_10_2011_Radon.Spe	09:40	4d23h31min	430260	591 ± 25
5	14_10_2011_Radonmessung.Spe	10:03	2d00h23min	174180	305 ± 13
6	17_10_2011_Radon.Spe	10:10	3d00h07min	259620	418 ± 18
7	19_10_2011_Radon.Spe	09:55	0d23h48min	85680	164 ± 7
8	25_10_2011_Radonmessung.Spe	11:36	6d01h41min	524460	664 ± 28
9	26_10_2011_Radonmessung.Spe	09:50	0d22h14min	80040	154 ± 6
10	27_10_2011_Radon.Spe	10:35	1d00h45min	89100	170 ± 7
11	28_10_2011_Radonmessung.Spe	10:34	0d23h59min	86340	165 ± 7
12	31_10_2011_Radonmessung.Spe	09:58	2d22h24min	253440	410 ± 17
13	02_11_2011_Radonmessung.Spe	10:11	2d00h13min	173580	304 ± 13
14	04_11_2011_Radonmessung.Spe	10:32	2d00h21min	174060	304 ± 13
15	09_11_2011_Radonmessung.Spe	10:19	1d21h59min	165540	292 ± 12
16	14_11_2011_Radonmessung.Spe	10:24	2d21h19min	249540	405 ± 17

Table G.2.: Measurements setup V3.1. Measurements 1-16, first part.

Measure	File name	Date air Probe	Enrichement time	Enrichement time in (s)	Radon air probe activity (Bq)
17	15_11_2011_Radonmessung.Spe	11:10	1d00h46min	89160	170 ± 7
18	18_11_2011_Radonmessung.Spe	10:02	2d22h52min	255120	412 ± 17
19	21_11_2011_Radonmessung.Spe	10:49	3d00h47min	262020	421 ± 18
20	22_11_2011_Radonmessung.Spe	10:01	0d23h12min	83520	160 ± 7
21	18_01_2012_Radonmessung.Spe	10:43	1d23h30min	171000	300 ± 13
22	19_01_2012_Radonmessung.Spe	14:39	1d03h56min	100560	189 ± 8
23	20_01_2012_Radonmessung.Spe	11:23	0d20h44min	74640	144 ± 6
24	31_01_2012_Radonmessung.Spe	11:07	10d23h44min	949440	859 ± 36
25	01_02_2012_Radonmessung.Spe	11:01	0d23h54min	86040	164 ± 7
26	07_02_2012_Radonmessung.Spe	10:39	3d23h04min	342240	510 ± 21
27	08_02_2012_Radonmessung.Spe	11:23	1d00h44min	89040	170 ± 7
28	13_02_2012_Radonmessung.Spe	15:49	5d04h26min	447960	606 ± 25
29	17_02_2012_Radonmessung.Spe	11:08	3d19h19min	328740	496 ± 21
30	27_02_2012_Radonmessung.Spe	14:54	5d23h19min	515940	658 ± 28
31	28_02_2012_Radonmessung.Spe	10:41	0d19h47min	71220	138 ± 6

Table G.3.: Measurements setup V3.1. Measurements 17-31, first part.

Measure	Emanation Rate	Differential time	Differential time in (s)	$A_{Rn}e^{-\lambda_{Rn}t_{diff}}$ in (Bq)	Measurement time (s)
1	0.382 ± 0.016	2h58min	10680	406 ± 17	7242
2	0.382 ± 0.016	3h05min	11100	513 ± 22	5959
3	0.382 ± 0.016	2h47min	10020	399 ± 17	7218
4	0.382 ± 0.016	2h43min	9780	579 ± 24	7200
5	0.382 ± 0.016	2h52min	10320	298 ± 13	7295
6	0.382 ± 0.016	2h47min	10020	409 ± 17	9167
7	0.382 ± 0.016	2h08min	7680	161 ± 7	7235
8	0.382 ± 0.016	2h23min	8580	652 ± 27	7867
9	0.382 ± 0.016	2h16min	8160	151 ± 6	7533
10	0.382 ± 0.016	3h29min	12540	165 ± 7	12332
11	0.382 ± 0.016	2h21min	8460	162 ± 7	7436
12	0.382 ± 0.016	2h33min	9180	402 ± 17	7415
13	0.382 ± 0.016	2h21min	8460	298 ± 13	7204
14	0.382 ± 0.016	2h23min	8580	299 ± 13	7518
15	0.382 ± 0.016	2h26min	8760	287 ± 12	7235
16	0.382 ± 0.016	2h39min	9540	397 ± 17	7222
17	0.382 ± 0.016	2h18min	8280	167 ± 7	8372

Table G.4.: Measurements setup V3.1. Measurements 1-17, second part.

Measure	Emanation Rate	Differential time	Differential time in (s)	$A_{Rn}e^{-\lambda_{Rn}t_{diff}}$ in (Bq)	Measurement time (s)
18	0.382 ± 0.016	2h40min	9600	404 ± 17	7387
19	0.382 ± 0.016	2h16min	8760	413 ± 17	7199
20	0.382 ± 0.016	2h41min	9660	157 ± 7	11942
21	0.382 ± 0.016	2h56min	10560	293 ± 12	7203
22	0.382 ± 0.016	3h02min	10920	185 ± 8	7205
23	0.382 ± 0.016	4h05min	14700	140 ± 6	7392
24	0.382 ± 0.016	2h34min	9240	843 ± 35	8170
25	0.382 ± 0.016	2h47min	10020	161 ± 7	7224
26	0.382 ± 0.016	4h55min	17640	491 ± 21	7309
27	0.382 ± 0.016	5h25min	19500	163 ± 7	7227
28	0.382 ± 0.016	2h42min	9720	594 ± 25	7201
29	0.382 ± 0.016	4h29min	16140	479 ± 20	3609
30	0.382 ± 0.016	2h29min	8940	646 ± 27	6489
31	0.382 ± 0.016	4h01min	14460	134 ± 6	7981

Table G.5.: Measurements setup V3.1. Measurements 18-31, second part.

Measure	Solid angle (Sr)	Area ^{222}Rn	Area ^{218}Po	Area ^{214}Po	Efficiency (%)
1	4.23 ± 0.24	277130 ± 1060	268387 ± 1052	161718 ± 473	28.22 ± 1.99
2	4.23 ± 0.24	209969 ± 879	211467 ± 866	103852 ± 381	20.58 ± 1.45
3	4.23 ± 0.24	262662 ± 1004	259085 ± 1003	145751 ± 453	27.33 ± 1.93
4	4.23 ± 0.24	233161 ± 915	223403 ± 909	126250 ± 404	16.74 ± 1.18
5	4.23 ± 0.24	209309 ± 857	210579 ± 847	121883 ± 420	28.83 ± 2.04
6	4.23 ± 0.24	173680 ± 764	164020 ± 756	120768 ± 450	13.87 ± 0.98
7	4.23 ± 0.24	110376 ± 730	108761 ± 722	61763 ± 300	28.37 ± 2.01
8	4.23 ± 0.24	367363 ± 1674	389261 ± 1659	236878 ± 691	21.45 ± 1.52
9	4.23 ± 0.24	124850 ± 827	125908 ± 811	71445 ± 370	32.83 ± 2.33
10	4.23 ± 0.24	106072 ± 1080	108737 ± 1048	82384 ± 580	15.59 ± 1.11
11	4.23 ± 0.24	90535 ± 806	85714 ± 898	44999 ± 406	22.52 ± 1.6
12	4.23 ± 0.24	172163 ± 941	176183 ± 916	100795 ± 426	17.28 ± 1.22
13	4.23 ± 0.24	184353 ± 1490	185328 ± 1558	90007 ± 758	25.69 ± 1.82
14	4.23 ± 0.24	207774 ± 591	197541 ± 610	103261 ± 331	27.69 ± 1.96
15	4.23 ± 0.24	112510 ± 980	104686 ± 1057	55748 ± 490	16.25 ± 1.16
16	4.23 ± 0.24	218862 ± 603	207341 ± 615	106038 ± 334	22.84 ± 1.61
17	4.23 ± 0.24	94571 ± 16735	92344 ± 16356	50089 ± 8859	20.28 ± 3.86

Table G.6.: Measurements V3.1. Measurements 1-17, Third part.

Measure	Solid angle (Sr)	Area ^{222}Rn	Area ^{218}Po	Area ^{214}Po	Efficiency (%)
18	4.23 ± 0.24	133343 ± 479	125140 ± 494	65563 ± 264	13.38 ± 0.95
19	4.23 ± 0.24	175249 ± 521	166676 ± 528	84664 ± 300	17.65 ± 1.25
20	4.23 ± 0.24	150332 ± 546	141807 ± 549	103535 ± 341	24.06 ± 1.7
21	4.23 ± 0.24	164352 ± 610	157607 ± 643	82551 ± 294	23.3 ± 1.65
22	4.23 ± 0.24	110745 ± 567	108900 ± 660	57368 ± 277	24.89 ± 1.76
23	4.23 ± 0.24	83919 ± 460	80724 ± 496	41113 ± 242	24.32 ± 1.72
24	4.23 ± 0.24	504095 ± 944	483329 ± 964	273493 ± 544	21.93 ± 1.55
25	4.23 ± 0.24	109866 ± 574	108519 ± 571	58182 ± 269	28.31 ± 2
26	4.23 ± 0.24	294096 ± 1005	290041 ± 1007	162539 ± 465	24.54 ± 1.73
27	4.23 ± 0.24	77358 ± 490	76285 ± 495	40879 ± 224	19.7 ± 1.4
28	4.23 ± 0.24	244844 ± 684	255530 ± 669	125991 ± 369	17.15 ± 1.21
29	4.23 ± 0.24	115011 ± 587	115921 ± 654	30310 ± 188	19.92 ± 1.41
30	4.23 ± 0.24	292309 ± 1004	289084 ± 992	146213 ± 432	20.9 ± 1.48
31	4.23 ± 0.24	88999 ± 390	88655 ± 422	46905 ± 239	24.93 ± 1.76

Table G.7.: Measurements V3.1. Measurements 18-31, Third part.

G.3. Measurements with setup V3.2

Measure	File name	Date air Probe	Enrichement time	Enrichement time in (s)	Emanation Rate	Radon air probe activity (Bq)
1	16_06_2012_Radonmessung.Spe	11:28	1d02h26min	95160	0.382 ± 0.016	180 ± 8
2	18_06_2012_Radonmessung.Spe	11:04	1d23h36min	171360	0.382 ± 0.016	300 ± 13
3	20_06_2012_Radonmessung.Spe	12:32	1d02h01min	93660	0.382 ± 0.016	177 ± 7
4	21_06_2012_Radonmessung.Spe	09:36	0d21h04min	75840	0.382 ± 0.016	146 ± 6
5	22_06_2012_Radonmessung.Spe	09:29	0d23h53min	85980	0.382 ± 0.016	164 ± 7
6	27_06_2012_Radonmessung.Spe	10:47	5d01h18min	436680	0.382 ± 0.016	597 ± 25
7	02_07_2012_Radonmessung.Spe	10:16	4d23h29min	430140	0.382 ± 0.016	591 ± 25
8	04_07_2012_Radonmessung.Spe	09:35	1d23h19min	170340	0.382 ± 0.016	299 ± 13
9	05_07_2012_Radonmessung.Spe	10:22	1d00h47min	89220	0.382 ± 0.016	170 ± 7

Table G.8.: Measurements setup V3.2, first part.

Measure	Differential time	Differential time in (s)	$A_{Rn}e^{-\lambda_{Rn}t_{diff}}$ in (Bq)	Measurement time (s)
1	2h44min	9840	176 ± 7	7201
2	2h18min	8280	295 ± 12	7208
3	2h20min	8400	174 ± 7	7690
4	2h25min	8700	144 ± 6	8937
5	2h30min	9000	161 ± 7	7747
6	2h20min	8400	586 ± 25	7356
7	2h22min	8520	581 ± 24	7292
8	2h33min	9180	293 ± 12	8834
9	2h43min	9780	166 ± 7	7201

Table G.9.: Measurements setup V3.2, second part.

Measure	Solid angle (Sr)	Area ^{222}Rn	Area ^{218}Po	Area ^{214}Po	Efficiency (%)
1	4.23 ± 0.24	124733 ± 681	125685 ± 727	68808 ± 323	29.41 ± 2.08
2	4.23 ± 0.24	209430 ± 892	208325 ± 1003	115207 ± 388	29.47 ± 2.08
3	4.23 ± 0.24	88088 ± 674	86549 ± 675	50503 ± 269	19.67 ± 1.4
4	4.23 ± 0.24	106566 ± 815	108286 ± 826	70707 ± 373	24.85 ± 1.76
5	4.23 ± 0.24	88607 ± 617	90243 ± 610	51842 ± 269	21.26 ± 1.51
6	4.23 ± 0.24	271753 ± 998	265179 ± 962	153012 ± 451	18.87 ± 1.33
7	4.23 ± 0.24	339070 ± 932	325555 ± 1039	179467 ± 465	23.97 ± 1.69
8	4.23 ± 0.24	200166 ± 797	192601 ± 797	124199 ± 399	23.14 ± 1.64
9	4.23 ± 0.24	81652 ± 462	78641 ± 471	41491 ± 220	20.41 ± 1.44

Table G.10.: Measurements setup V3.2, third part.

G.4. Measurements of basement samples

Measure	File name	Date air probe	Differential time	Differential time in (s)	Measurement time (s)	Solid angle (Sr)
1	16_07_2012_messungkeller_1.Spe	11:50	0d03h45min	13500	7229	4.23 ± 0.24
2	17_07_2012_kellermessung_2.Spe	10:06	0d03h02min	10920	7224	4.23 ± 0.24
3	18_07_2012_messungkeller_3.Spe	12:21	0d03h23min	12180	7580	4.23 ± 0.24
4	19_07_2012_messungkeller_4.Spe	10:20	0d02h54min	10440	7507	4.23 ± 0.24
5	20_07_2012_kellermessung_5.Spe	10:19	0d02h54min	10440	7204	4.23 ± 0.24
6	23_07_2012_Kellermessung_6.Spe	09:43	0d03h11min	11460	7203	4.23 ± 0.24

Table G.11.: Basement measurements, first part.

Measure	Area ^{222}Rn	Area ^{218}Po	Area ^{214}Po
1	58 ± 12	49 ± 12	25 ± 5
2	N.A	89 ± 21	46 ± 9
3	26 ± 7	34 ± 7	21 ± 4
4	51 ± 22	35 ± 17	32 ± 17
5	80 ± 19	43 ± 1	41 ± 10
6	90 ± 67	69 ± 52	34 ± 26

Table G.12.: Basement measurements, second part.

G.5. Measurements of floor samples

Measure	File name	Date air probe	Differential time	Differential time in (s)	Measurement time (s)	Solid angle (Sr)
1	24_07_2012_Etage_keller.Spe	09:41	03h09min	11340	7204	4.23 ± 0.24
2	25_07_2012_etage_erdgeschoss.Spe	09:50	03h07min	11220	7203	4.23 ± 0.24
3	26_07_2012_Etage_1.Spe	09:43	02h58min	10680	7316	4.23 ± 0.24
4	27_07_2012_etage_2.Spe	09:41	03h07min	11220	7203	4.23 ± 0.24
5	30_07_2012_etage_3.Spe	09:49	03h06min	11160	7202	4.23 ± 0.24
6	28_08_2012_etage_4.Spe	09:38	02h59min	10740	7260	4.23 ± 0.24
7	29_08_2012_etage_5.Spe	09:31	06h06min	11160	7202	4.23 ± 0.24

Table G.13.: Floor measurements, first part.

Measure	Area ^{222}Rn	Area ^{218}Po	Area ^{214}Po
1	65 ± 18	61 ± 13	43 ± 10
2	32 ± 5	19 ± 4	5 ± 2
3	25 ± 22	10 ± 6	N.A
4	50 ± 27	23 ± 13	20 ± 10
5	10 ± 3	N.A	N.A
6	31 ± 15	22 ± 10	17 ± 7
7	47 ± 6	21 ± 5	10 ± 3

Table G.14.: Floor measurements, second part.

G.6. Measurements of background samples

Measure	File name	Date air probe	Differential time	Differential time in (s)	Measurement time (s)	Solid angle (Sr)
1	13_07_2012_background_1.Spe	10:10; 18.10.2011	269d03h14min	23253240	7221	4.23 ± 0.24
2	18_09_2012_background_2.Spe	16:54; 13.07.2012	66d20h23min	5775780	7213	4.23 ± 0.24

Table G.15.: Background measurements, first part.

Measure	Area ^{222}Rn	Area ^{218}Po	Area ^{214}Po
1	7 ± 2	2 ± 1	1 ± 1
2	17 ± 1	7 ± 1	5 ± 1

Table G.16.: Background measurements, second part.

Bibliography

[Ama] J. Amaro. *http://www.ugr.es/ amaro/radiactividad/tema4/node17.html*. Universidad de Granada.

[ap] T. N. academies press. *Decay scheme for natural occurring 238U chain*.

[Bar] K. Barbalace. *Periodic Table of Elements - Radon - Rn*. Environmental-Chemistry.com. 1995 - 2012. Accessed on-line: 10/30/2012.

[Bor] G. Bortels and P. Collaers. *Analitical Function for fitting peaks in alpha-particle spectra from Si Detectors*.

[con] *http://www.bvsde.paho.org/bvstox/i/fulltext/toxprofiles/radon.pdf*.

[dep] *http://chemistry.beloit.edu/edetc/SlideShow/slides/contents/pn.html*.

[epa] *United States Environmental Protection Agency*. http://www.epa.gov/.

[esc] *https://lp.uni-goettingen.de/get/text/5819*.

[fmt] *http://en.wikipedia.org/wiki/Mean_free_path#cite_note-2*.

[God] T. Godish. *"Indoor Environment Quality"*. FL. CRC Press LLC.

[Hod97] P. Hodgson, E. Gadioli and E. Erba. *Introductory nuclear physics*. Oxford science publications. Clarendon Press, 1997.

[Ind] C. Industries. *Spectroscopy Preamplifier Model 970-D, manual instructions*.

[Ind76] C. Industries. *Spectroscopy Preamplifier Model 2010, manual instructions*. 1976.

[Kno89] G. Knoll. *Radiation detection and measurement*. Wiley, 1989.

[Lab] B. N. Laboratory. *B.N.L National Nuclear Data Center*.

[Lap65] R. E. Lapp. *http://www.chemtopics.com/elements/noble/noble.htm*. 1965.

[Leo94] W. Leo. *Techniques for Nuclear and Particle Physics Experiments: A How-To Approach*. Springer, 1994.

[liq] A. liquide. *http://encyclopedia.airliquide.com/images_encyclopedie/VaporPressureGraph/nitrogen_vapor_pressure.gif*.

[Net94] M. Nettebrock. *Entwicklung von Nachweisverfahren für radiaktive Isotope hoher Radiotoxizität in Umweltproben*. Westfälischen Wilhelms Universität Münster, 1994.

[ni] *NI USB-6008/6009*. http://www.ni.com/pdf/manuals/371303m.pdf.

[nIDE] P.-W. P. nach IEC 751DIN EN 60751. *http:grundpraktikum.physik.uni-saaland.de/scripts/Platin_Widerstandthermometer.pdf*.

[Nus11] A. Nustede. *Aktivitätsbestimmung radonhaltiger Umweltproben und Quellen mittels Halbleiterdetektoren im kernphysikalischen Praktikum*. Westfälische Wilhelms-Universitat Münster, Juli 2011.

[Orta] Ortec. *MAESTRO 32-MCA emulator for Microsoft Windows, Software User's Manual. V6.0*.

[Ortb] Ortec. *Model 926 ADCAM® Multichannel Buffer Hardware Manual*.

[Pro] E. Profio. *Radiation shielding and dosimetry*.

[R.W02] R.Whitcher. *Calculation of the Averange Solid Angle Subtendet by a Detector to Source un a Parallel Plane by a Monte Carlo Method*. Vol. 102, No.4, pp. 365-369, 2002.

[sil] *http://www.siliconfareast.com/sigegaas.htm*.

[Tä12] A. Täschner. *Fehlerrechung and Least Square Fits*. 2012.

[War] d. o. p. Warwick. *Description of the electronic bands in solids[8]*..

Acknowledgements

In these last lines I would like to thank all people who have helped me during the master period.
First, I would like to express my gratitude to Prof. Dr. Alfons Khoukaz for giving me the opportunity to work in his group, supporting me and giving me new ideas to make face all problems.
My next gratitude will be to Esperanza Köhler and Alexander Täschner for spending hours and hours reading my master thesis and searching errors. Without their tips, I wouldn't write this master thesis.
The next gratitude is to Andrea Nustede, I would like to thank you for all hours together when I started my master thesis, all advices during my first measurements and to start me the way of this master. I would like to thank Daniel Bonaventura for helping me during the installation of the new setup.
The next thanks will go to Elena Ceballos Romero, Markus Michael, David Regalado Lamprea and Michèle Neumann. I would like to say you thanks for every moment here together, for every tea, every beer and I hope in the future we can meet one more time to spend hours and remember the master pauses.
In this point I would like to cite my family who helped me every day from Spain, my mother Maria Dolores Mayo Rodriguez and my brother Francisco Javier Pérez Mayo, thank you one more time to give me the opportunity to do this thesis.
Finally I would like to finish this thesis with a person who I have met this year and who has given me every day reasons to stand up and to do a better work. Vielen Dank meine Laura.

Affidavit

Ich versichere, dass ich die vorliegende Arbeit selbständig verfasst und keine anderen als die angegebenen Hilfsmittel verwendet habe. Alle Textstellen, die dem Wortlaut oder dem Sinn nach anderen Werken entnommen sind, wurden unter der Angabe der Quelle deutlich gekennzeichnet.

Münster, Februar 2013

.....
(Manuel Pérez Mayo)